Generalized Branching in Circle Packing

A Dissertation Presented for

the Doctor of Philosphy

Degree

The University of Tennessee, Knoxville

James Russell Ashe

May 2012

© by James Russell Ashe, 2012
All Rights Reserved.

To my wonderful family, both here and gone

Acknowledgements

I have been truly blessed by the people who have graced my life. Credit must be given to the department for accepting this student on the basis of potential rather than background. A possibility I would have not thought possible had it not been for the guidance of David Dobbs. When I first walked into Pavlos Tzermias' class I truly knew nothing about mathematics, his inspiring teaching was the fire that steeled my mind. Of course I owe my advisor Ken Stephenson a debt of gratitude. Not only for accepting me as his student, but for his contagious enthusiasm and love of math. Unlike many other fields, an advisor in mathematics takes on a burden with a student that may yield no professional rewards. I appreciate his patience and value the friendship which has grown over the years.

I should also thank Pam Armentrout for her dedication to us graduate students. There are many other people who deserve recognition. The entire Mathematics department of the University of Tennessee is an example of excellence. All of my instructors have been accessible and dedicated teachers. All of the staff has been helpful and professional.

Nothing I have accomplished would have been possible or meaningful without the love and support of my family. I need to thank my brother and sister-in-law, who always had an open door and a cold drink. My beautiful baby girl has been a wonderful motivator, and I was only able to capitalize on that motivation due to the help of both my mother and mother-in-law. I also appreciate the emotional support and prayers of both my parents. Their faith in me never waned. Natives of Tennessee, both sets of my grandparents grew up in stark poverty with limited opportunities. I will always cherish what their sacrifices have created, and work to follow their example. Finally, I want to thank my wife, whose love has shouldered the greatest burden in this journey.

Abstract

Circle packings are configurations of circle with prescribed patterns of tangency. They relate to a surprisingly diverse array of topics. Connections to Riemann surfaces, Apollonian packings, random walks, Brownian motion, and many other topics have been discovered. Of these none has garnered more interest than circle packings' relationship to analytical functions. With a high degree of faithfulness, maps between circle packings exhibit essentially the same geometric properties as seen in classical analytical functions. With this as motivation, an entire theory of discrete analytic function theory has been developed. However limitations in this theory due to the discreteness of circle packings are shown to be unavoidable. This thesis explores methods to introduce continuous parameters for the purpose of overcoming these difficulties. Our topics include, packings with deep overlaps, fractional branching, and shift-points. Using the software package `CirclePack`, examples of some previously non-realizable discrete functions in circle packing are shown to computational exist using these techniques. Some necessary theory is developed including a generalization for overlapping packings and some results for expressing singularities associated with faces.

Contents

1 Introduction **1**

1.1 Background 1
1.2 Overview 2
1.3 Fundamentals 4
1.4 Discrete Analytical Functions and Branching 6
1.5 Software Acknowledgments 8

2 Motifs **9**

2.1 Packings with Overlaps 10
2.2 Monotonicity and Existence of Triangles with Deep Overlaps 14
2.3 Admissibility 20
2.4 Existence and Uniqueness of Labels for Decorated Complexes 23

3 Coherence **27**

3.1 Chains and the Fundamental Group 28
3.2 Chain Developments and Layouts 30
3.3 Coherence 30

4 Discretization Issues **39**

4.1 A Measure of Incoherence 40
4.2 Methods 40
4.3 A Quadratic Polynomial 41
4.4 The Ahlfors Function 41
4.5 The Weierstrass Function 46

5 Generalized Branching **55**

6 Fractional Branching **58**

6.1 Fractional Branching on Three Vertices 60
6.2 Uniqueness of Fractional Branchings 63
6.3 Fractional Branching on Four Vertices 71

7 Shift-Branching **75**
7.1 Monotonicity in Shift-Points 78
7.2 Existence and Uniqueness of Motifs with Shift-Points 82
7.3 Modified Shift-Points 84

8 Experiments **90**
8.1 Methods 91
8.2 Experiments on a Quadratic Polynomial 93
8.3 The Ahlfors Function 95
8.3.1 Example 1: Annulus with Reflexive Symmetry 96
8.3.2 Example 2: A Non-Symmetric Annulus 99
8.3.3 Example 3: A Coarse Non-symmetric Annulus 99
8.4 The Weierstrass Function 104

Bibliography **109**

Vita **114**

List of Figures

1.1 Circle packings in $\mathbb{C}$, $\mathbb{D}$, and $\mathbb{P}$. 3
1.2 The Owl packing with three different set of edge assignments. 3
1.3 Hierarchy of circle packing structures in a tangency packing. 4
1.4 A branched flower. 7
1.5 Branched circle packings of the Owl. 7

2.1 Overlapping circles. 10
2.2 Deep overlapping circles. 11
2.3 Projection of overlapping circles from $\mathbb{H}$ to $\mathbb{C}$. 12
2.4 Sets of radii and edge assignments which cannot form triangles. 13
2.5 The auxiliary circle is used to describe the triangle. 18
2.6 Non-monotonicity of triangles when using inversive distance as a parameter. 20

3.1 Two different layouts of the same motif, $K(R_1, I, A_1)$. 27
3.2 Two homotopic face chains. 29
3.3 A locally coherent but globally incoherent motif. 33
3.4 Another locally coherent but globally incoherent annulus. 34
3.5 Turning angle of a non-simple polygon. 35
3.6 Chains passing through and around an incoherent sub-motif. 37

4.1 A discrete quadratic polynomial. 42
4.2 A coarse discrete polynomial. 42
4.3 Two different motifs and layouts of an annulus. 45
4.4 The Ahlfors Packing of the example from Figure 4.3. 45
4.5 The complex is modified with a Whitehead move. 47
4.6 Function elements layout the incoherent motif. 48
4.7 The torus "unwrapped". 48
4.8 The latticeΛ generated by the fundamental region Ω. 49
4.9 A lattice generated by a circle packing of a fundamental region. 51
4.10 The fundamental region of a symmetric 16 vertex torus. 52
4.11 The fundamental region of a symmetric 48 hex packed torus. 53
4.12 Breaking the symmetry of the symmetric 16 vertex torus. 54
4.13 Breaking the symmetry of the symmetric 48 hex packed torus. 54

5.1 A generalized branched point. 56
5.2 Laying out a generalized branched motif. 57

6.1 Complex of a fractured motif. 59
6.2 Three fractured points are needed. 61
6.3 The "frac-branch property" 62
6.4 Fractured branched circle packings in $\mathbb{C}$ and $\mathbb{D}$. 64
6.5 Detail of a simple fractured branched circle packing. 65
6.6 Fractured branched circle packing on $\mathbb{P}$. 66
6.7 Non-uniqueness of a quasi-coherent flower. 67
6.8 Error for different angle assignments on Example 6.6. 69
6.9 A fractured branched circle packing with an auxiliary motif and shepherd circles. . . 70
6.10 Creating a fractured branched packing over four vertices from one with three. 73
6.11 The fractional branching is transferred to another face. 74

7.1 The shift-circle. 75
7.2 A traditional branch point and shift-point. 76
7.3 Laying out a shift-point. 77
7.4 Placement of the jump-petal on a shift-circle 78
7.5 Increasing a petal on a shift-point. 80
7.6 Change of the shift-point petal angles 82
7.7 Realizing a shift-point as a generalized branch point. 83
7.8 How the phase angle changes the layout of a shift-point. 85
7.9 The choice of the lead-petal is arbitrary in a modified shift-point. 86
7.10 Incremental changes of the shift-ratio on a shift-point. 87
7.11 Various branched circle packings with shift-points. 88
7.12 More branched circle packings with shift-points. 89

8.1 A shift-point converted to a generalized branch point. 92
8.2 Quadratic polynomial adjusted with shift-point $\mathfrak{C}(x, \pi)$ using parameter x. 94
8.3 Quadratic polynomial adjusted with shift-point $\mathfrak{C}(x, 3\pi)$ using parameter x. 94
8.4 The generalized packing from Figure 8.3 adjusted with a separated flower. 95
8.5 An annulus with reflexive and translational symmetry. 96
8.6 Example 1: an annulus with reflexive symmetry. 97
8.7 A conversion applied to Example 1. 98
8.8 Details of the conversion of Example 1. 100
8.9 Example 2: an annulus with no combinatorial symmetry is created from Example 1. 101
8.10 Progressive adjustments of Example 2 using shift-points 102
8.11 Two views of the adjusted solution for Example 2 on $\mathbb{P}$. 103
8.12 The error for Example 2 with a single shift-point $\mathfrak{C}(x, \varphi)$. 103
8.13 The conversion used to adjust the edge assignments for Example 3. 105
8.14 Example 3 made coherent via adjusted edge assignments. 106

8.15 The torus used in Example 4. 106
8.16 Different views of E_K for Example 4 adjusted at a single shift-point 108

Chapter 1

Introduction

1.1 Background

Questions involving mutually tangent circles date back to the origins of mathematics and are among some of the most elegant of the classical theorems. The Circles of Apollonius, Descartes's kissing circles, Sangaku puzzles helped give birth to mathematics. Though the golden age of geometry rose and set with Hellenistic culture, geometry held a prominent place in mathematics deep into the nineteenth century. Modern mathematics saw an explosion of diversity with its efforts split between application in the natural world and deep generalizations. Geometry's use in the applied sciences had mostly been tapped, and so interest in the field fell as questions about connectedness and boundary replaced those of length and angle. Thus it is somewhat ironic that first Topology and then computational modeling has helped redirect mathematics to geometry.

Motivated in his search to solve the Poincaré Conjecture, Thurston employed hyperbolic geometry, a product of the nineteenth century, to classify 3-manifolds. Thurston's notes relate the topology of 3-manifolds to the surfaces they support. The Geometrization Conjecture which followed was the directing force of geometric topology for over three decades. Even after its proof by Perelman, albeit by methods foreign to Thurston's original insight, it continues to be a paragon of geometric methods.

Along the way Thurston independently proved what is now known as the Koebe-Andreev-Thurston Theorem (Theorem 1.3) as a crucial ingredient of his Geometrization program. This seminal theorem along with other ideas foundational to circle packing were included in the infamous Chapter 13 of his notes. However circle packing still did not garner much interest until a 1985 Purdue University conference [46] when Thurston suggested that circle packings could be used to approximate Riemann maps from the plane to the unit disc (this was later proved by Rodin and Sullivan [37]).

A burst of activity followed, and Circle packing has since gathered contributors from analysis, topology, combinatorics, and geometry. Taken collectively it has been noted that their work gives form to two distinct but not disparate veins. There are the analytic and combinatorial circle packers who were born from Thurston's talk. Connections to classical complex analysis exemplified through

developing discrete analogues has been their focus. The other vein is more geometric and topological in their aim. Finding inspiration in the pure aesthetics of the relationship between circles, their topology, and combinatorics. Of these two groups this thesis clearly falls in the former, however a fair amount of overlap will occur. For an excellent exposition of circle packing and its history, the interested reader should see [10].

Examples of circle packings are shown in Figure 1.1 using circle packing's unofficial mascot, Ken Stephenon's "Owl". The circles in the figure are placed so that they are externally tangent. If not stated otherwise, it is usually assumed that tangencies are fixed in this way. Indeed external tangencies have become the standard even though substantial work has been done using overlaps. The preference may be owing to the fact with overlaps similar results hold at a greater computational cost. Additionally, sans a computer, they are more difficult to draw. Yet packings with overlaps are very appealing and questions regarding them are still of much interest.

"Tangencies" can also be kept between non-intersecting circles. The distance being determined by a more general idea called inversive distance which includes both overlapping and separated circle packings, e.g., Figure 1.2. This idea was introduced by Philip Bowers and Stephenson as a generalization of the K-A-T theorem in [13]; what has been called the Bowers-Stephenson conjecture. They proposed that inversive circle packings of closed triangulations are (globally) rigid, i.e., radii for circle packings are determined up to Möbius transformation by their triangulations. Using a variational principle Ren Guo has recently shown local rigidity for inversive circle packings [24], and Luo has used this result to prove the Bowers-Stephenson conjecture in the positive for closed hyperbolic and Euclidean surfaces [32]. Even more recently Jiming Ma and Jean-Marc Schlenker claimed to have found a counterexample for the conjecture on the sphere [33].

1.2 Overview

Circle packings here are configurations of circles in one of the standard geometries $\mathbb{G} = \mathbb{P}$, $\mathbb{D}$, or $\mathbb{C}$. Traditionally, circles in a circle packing are placed according to an abstract simplicial 2-complex. A desired angle sum is associated with each interior vertex, and a set of radii, a *label*, is computed such that the sum of angles at each flower (see Figure 1.3) meets the target value. Typically it is also assumed that a circle will be placed such that it is externally tangent to all of its neighbors. Questions involving the computation of a label: Does there exist a label for this complex and targeted angles? Is it unique? Can the associated circles be consistently placed in a geometry $\mathbb{G}$?

When the complex is simply connected, all the above have been answered in the affirmative (see [44] for details). Together these qualities allow simply connected circle packings to be used as the foundation for a theory of discrete analytic functions. We follow a similar path with two additions.

First, in addendum to the target angles, radii are computed such that edges between circles have prescribed inversive distances which include deep overlaps. The collection of inversive distances for edges is called the *edge assignment*, denoted I; together with the angles A these two sets of assignments are called the complex's *decorations*. This raises issues about existence and monotonicity, and it also imposes local constraints which translate to global constraints. Conditions for a unique label to exist for target angles and edge values are investigated in Chapter 2.

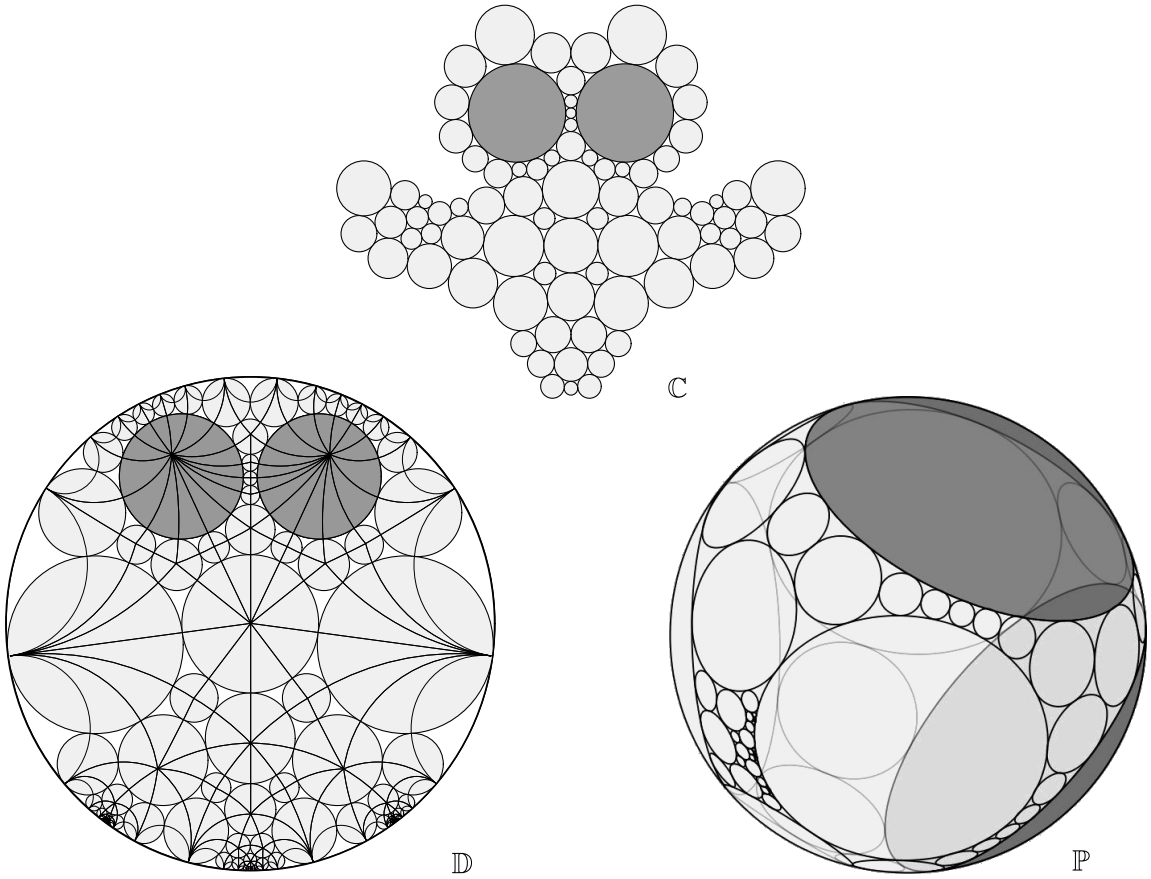


Figure 1.1: Circle packings in $\mathbb{C}$, $\mathbb{D}$, and $\mathbb{P}$. Each packing uses Stephenson's "Owl" complex.

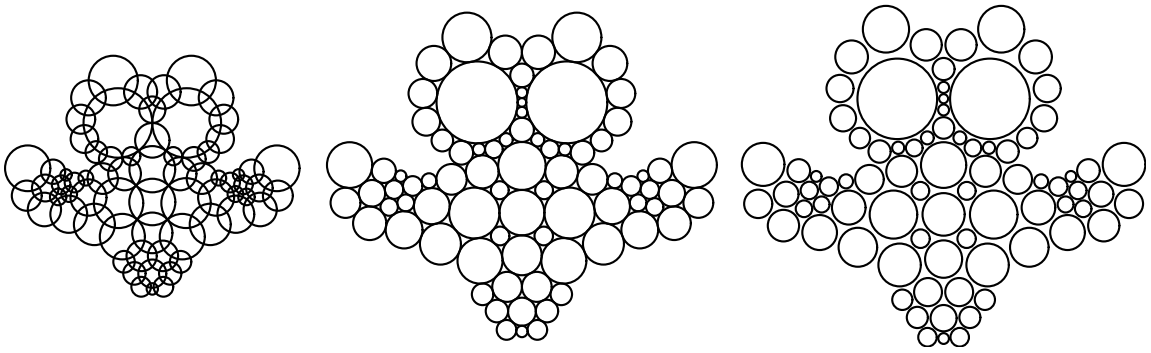


Figure 1.2: The Owl packing with three different set of edge assignments. These three packings have identical complexes and border radii, but have different edge assignments of 0, 1, and $3/2$ from left to right.

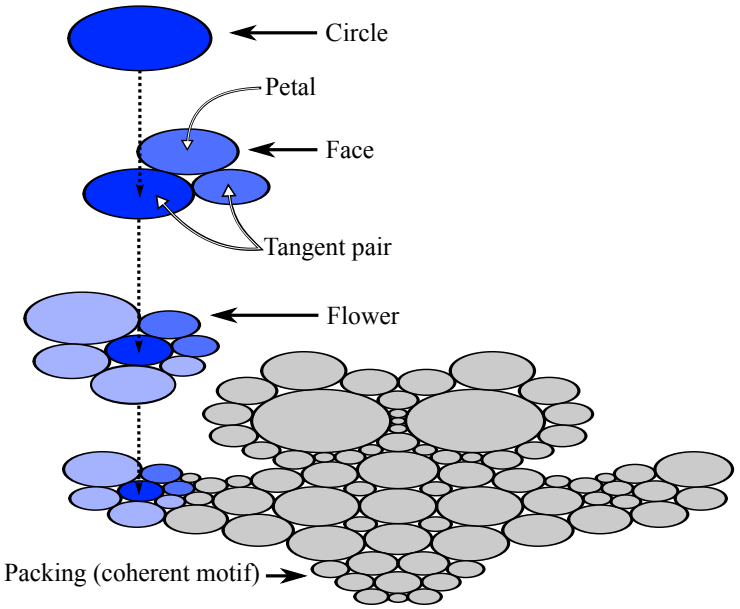


Figure 1.3: Hierarchy of circle packing structures in a tangency packing.

Second, non-simply connected complexes are a major focus. Because radii have been found meeting the prescriptions of a complex does not mean there is any consistent way to place the circles in a geometry, i.e., for the radii to be realized as a circle packing. For simply connected complexes, the radii form a circle packing when they do so locally. However this condition does not suffice for non-simply connected complexes. This is covered in Chapter 3.

A label meeting the assignments of its complex may be a circle packing, or it may be nothing more than an amorphous structure having no consistent layout. This is a *motif*. The inherent discreteness of circle packing precludes creating analogues of certain classical functions (as seen in Chapter 4). The use of motifs allow the description of structures which fail to be circle packings within localized areas, yet they are circle packings elsewhere. These areas of ambiguity, to be called *generalized branching* in Chapter 5, are like black holes where their interiors may be nonsense, but when traveling safely around the outside, everything else appears like a normal circle packing.

Types of generalized branching are introduced in Chapters 6 and 7. The shift-points from Chapter 7 allow for continuous parameterization while preserving rigidity. In Chapter 8 generalized branch points are used to manipulate inconsistent motifs into "circle packings" with confined sub-complexes of generalized branching.

1.3 Fundamentals

Definition 1.1. Following this topic's conventions (see [44]), the pattern of these circles will be encoded in an abstract simplicial 2-complex, shortened to *complex*, which is (simplicially equivalent to) a triangulation of an oriented topological surface. It is thus composed of vertices, edges, and

oriented faces. It will be assumed that every complex is face connected and finite. The notation K will be used to denote both a complex and its realization as a topological surface.

A complex is just an abstract combinatorial object. It is a set of instructions telling us how the circles for a structure (like the one shown in Figure 1.3) are suppose to be placed in a geometric setting. As such, complexes possess no geometric or metric information. This comes when actual circles are associated with the complex and placed according to its pattern.

The collection of faces in a complex at a common vertex v is called the *flower* with *nexus* v. The vertices neighboring this flower's nexus are its *petals*. We will use $\sim$ to denote when vertices are neighbors or when faces share edges. For example, $v_i \sim \{v_j, v_k\}$ means that the vertices v_j and v_k both neighbor the vertex v_i.

In general we will use possession to indicate when a structure is an element of another structure, e.g., v is the flower's nexus. The names of these structures will be applied to both the abstract complex and the circle configurations once they have been realized in a geometric setting (see Figure 1.3).

Given a complex K, denote its collection of vertices, edges, and faces with V, E, and F, respectively. Prefixes of "∂" and "int" will denote border and interior subsets of these collections, respectively, e.g., ∂V and int$V$. Border edges are defined as those composed strictly of border vertices; else they are called interior. Border faces are those composed of at least one border vertex, otherwise they are called interior.

Inversive distance is a number encoding a relationship between circles; invariant to geometry, this number specifies where a circle is to be placed relative to its neighbor. Details are provided in Section 2.1 for now we write D_{ij} for this distance. In $\mathbb{C}$ one might like to consider circles with infinite radii, bounding hyperplanes. Though easy to draw, the added complication of dealing with these special cases is cumbersome, and thus avoided here.

A label provides circles, a complex instructs which circles are neighbors, and the edge assignment provides the inversive distance between neighboring circles. Let $C(v_i)$ and $C(v_j)$ be two circles in a geometry with radii r_i and r_j given by a label R for two neighboring vertices $v_i \sim v_j$ in a complex K. If the circles of $C(v_i)$ and $C(v_j)$ have a specified inversive distance then we say that the two circles are *contiguous*. If a circle is placed (in a geometry) such that it is contiguous to each of its neighbors we say that it has been placed contiguously. Contiguousness is meant to be a generalization of tangency, which implies external tangencies.

Definition 1.2. A collection $P = \{C(v_i)\}$ of circles in $\mathbb{G}$ is said to be a *circle packing* for a complex K with edge assignment I if

1. P has one and only one circle $C(v_i)$ associated with each vertex v_i in K.
2. $C(v_i)$ and $C(v_j)$ are contiguous whenever $v_i \sim v_j$ in K.
3. Three circles $C(v_i)$, $C(v_j)$, $C(v_k)$ form a positively oriented triple in $\mathbb{G}$ whenever v_i, v_j, v_k form a positively oriented face of K.

A key result in circle packing is the already mentioned Koebe-Andreev-Thurston theorem:

Theorem 1.3. K-A-T. *Let K be a combinatorial sphere with edge assignment $I \equiv 1$. Then there exists an essentially unique circle packing P for K in $\mathbb{P}$.*

By essentially unique it is meant that a packing is unique up to Möbius transformations. For a proof see [44]. The existence and uniqueness of labels (with some assumptions on edge and angle assignments) is the subject of Chapter 2. Most of Chapter 2 deals with basic results for inversive packings with branch points, which have long been understood but have yet to appear in the literature. Small generalizations are also made which will find use in Chapters 6 and 8, and allow the concept to fit in nicely with the our overall theme. Along the way we hope to illuminate some of the potential of these types of packings, why they present unique difficulties, and hopefully allow some insight into further development.

1.4 Discrete Analytical Functions and Branching

Definition 1.4. A *discrete analytic function* is a map $f\colon Q \to P$ between circle packings that preserves edge assignments and orientation.

Discrete analytic functions relate circle packings to classical functions in two important ways: as analogues and approximations. Years of effort have shown that both can be done remarkably well. For a summary see [43, 44]. The list of analogues is long and ever growing.

The following quote best summarizes the behavior of the approximations. "*Classical analytic functions map infinitesimal circles to infinitesimal circles; discrete analytical functions map real circle to real circles* [44]." This was the basic intuition behind Thurston's conjecture. With a discrete analogue formulated for a class of functions, increasingly fine combinatorics converge to their classical counterpart, e.g., discrete polynomials converge to polynomials.

Combined these two connections allow circle packing to serve as a study of discrete analytic functions. However it is more than an analogy. The K-A-T theorem has been shown to actually imply the Riemann mapping theorem [26]. So circle packings can be seen to be fundamentally linked to classical analysis.

If limited to using only locally univalent packings, like the ones seen in Figure 1.1, our discrete analogues would be limited to locally univalent functions. Thus we need a version of branching.

Definition 1.5. A *branch point* of *order* $n \in \mathbb{Z}^+$ is an interior vertex v in a circle packing with an angle sum of $2\pi n$ (see Figures 1.4 and 1.5).

Modeling discrete analytical functions via circle packings was first extended to non-locally univalent packings by Tomasz Dubejko and Stephenson when they introduced branching using a similar definition [18, 19, 12, 21, 20]. Classically a branch point of a multi-valued function is a point of singularity wrapped with an arbitrarily small circuit. Branching is where key differences between the classical and discrete setting quickly manifest, and here it can be seen right away.

Circuits in motifs will necessarily be chains of the motif's discrete elements, i.e., vertices, edges, or faces. Furthermore traditional circle packings have no analogue for discontinuity. Later a sort of discontinuity will be inserted at "branch areas" using generalized branching, but this will be for special cases of an already rich library of discrete branched analogues. Additionally branching

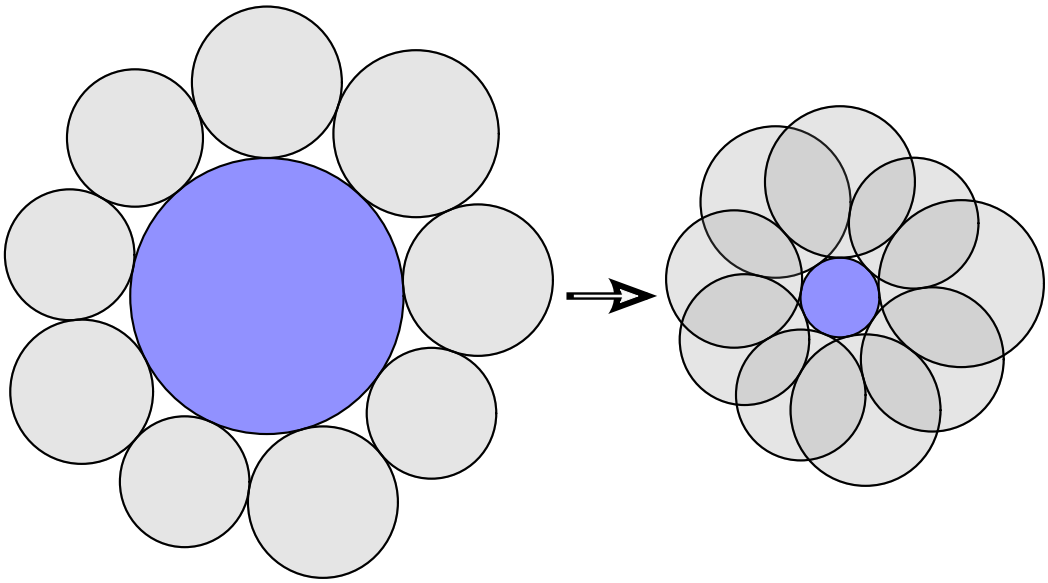


Figure 1.4: A branched flower.

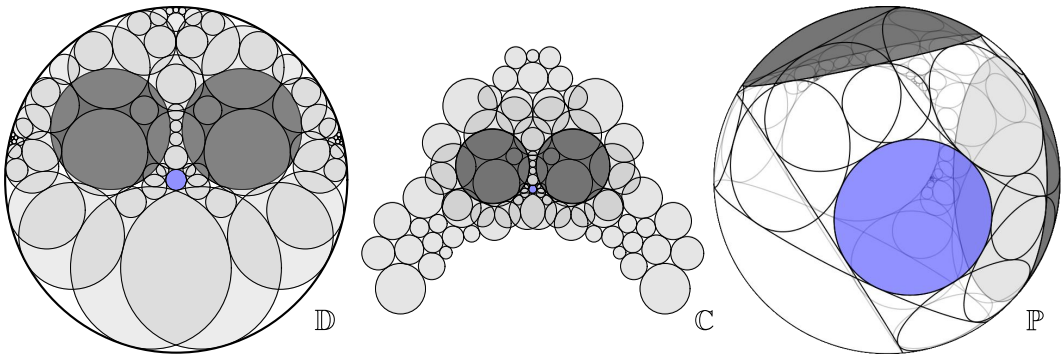


Figure 1.5: Branched circle packings of the Owl (from Figure 1.1). The branch point is colored in blue.

exposes compatibility issues with given angle assignment; a problem resulting from discreteness (see Definition 2.7).

Using circle packings one may consider the structures resulting from pasting together two-dimensional triangular faces as if they were pieces of cardboard. As long as the angle sums are fixed such structures are unique in $\mathbb{R}^3$ up to isomorphisms regardless of the angle sums' value [23]. Similar triangulations using circle patterns have been used to describe non-Euclidean surfaces, see [30]. However all angle assignments equaling integer multiples of 2π is a necessary condition for a circle packing to exist (see Chapter 2). Thus for our purposes avoiding a more general definition makes sense.

1.5 Software Acknowledgments

Computation of all labels and creation of all circle images were produced using the Java™program `CirclePack`. `CirclePack` is a free, open source software available under the GNU Public License; it is written, maintained, and copyrighted by Ken Stephenson. It requires only Java™1.6+, and can be run on any platform which supports Java. `CirclePack` can be downloaded from `http://www.math.utk.edu/~kens/CirclePack/downloads/`.

Special software extensions for computing and creating shift-points and fractional branchings in `CirclePack` were written by Stephenson and the author. These extensions are slated to be included in later versions of `CirclePack` but can also be made available upon request.

Many images seen throughout this work were modified using the free software `InkScape` and `GIMP`. This document was prepared in LaTeX with the aide of LyX. All these excellent programs are licensed under GNU public license, as is `CirclePack`. The equations in Chapter 2 and Figure 6.7 were produced using Maple™. Figures 6.8, 8.12, and 8.16 were created off-line with `MATLAB`™7.10 using data processed by `CirclePack`.

Chapter 2

Motifs

A pattern of circles with overlaps is a collection of circles where the distance between two vertices is made rigid by specifying an angle for which their corresponding circles must overlap. Angle of overlap is measured at the tangents where the overlapping circles intersect (see Figures 2.1 and 2.2). Thurston was apparently the first to consider such packings. He modeled convex polyhedron formed by sets of intersecting hyperplanes. These hyperplanes intersect the boundary as circles forming circles on the sphere with overlaps related to the polyhedron's dihedral angles. This then allowed Thurston to reproduce results by E. M. Andreev ([2, 3]) on 3-dimensional finite volume polyhedra.

Thurston's proof of the existence and uniqueness of these motifs turned out to be a rediscovery and generalization of a forgotten 1936 result of Paul Koebe's [31], what has come to be called the Koebe-Andreev-Thurston Theorem. The K-A-T theorem played a role in Thurston's classification of 3-manifolds for which he was awarded the Fields Medal in 1982.

In 1985 Thurston conjectured that circle packings could provide a computational method for approximating Riemann mappings [46]. This lecture, not the above mentioned results, kindled an interest in circle packings. Early developments using circle packings as discrete analytic functions included packings with overlaps, and using overlaps has been essential to some important results such as in the K-A-T theorem or Oded Schramm's square grid packing [40]. However the general practice has been to focus on external tangencies and treat overlaps as a special case.

This preference is probably due to the fact that overlaps are an added complication which often comes without benefit. Additionally there is the issue of aesthetics. Problems involving externally tangent circles sprinkle the history of mathematics all the way to its origins, e.g., Descartes, Sangaku problems, Apollonius etc. Externally tangent circles are easier to compute, draw, and arguably make better pictures.

Inversive distance is a generalization of the notion of overlapping circles. Inversive distances were introduced by H. S. M. Coxster as an inversion invariant means to relate non-intersecting circles[16]. Let r_a and r_b be the radii of two concentric circles which are the (circle) inversion images of two non-intersecting circles. Coxster defined the inversive distance (in the plane) as the natural logarithm of the ratio of r_a and r_b (larger over the smaller). It since has been extended for hyperbolic and spherical geometry and to include intersecting circles.

Ken Stephenson and Phil Bowers [44] applied inversive distance towards circle packings as a generalization of Koebe-Andreev-Thurston's overlapping circle packings. Allowing circle packings to include inversive distances greater than 1 (separated circles) or less than 0 (circles with deep overlaps) introduces complications about the existence and monotonicity of faces. Ren Guo [24] used a variational approach to show that packings with separated circles are locally rigid in $\mathbb{C}$ and $\mathbb{D}$, however convexity was lost when applied to the global case. Rivin extended the K-A-T theorem for packings which include deep overlaps by identifying an additional geometric constraint which avoids incompatibilities [36].

2.1 Packings with Overlaps

The inversive distance between two neighboring vertices in a complex, say v_i and v_j, will be denoted $\sigma_{ij} = \sigma(i,j)$. A collection of inversive distances will be assigned to each of a complex's edges. In collaboration with the target angles sums, these edge assignment will determine the radii of a packing's circles. The distances and the complex's tangency pattern will be used to locate circles in a geometry.

When two circles associated with a complex K are said to be *contiguous* it is to be assumed that their location agrees with their edge assignment. Contiguousness is used in place of tangency in order to emphasize that it is a generalization of external tangencies. For intersecting circles the relation between σ_{ij} and an overlapping angle φ_{ij} is $\cos(\varphi_{ij}) = \sigma_{ij}$ (see Figure 2.1 and 2.2). This is for both the Euclidean and hyperbolic cases, and can be verified using their respective Law of Cosines.

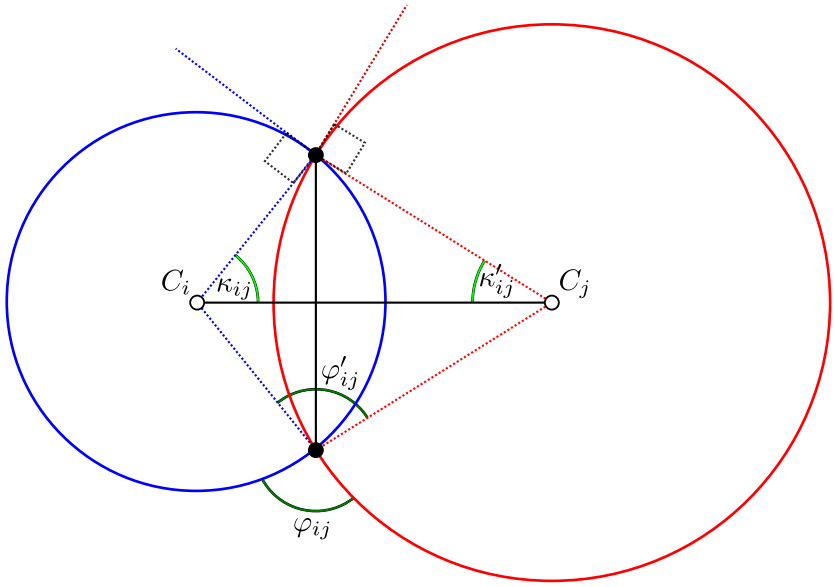


Figure 2.1: Overlapping circles. $\varphi_{ij} + \varphi'_{ij} = \pi$ for the edge $e(i,j)$.

Inversive distances are Möbius invariant; more specifically they are independent of geometry and constant under projections [11]. We will write $D_{\mathbb{G}}(v_x, v_y)$ for the distance in a geometry $\mathbb{G}$ between the circles for two vertices v_x and v_y, or just write D_{xy} when $\mathbb{G}$ is understood. In a triangle determined by circles, the length $D_{\mathbb{G}}(v_i, v_j)$ is determined as the side opposite the obtuse angle φ_{ij} in a triangle with one side from radii $R(v_i) = r_i$ and $R(v_j) = r_j$ (see Figure 2.1). So then by applying the appropriate Law of Cosines we can find the inversive distance in a given geometry. The inversive distance in $\mathbb{C}$ between vertices v_i and v_j is given by

$$\sigma_{ij} = \frac{D_{\mathbb{C}}(v_i, v_j)^2 - (r_i^2 + r_j^2)}{2r_i r_j}, \tag{2.1}$$

and in $\mathbb{D}$ the inversive distance is

$$\sigma_{ij} = \frac{\cosh D_{\mathbb{D}}(v_i, v_j) - \cosh r_i \cosh r_j}{\sinh r_i \sinh r_j} \tag{2.2}$$

where $D_{\mathbb{G}}(v_i, v_j)$ is the distance between the two vertices.

These two formulas are related by stereographic projection. Model hyperbolic two-space as the surface of a hemisphere in $\mathbb{H}^3$ intersecting $\mathbb{C}$ perpendicularly. Send circles and lines from $\mathbb{H}$ onto $\mathbb{C}$ by projecting from the point $(0, 0, -1)$, see Figure 2.3. If one or both of the circles are horocycles the inversive distance can be found using the projection on the plane (on the plane we assume all circles are finite).

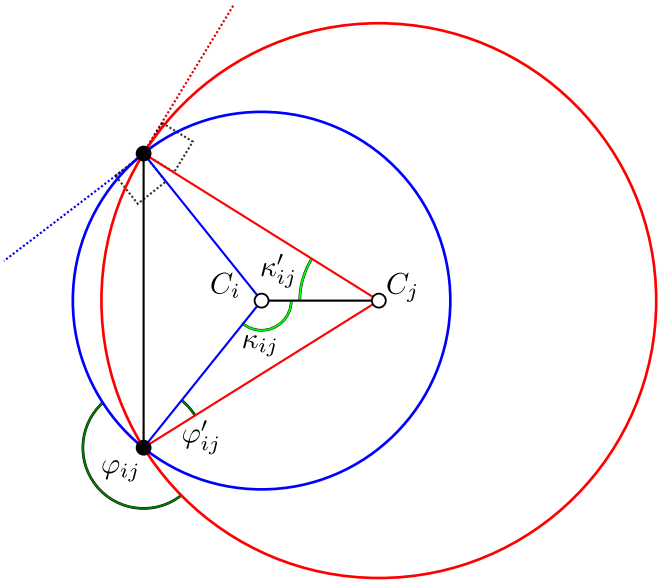


Figure 2.2: Deep overlapping circles.

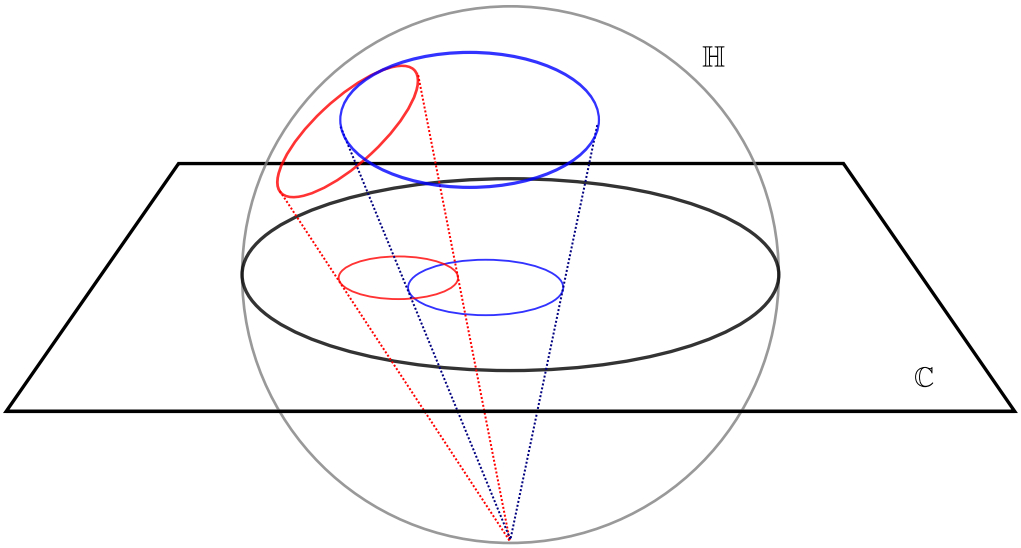


Figure 2.3: Projection of overlapping circles from $\mathbb{H}$ to $\mathbb{C}$.

Definition 2.1. An *angle (sum) assignment* is a collection of angles

$$A = \{A(v_1), \ldots, A(v_m) \,|\, A(v_i) \in (0, \infty)\},$$

one associated with each interior vertex v_j of K. An *edge assignment* is a collection of inversive distances

$$I = \{\sigma_{ij} \in [-1, \infty) \,|\, v_i \sim v_j \text{ and } \sigma_{ij} = \sigma_{ji}\},$$

one associated with each edge $v_i \sim v_j$ of K. Collectively the angle and edge assignments are called *decorations* for K. A *decorated complex* is a complex with attached decorations, denoted $K(I, A)$. A *label* R for K in $\mathbb{C}$, $\mathbb{D}$, or ,$\mathbb{P}$ is a set $R = \{r_1, r_2, \ldots\}$ of radii paired with vertices in K. Each radii is a real number $(0, \infty)$ when in $\mathbb{C}$, $(0, \infty]$ when in $\mathbb{D}$, and $(0, \pi]$ when in $\mathbb{P}$.

The most familiar type of packing is when every edge assignment is an external tangency, i.e., $I = 1$ for every edge in K or equivalently $I \equiv 1$. Call this special case a *tangency packing* (later a *tangency motif*). The radii of tangency packings are typically computed by assigning angle sums to a complex and applying the *Circle Packing Algorithm* [14]. The monotonicity of triangles with overlaps (shown below) will allow decorated complexes to be similarly computed. This broadens the type of packings under consideration, but it will be seen that it also places further limitations on which packings can be computed.

As one might imagine, attaching just any label to a complex does not produce a circle packing. For simply connected complexes the theory's elegance renders the classification of labels which are not circle packings somewhat pointless. However this work includes non-simply connected complexes that have a greater variety of decorations, and it will behoove us to make the distinction. Hence we introduce the definition *motif* below; A label meeting the criteria of a complex's decorations which has not been actually placed into a geometry.

Let K be a decorated complex. Assuming that the three edge assignments and radii for a face form a triangle then the angle at each center can be computed using the Law of Cosines appropriate for the radii's geometry and Equation 2.1 or 2.2. For the face $\{v_i, v_j, v_k\}$ and circles $\{C(v_i), C(v_j), C(v_k)\}$ call the angle at the center of $C(v_i)$ the *face angle* at v_i, denoted $\theta(r_i; r_j, r_k)$. The sum of all face angles at v_i is the *angle sum* at v_i, denoted $\theta(r_i)$. Because the curvature in each of the geometries is constant this angle is not dependent on the location of the circles, and can thus be measured without placing any actual circles.

Definition 2.2. Let R be a label such that $\theta(r_i) = A(v_i)$ for each interior vertex in a decorated complex $K(I, A)$. Then $K(R, I, A)$ is called a *motif*. A *sub-motif* is a motif $K'(R, I, A)$ on the sub-complex $K' \subset K$ with decorations and radii restricted to components of K'. A motif in $\mathbb{D}$ such that each border radius is ∞ is called a *maximal motif*.

Inversive distances can describe externally tangent, overlapping, and separated motifs. However it is common practice to only refer to inversive distances if the motif has separated circles. Here the term will generally refer to the edges of all motifs. The language will be kept as general as possible, but for existence reasons most of our results will require motifs to have no separated circles, i.e., $\sigma_{ij} \leq 1$ for all $\sigma \in I$.

The traditional restriction on overlaps is that the angle must be between 0 and $\frac{\pi}{2}$; corresponding to inversive distances in $[0, 1]$. Edge assignments in $[-1, 0)$ and in $(1, \infty)$ may give lengths that are not realizable as triangles (see Figure 2.4). For this reason we will (in general) use inversive distances from 0 to 1 (overlaps from 0 to $\frac{\pi}{2}$), and require additional special conditions for distances from -1 to 1 (see Lemma 2.3).

To extend discrete versions of analytical functions beyond locally univalent functions the idea of branching was introduced by Tomasz Dubejko and Stephenson [18]. A branch point is a flower with petals that circumnavigate the nexus more than once (see Definition 1.5). Given our geometries this necessarily means that a branch point can be realized in a circle packing if and only if its angle sum is an integral multiple of 2π there. While the typical existence and uniqueness results for overlapping locally univalent packings has been developed, to the best of our knowledge this is the

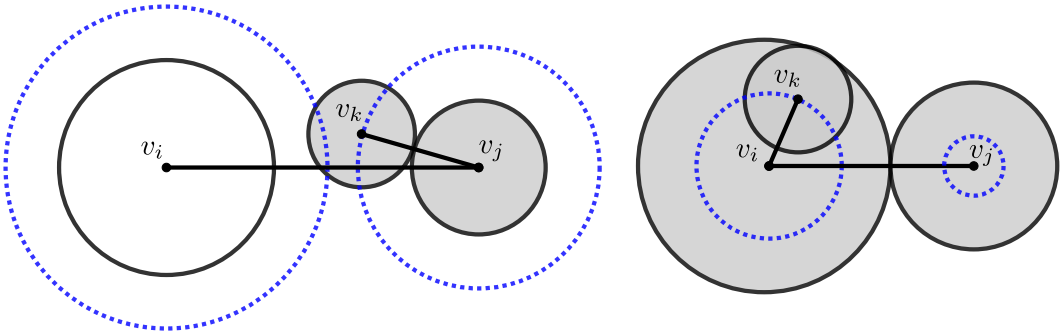


Figure 2.4: Sets of radii and edge assignments which cannot form triangles. On the left, $\sigma_{ij} > 1$ and $\sigma_{ik} = \sigma_{kj} = 1$. On the right, $\sigma_{ij} = 1$ and $\sigma_{ik} = \sigma_{jk} = -1$. For both set of circles, the dashed blue paths indicate possible locations for C_k. If the radii and edge assignments could be realized as a triangle then these blue paths would intersect.

first formal investigation of branched overlap packings. Although they are not found in the literature these results for branched motifs (such that $\sigma_{ij} \in [0,1]$) are understood to have been established. A special case allowing for deep overlaps is developed here.

2.2 Monotonicity and Existence of Triangles with Deep Overlaps

Packings are composed of faces. As such, key to building packings is first establishing the existence and monotonicity of these basic building blocks. For this section assume that $\{v_i, v_j, v_k\}$ is a face of K with edge assignments $I = \{\sigma_{ij}, \sigma_{ik}, \sigma_{jk}\}$ and label $R = \{R(v_i), R(v_j), R(v_k)\}$ in $\mathbb{C}$ or $\mathbb{D}$.

Lemma 2.3. (Existence) *For any label R there exists a triangle if one of the following sets of conditions is met.*

1. $\sigma_{ij}, \sigma_{ik}, \sigma_{jk} \in [0,1]$ *(overlaps are all between 0 and $\frac{\pi}{2}$).*
2. $\cos^{-1}(\sigma_{ij}) + \cos^{-1}(\sigma_{ik}) + \cos^{-1}(\sigma_{jk}) \leq \pi$.

Proof. The length D_{xy} is defined as the length of the edge opposite the obtuse angle φ'_{xy} in a triangle with sides formed by radii r_x and r_y see (Figure 2.1). From Equations 2.1 and 2.2 we get,

$$D_{xy} = \begin{cases} \text{for } \mathbb{C}, & D_{\mathbb{C}}(v_x, v_y) = \sqrt{r_x^2 + r_y^2 + 2\sigma_{xy} r_x r_y} \\ \text{for } \mathbb{D}, & D_{\mathbb{D}}(v_x, v_y) = \cosh^{-1}(\cosh(r_x)\cosh(r_y) + \sigma_{xy}\sinh(r_x)\sinh(r_y)) \end{cases} \tag{2.3}$$

Realization of a triangle can now be reduced to confirming the triangle inequality among the edge lengths.

Part 1. If $0 \leq \sigma_{xy} \leq 1$ then in $\mathbb{C}$ we have,

$$r_x + r_y \quad \geq \quad D_{xy} \geq \sqrt{r_x^2 + r_y^2} \geq \max\{r_x, r_y\}$$

and with finite radii in $\mathbb{D}$ we have,

$$r_x + r_y \geq D_{xy} \geq \cosh^{-1}(\cosh(r_x)\cosh(r_y)) \geq \max\{r_x, r_y\}$$

since $\cosh(x) \geq 1$.

Both cases imply that

$$\begin{aligned} D_{ij} + D_{ik} &\geq \max\{r_i, r_j\} + \max\{r_i, r_k\} \\ &\geq r_j + r_k \geq D_{jk}. \end{aligned}$$

Now we treat the case in $\mathbb{D}$ when one or more of the circles are horocycles. Equation 2.2 is only defined for finite radii ($D_{ij} < \infty$), but we can use the angle overlap $\varphi_{ij} = \cos(\sigma_{ij})$ in an explicit construction. First assume that there is at least one finite radius, say r_i. Place C_i at the origin of the disc and then place the horocycle C_j contiguous to C_i (according to its edge assignment σ_{ij}).

Now place the remaining circle C_k contiguous to C_i, and rotate this circle counter-clockwise around C_i (while preserving σ_{ik}). This rotation is centered at the origin and thus preserves the Euclidean radii of C_k in the projection map. So by the Euclidean part above, there must be a rotation such that $D_{jk} = \sigma_{jk}$ (Note this could have been done for finite radii in place of a direct computation).

Now suppose that all three circles are horocycles. Place any triple of Euclidean circles $\{C(\overline{r_i}), C(\overline{r_j}), C(\overline{r_k})\}$ in $\mathbb{C}$ according to the edge assignments. There is a circle $D(\overline{r_d})$ such that $C(\overline{r_i})$ and $C(\overline{r_j})$ are both internally tangent to D_d. By the Euclidean part above, $\overline{r_k}$ can be increased or decreased such that $C(r_k)$ is also internally tangent to $D(\overline{r_d})$. Scale all four circles so that $r_d = 1$ and then project to $\mathbb{D}$ making $D(\overline{r_d})$ the unit circle making the three scaled circles are the desired horocycles.

Part 2. First we show that the triangle inequality holds for the special case when $\sigma_{ij}, \sigma_{ik} = 1$ and $\sigma_{jk} \in [-1, 0)$.

In $\mathbb{C}$ this gives

$$\begin{aligned} D_{ij} + D_{jk} &= r_i + r_j + \sqrt{r_j^2 + r_k^2 + 2\sigma_{jk} r_j r_k} \\ &\geq r_i + r_j + \sqrt{(r_j + r_k)^2} \\ &= r_i + r_j + |r_j - r_k| \\ &\geq r_i + r_k = D_{ik}. \end{aligned}$$

The case for $\mathbb{D}$ can be shown using the Euclidean case as remarked above.

Now suppose that $\sum \cos^{-1}(\sigma) < \pi$. The supplementary angles in such an assignment will sum to less than 2π meaning that they can define an interstice with positive area. A circle can be placed externally tangent to the three circles, and a flower with the edge assignments can be built by part 1.

Now suppose that $\cos^{-1}(\sigma_{ij}) + \cos^{-1}(\sigma_{ik}) + \cos^{-1}(\sigma_{jk}) = \pi$. Then it can be shown that the three circles pass through a common point, say p, since

$$\pi - \varphi_{ij} + \pi - \varphi_{ik} + \pi - \varphi_{jk} = 2\pi.$$

Consider this point a circle of zero radius with center p. By part 1, placing p externally tangent to C_i, C_j, and C_k a flower with nexus p can be built such that the edge assignments (σ_{ij}, σ_{ik}, σ_{jk}) are met on the petal edges. □

Monotonicity for these faces is the next step. Parts 1 and 2 of Lemma 2.3 are two cases distinguished by the difference in how the length of edges change with respect to a radius. When the inversive distance between two circles is 0 or greater this change is positive, but this is not necessarily the case if it is less than 0.

Lemma 2.4. (Monotonicity) *Let I satisfies the conditions of Lemma 2.3. Then for any label R the following hold:*

1. *The face angle $\theta(r_i; r_j, r_k)$ is a decreasing continuous function with respect to r_i, and*

$$\lim_{r_i \to 0^+} \theta(r_i; r_j, r_k) = \pi - \cos^{-1}(\sigma_{jk}).$$

2. *The face angles $\theta(r_j; r_i, r_k)$ and $\theta(r_k; r_i, r_j)$ are increasing continuous functions with respect to r_i, and*

$$\lim_{r_i \to 0^+} \theta(r_j; r_i, r_k) = \begin{cases} \cos^{-1}\left(\frac{r_j + \sigma_{jk} r_k}{\sqrt{r_j^2 + r_k^2 + 2\sigma_{jk} r_j^2 r_k^2}}\right) & \text{in } \mathbb{C} \\ \cos^{-1}\left(\frac{-\cosh(r_j) + \sigma_{jk} \cosh(r_k) \sinh(r_j) \sinh(r_k) + \cosh(r_j)^2 \cosh(r_k)}{\sinh(r_j)\sqrt{(\sigma_{jk} \sinh(r_j) \sinh(r_k) + \cosh(r_j) \cosh(r_k))^2 - 1}}\right) & \text{in } \mathbb{D}. \end{cases}$$

If each edge assignment is in $[0, 1]$ then parts 1 and 2 are strictly decreasing and increasing, respectively.

Proof. Continuity follows from using Equations 2.3 in the Euclidean or hyperbolic Law of Cosines. It is then not difficult to obtain the limits. Suppose two circles C_x and C_y have an edge assignment $\sigma_{xy} \in (0, 1)$ then there exists a point $p_{xy} = C_x \cap C_y$. Call $\kappa_{xy} = \angle C_x C_y p_{xy}$ the *kite angle*, i.e., the angle formed by the overlap (see Figure 2.1 and 2.2). There will actually be two such points, but because of symmetry the resulting triangles will be similar.

Using the appropriate Law of Cosines we find the kite angle and its derivative with respect to r_x and r_y. For the Euclidean angles let $E(\sigma_{xy}) = r_x^2 + r_y^2 + 2\sigma_{xy} r_x r_y$.

$$\kappa_{xy} = \cos^{-1}\left(\frac{r_x + \sigma_{xy} r_y}{\sqrt{E(\sigma_{xy})}}\right)$$

$$\frac{d}{dr_x}\kappa_{xy} = \frac{-r_y\sqrt{1 - \sigma_{xy}^2}}{E(\sigma_{xy})} < 0 \tag{2.4}$$

$$\frac{d}{dr_y}\kappa_{xy} = \frac{r_y(1 - \sigma_{xy}^2)}{E(\sigma_{xy})^{3/2}\sqrt{(1 - \sigma_{xy}^2)E(\sigma_{xy})^{-1}}} > 0 \tag{2.5}$$

It only needs to be verified that $E(\sigma_{xy}) > 0$. For this, note that $E(-1) = (r_x - r_y)^2 \geq 0$ and that $\frac{d}{d\sigma_{xy}} E > 0$.

For the hyperbolic angles let, $H(\sigma_{xy}) = \sigma_{xy} \sinh(r_x) \sinh(r_y) + \cosh(r_x) \cosh(r_y)$, we have

$$\kappa_{xy} = \cos^{-1}\left(\frac{-\cosh(r_y) + \cosh(r_x)\sigma_{xy} \sinh(r_x) \sinh(r_y) + \cosh(r_x)^2 \cosh(r_y)}{\sinh(r_x)\sqrt{H(\sigma_{xy})^2 - 1}}\right) \tag{2.6}$$

$$\frac{d}{dr_x}\kappa_{xy} = \frac{-\sinh(r_y) H(\sigma_{xy})(1 - \sigma_{xy}^2)}{(H(\sigma_{xy}) - 1)^{3/2}(H(\sigma_{xy}) + 1)^{3/2}\sqrt{\frac{1 - \sigma_{xy}^2}{(H(\sigma_{xy}) - 1)(H(\sigma_{xy} + 1)}}} \tag{2.7}$$

$$\frac{d}{dr_y}\kappa_{xy} = \frac{\sinh(r_x)(1-\sigma_{xy}^2)}{(H(\sigma_{xy})-1)^{3/2}(H(\sigma_{xy})+1)^{3/2}\sqrt{\frac{1-\sigma_{xy}^2}{(H(\sigma_{xy})-1)(H(\sigma_{xy}+1)}}} \tag{2.8}$$

in $\mathbb{D}$. $H(-1)-1 = \cosh(r_x - r_y) - 1 \geq 0$ and $\frac{d}{d\sigma_{xy}}H = \sinh(r_x)\sinh(r_y) > 0$ together imply that $\frac{d}{dr_x}\kappa_{xy} < 0$ and $\frac{d}{dr_y}\kappa_{xy} > 0$ as well. If C_y is a horocycle then the kite angle is the limit of Equation 2.6 as $r_y \to \infty$,

$$\kappa_{xy} = \cos^{-1}\left(\frac{\sigma_{xy}\cosh(r_x)+\sinh(r_x)}{\sigma_{xy}\sinh(r_x)+\cosh(r_x)}\right), \text{ and}$$

$$\frac{d}{dr_x}\kappa_{xy} = -\sqrt{1-\left(\frac{\sigma_{xy}\cosh(r_x)+\sinh(r_x)}{\sigma_{xy}\sinh(r_x)+\cosh(r_x)}\right)^2} < 0. \tag{2.9}$$

Like all angles at the boundary the opposite kite angle will be 0 when C_y is a horocycle. So the kite angle is a decreasing function of r_x.

When $\cos^{-1}(\sigma_{ij}) + \cos^{-1}(\sigma_{ik}) + \cos^{-1}(\sigma_{jk}) = \pi$ all three circles meet at a common point of intersection. Referring to Figure 2.1 it can be seen that this happens because $3\pi - \sum\cos^{-1}(\sigma) = 2\pi$. Choose the points of intersection such that $p_{ij} = p_{ik} = p_{jk}$. The monotonicity of the kite angles then proves the lemma when $\sum\cos^{-1}(\sigma) = \pi$ since then $\theta(r_i; r_j, r_k) = \kappa_{ij}+\kappa_{ik}$ and $\theta(r_j; r_i, r_k) = \kappa_{ji}+\kappa_{jk}$.

It is left to extend this argument for edge assignments such that $\sum\cos^{-1}(\sigma) < \pi$. In this case the points of intersection are not identical, but they can be chosen such that they form an interstice. Let the auxiliary circle C_ℓ be defined by the vertices of this interstice. C_ℓ lies over the interstice passing through p_{ij}, p_{ik}, and p_{jk}. This creates an auxiliary flower composed of three faces; use C_ℓ's placement to provide edge assignments. So $\sum\cos^{-1}(\sigma) = \pi$ for each of the flowers faces. Referring to Figure 2.5, the first part of this lemma implies that increasing r_i decreases the auxiliary angle at v_i (in the auxiliary flower) and increases the auxiliary angles at v_j and v_k. It also increases the angle sum of the flower at v_ℓ.

The auxiliary flower must have an angle sum of 2π to represent our original triangle, but this angle sum has been increased to some value over 2π. Again applying the monotonicity shown above, increasing r_ℓ will decrease its angle sum while further increasing the angles at v_j and v_k. However this also increases the angle at v_i. In the Euclidean case the angles at v_i, v_j, and v_k must sum to π. The fact that the increase of r_i and r_ℓ both increase the angles at v_j and v_k imply that the total effect must sum to a decrease in the angle at v_i.

For the hyperbolic case move the flower via a Möbius map so that C_i is centered at the origin (if no radius is finite then the angle cannot change). Increasing r_i increases $\theta(r_\ell) > 2\pi$. Just as above, r_ℓ must be increased which cannot decrease the angles at v_j and v_k (either angle will increase if their circles are not horocycles), but this also increases the angle at v_i. The distances D_{ij} and D_{ik} have not changed due to r_ℓ so neither have the Euclidean radii of r_j and r_k. By the Euclidean part above, the Euclidean angle at v_i increases, and thus the hyperbolic angle at v_i does as well.

The second part of this lemma has been shown before most famously by Thurston in the infamous Chapter 13 of the *Notes* [45]. A somewhat more direct albeit less elegant proof is provided here for

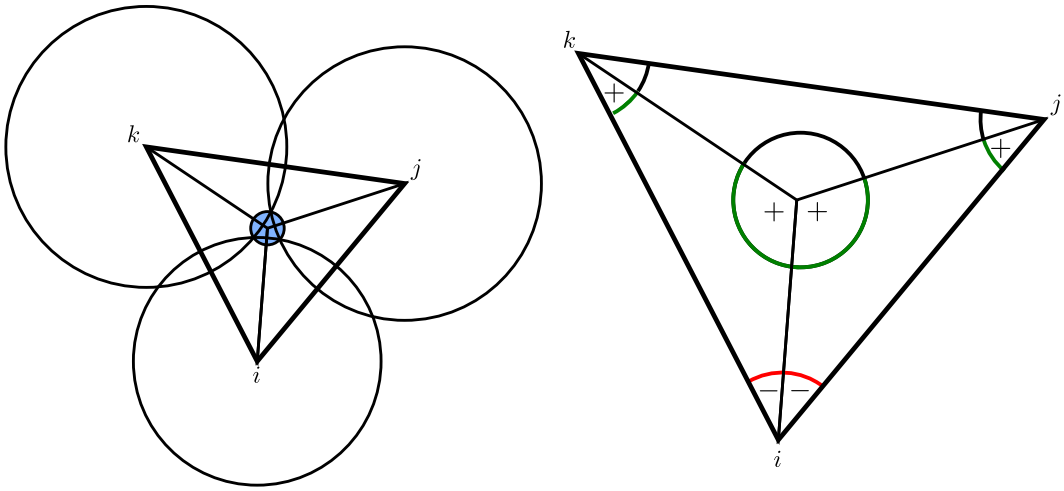


Figure 2.5: The auxiliary circle is used to describe the triangle. The auxiliary circle C_ℓ is colored blue on the left. The picture on the right illustrates how the angles change if the circle at i is increased.

completeness. The change in edge length is a key difference in this case. In $\mathbb{C}$,

$$\begin{aligned}
&\tfrac{d}{dr_i}\theta(r_i;r_j,r_k)\\
&\qquad = -\frac{\begin{array}{c} r_i^3(r_j^2(1-\sigma_{ij}^2)+2r_kr_j(\sigma_{jk}+\sigma_{ik})+r_k^2(1-\sigma_{ik}^2))\\ +3r_jr_kr_i^2(r_j(\sigma_{ik}+\sigma_{jk}\sigma_{ij})+r_k(\sigma_{ij}+\sigma_{jk}\sigma_{ik}))\\ +r_j^2r_k^2(r_j(\sigma_{ij}+\sigma_{jk}\sigma_{ik})+r_k(\sigma_{ik}+\sigma_{ij}\sigma_{jk}))\\ +r_ir_jr_k(r_j^2(\sigma_{jk}+\sigma_{ij}\sigma_{ik})+r_jr_k(2+4\sigma_{ij}\sigma_{jk}\sigma_{ik}+\sigma_{ij}^2+\sigma_{ik}^2)+r_k^2(\sigma_{jk}+\sigma_{ij}\sigma_{ik})) \end{array}}{E(\sigma_{ij})E(\sigma_{ik})\left(\begin{array}{c} r_i^2(r_j^2(1-\sigma_{ij}^2)+r_k^2(1-\sigma_{ik}^2)+2r_jr_k(\sigma_{jk}+\sigma_{ik}\sigma_{ij}))\\ +2r_ir_jr_k(r_j(\sigma_{ik}+\sigma_{ij}\sigma_{jk})+r_k(\sigma_{ij}+\sigma_{ik}\sigma_{jk}))\\ +r_j^2r_k^2(1-\sigma_{jk}^2)\end{array}\right)^{1/2}},
\end{aligned} \tag{2.10}$$

and

$$\begin{aligned}
&\tfrac{d}{dr_i}\theta(r_j;r_i,r_k)\\
&\qquad = \frac{(r_ir_j^2-\sigma_{ij}r_ir_j^2)+\sigma_{ik}r_j^2r_k+\sigma_{ij}\sigma_{ik}r_ir_jr_k+\sigma_{jk}r_ir_jr_k+\sigma_{ij}\sigma_{jk}r_j^2r_k}{E(\sigma_{ij})\left(\begin{array}{l} (r_i^2r_j^2-r_i^2r_j^2\sigma_{ij}^2)+(r_i^2r_k^2-r_i^2r_k^2\sigma_{ik}^2)+(r_j^2r_k^2-r_j^2r_k^2\sigma_{jk}^2)\\ +2r_ir_jr_k^2\sigma_{ij}+2r_i^2r_jr_k\sigma_{jk}+2r_ir_j^2r_k\sigma_{ik}\\ +2r_i^2r_jr_k\sigma_{ij}\sigma_{ik}+2r_ir_j^2r_k\sigma_{ij}\sigma_{jk}+2r_ir_jr_k^2\sigma_{ij}\sigma_{jk}\end{array}\right)^{1/2}}.
\end{aligned} \tag{2.11}$$

Which we can see is negative and positive, respectively, when σ_{ij}, σ_{ik}, and $\sigma_{jk} \in [0,1]$.

Use $\overline{C_x}$ to denote the hyperbolic circle C_x in $\mathbb{C}$. Map the triangle via Möbius transformation so that C_i is centered at the origin.

$$\frac{d}{dr_x}D_{xy} = \frac{\sigma_{xy}\cosh(r_x)\sinh(r_y)+\sinh(r_x)\cosh(r_y)}{\sqrt{H(\sigma_{xy})^2-1}} \geq 0$$

and real when $\sigma_{xy} \geq 0$. So increasing C_i will not only increase $\overline{C_i}$, but will also move C_j and C_k towards the boundary. If one or both are horocycles they will already be on the boundary, but

their Euclidean radius must decrease as C_i is at the origin and increasing. The fact that $\overline{C_j}$ and $\overline{C_k}$ decrease while $\overline{C_i}$ increases imply by Equations 2.10 and 2.11 that the Euclidean angle $\overline{\theta(r_i)}$ decreases; thus the hyperbolic angle $\theta(r_i)$ decreases since C_i is at the origin. A similar argument can be made to show that $\theta(r_j; r_i, r_k)$ decreases with respect to r_i in $\mathbb{D}$. □

Lemma 2.5. *Suppose a triangle exists with label R and edge assignments $I = \{\sigma_{ij}, \sigma_{ik}, \sigma_{jk}\}$. If $\{\sigma_{ij}, \sigma_{ik}, \sigma_{jk} \pm \epsilon\}$ meets the conditions for Lemma 2.3 for some $\epsilon > 0$ then*

$$\frac{d}{d\sigma_{jk}}\theta(r_i; r_j, r_k) > 0.$$

Proof. From Equation 2.3 we find that for $\sigma_{xy} \geq -1$.

$$\frac{d}{d\sigma_{xy}}D_{xy} = \frac{r_x r_y}{\sqrt{r_x^2 + r_y^2 + 2\sigma_{xy} r_x r_y}} > 0$$

since $r_x^2 + r_y^2 \geq 2r_x r_y$. For the hyperbolic case ($H(\sigma_{xy})$ is as defined in Lemma 2.4),

$$\frac{d}{d\sigma_{xy}}D_{xy} = \frac{\sinh(r_x)\sinh(r_y)}{\sqrt{H(\sigma_{xy})^2 - 1}} > 0.$$

Now by the Euclidean Law of Cosines

$$\frac{d}{dD_{jk}}\cos^{-1}\left(\frac{D_{ij}^2 + D_{ik}^2 - D_{jk}^2}{2D_{ij}D_{ik}}\right) = \frac{2D_{jk}}{D_{ij}D_{ik}\sqrt{4 - \frac{(D_{ij}^2 + D_{ik}^2 - D_{jk}^2)^2}{D_{ij}^2 D_{ik}^2}}} > 0,$$

and the hyperbolic Law of Cosines

$$\begin{aligned}&\frac{d}{dD_{jk}}\cos^{-1}\left(\frac{\cosh(D_{ij})\cosh(D_{ik}) - \cosh(D_{jk})}{\sinh(D_{ij})\sinh(D_{ik})}\right)\\ =&\frac{\sinh(D_{jk})}{\sinh(D_{ij})\sinh(D_{ik})\sqrt{1 - \left(\frac{\cosh(D_{ij})\cosh(D_{ik}) - \cosh(D_{jk})}{\sinh(D_{ij})\sinh(D_{ik})}\right)^2}} > 0.\end{aligned}$$

The values in both radicals above are positive because of the assumption that the triangle inequality holds. □

Lemma 2.5 means that as a parameter, inversive distance on the petal edges can monotonically increase the angle sum of a flower. However unlike the circle radii, the effects on the other triangle angles are not consistent. Figure 2.6 shows how increasing an edge length can cause adjacent angles to either increase or decrease depending on edge length. Using edge assignments as a parameter thus comes at the cost of monotonicity, an important characteristic for showing existence, uniqueness, and other results.

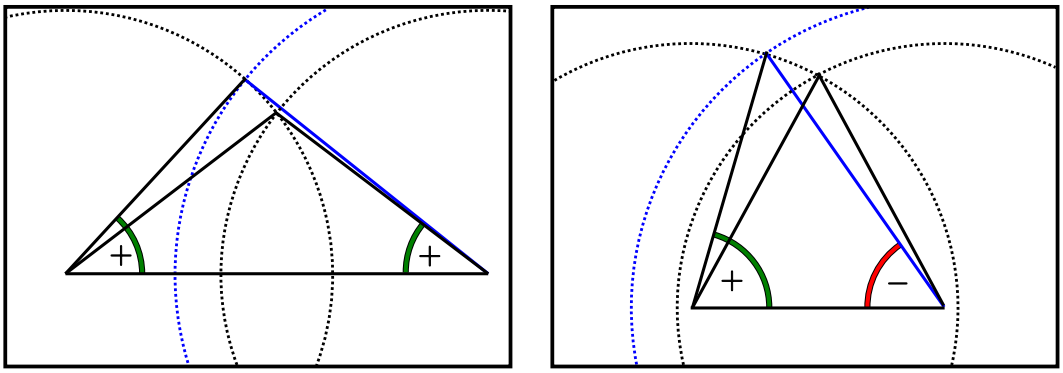


Figure 2.6: Non-monotonicity of triangles when using inversive distance as a parameter. The blue edge indicates where the inversive distance has been increased. In both case the angle across from the increasing edge changes positively, however the adjacent angle changes positively on the left and negatively on the right.

2.3 Admissibility

Transferring ideas and concepts from the continuous setting to the discrete has a discretization effect, a consequence in difference of behavior. Branching significantly elevates the discretization effect, and as such will be an important concept in this thesis.

The introduction of *admissibility* outlines how discretization limits conditions for existence locally. What is not immediately clear is that it also encapsulates global conditions. Try to construct, for example, a coherent simply connected motif with only two finite border circles, or a branched motif with only three border circles. Like a bike chain without enough links, it is easy to see how the border chain is limited by the lack of flexibility. This is a combinatorial restriction born by the boundary. Below is how this restriction is stated in [44] for tangency packings.

Definition 2.6. Given a combinatorial closed or open disc K with a set of interior vertices $\beta(K) = \{v_1, v_2, ...\}$ including possible repetitions, K is said to be a *branch structure* for $\beta(K)$ if the following condition holds: for each simple, closed, positively oriented edge-path $\gamma = \{e_{(1,2)}, e_{(2,3)}, ..., e_{(k-1,k)}\}$ in K the inequality $|\gamma| > (2N+2)$ holds, where N is the number of points of $\beta(K)$ inside γ, counting repetitions.

Call $\beta(K)$ the *branch set* and $|\beta(K)|$ the *branch order*; note that $\beta(K)$ can be empty. This definition was an important step in the original studies of branched packings. It was independently formulated by Dubejko and Bowers who both showed that it is a necessary and sufficient condition for the existence of externally tangent circle packings with interior angle sums of $\theta(v_i) = 2\pi + 2\pi n_i$ where n_i is the number of times v_i occurs in $\beta(K)$, i.e., a branched circle packing of degree $|\beta(K)|$ [18, 9].

The inclusion of edge assignments as a decoration augments the restrictions described by Definition 2.6. A tangency n-flower (edge assignments all 1) must have at least n petals if its face angles are to sum to $2\pi(n-1)$. The face angles are bounded by π so obtainable angles are restrained by combinatorics. For example, If you were to set edge assignments to $\frac{1}{2}\pi$ on the border

edges of the same flower, you would bound every face angle by $\frac{1}{2}\pi$, and so the minimum number of faces you would need goes up by a factor of two. These are local restrictions, but there are also global restrictions.

Imagine we have a circle packing with three border circles, as one might have from the projection of a sphere packing with a punctured face. Restricting circles to finite radii, it is easy to see that this packing could not do with any fewer border circles. Now assign an angle sum of 4π to any interior vertex. We will only have a circle packing if the border circles can circumnavigate the complex twice, however this is not possible with just three border circles (this will be justified in Chapter 3). Even though the complex is locally compatible with its curvature assignment, it fails to be compatible globally. How local and global properties interact is a recurring theme in circle packing and will be a major theme in this thesis. Global properties are investigated in Chapters 3 and 4, but first sufficient conditions for a label to exist on a decorated complex are established.

Since I is injectively paired with E the three edges in a face $f \in F$ each have an associated edge assignment $\sigma_{ij} \in I$. Identify the assignment for this face's edge $h = 1, 2, 3$ with $f(\sigma_h)$.

Definition 2.7. A decorated complex $K(I, A)$ in $\mathbb{C}$ or $\mathbb{D}$ is *admissible* if it has the following properties:

1. $\sigma_{ij} \in [-1, 1]$ for each $\sigma_{ij} \in I$.
2. For every face $f \in F$ either $\sum_{j=1\ldots3} \cos^{-1}(f(\sigma_j)) \leq \pi$ or $f(\sigma_j) \geq 0$ for $j = 1, 2, 3$.
3. For any simply connected sub-complex $K' \subseteq K$ with edges, faces, and vertices E, F, V we have
$$\sum_{v \in \text{int}V} A(v) < \pi\,|F| - \sum_{f \in F} \sum_{j=1\ldots3} \cos^{-1}(f(\sigma_j)) \leq \pi\,|F|\,.$$
Furthermore, $\pi\,|\text{int}F| < \sum_{v \in \text{int}V} A(v)$ in $\mathbb{C}$ where int$F$ is the set of strictly interior faces.

In the next section it will be shown that admissibility implies a label exists such that the criteria of the decorated complex are satisfied. To be clear, there are decorated complexes that fail to meet parts 1 or 2 of Definition 2.7, yet still have labels. Examples for separated and deeply overlapping motifs abound. One might toss a collection of circles randomly onto a $\mathbb{G}$ and make assignments retroactively based on how the circles happen to have fallen. However allowing for unrestrained edge assignments creates an equally wild label space. Consider a complex where each edge assignment is -1. If all radii are identical then the circles can be placed in $\mathbb{C}$ so they satisfy their edge assignments. Change one of these radii infinitesimally and this is no longer the case. Thus admissibility does not characterize all labels which exist for decorated complexes; rather it restricts our investigation to cases better suited for our applications.

Theorem 2.8. *Let $K(I, A)$ be simply connected with $I \equiv 1$ and $A(v)$ an integral multiple of 2π for every interior vertex v. Then $K(I, A)$ is a branch structure if and only if it is admissible.*

Proof. K is simply connected so any simple closed edge path is the border of a simply connected sub-complex. Hence it suffices to show the result for a closed disc K. First, two quick equalities. $\sum A(v) = 2\pi(\text{int}V + n)$ for some $n \in \mathbb{Z}^+$ such that $n \leq N$ by assumption. Secondly, there are 3

edges per face. Excluding the border edges, this double counts the number of edges. Noting that $\partial V = \partial E$ this gives,

$$E = \frac{1}{2}(3F - \partial V) + \partial V = \frac{3}{2}F + \frac{1}{2}\partial V.$$

Together with the Euler characteristic, $\lambda(K) = 1$, this implies that

$$\begin{aligned} V - \frac{3}{2}F - \frac{1}{2}\partial V + F &= 1 \\ \Rightarrow 2\text{int}V + \partial V - 2 &= F. \end{aligned} \tag{2.12}$$

Suppose that K is a branch structure. $N < \frac{\partial V - 2}{2}$ implies that,

$$\begin{aligned} \sum A(v) = 2\pi(\text{int}V + N) &< 2\pi\text{int}V + 2\pi\left(\frac{\partial V - 2}{2}\right) \\ &< \pi(2\text{int}V + \partial V - 2) \\ &< \pi F. \end{aligned}$$

It is left to show that $|\text{int}F|\,\pi < \sum_{v_i \in \text{int}V} A(v_i)$ in $\mathbb{C}$. Each $f \in \partial F$ has at most one border edge, but each $v \in \partial V$ is in one or more faces so $\partial F \geq \partial V$. Together with the assumption $N \geq 1$ and Equation 2.12 this implies,

$$\begin{aligned} \text{int}F + \partial F &= 2\text{int}V + \partial V - 2 \\ \text{int}F + 2 &\leq 2\text{int}V. \end{aligned}$$

Because each Euclidean face must have angles summing to π this gives,

$$\Rightarrow \pi\text{int}F < 2\pi\text{int}V + 2\pi N = \sum A(v).$$

So K is admissible.

Conversely, suppose that K is admissible. $\sum A(v) = 2\pi(\text{int}V + N) < \pi F$ implies that,

$$\begin{aligned} 2\text{int}V + 2N &< F \\ \Rightarrow 2 + 2N &< F - 2\text{int}V + 2 \\ &< (2\text{int}V + \partial V - 2) - 2\text{int}V + 2 \\ &< \partial V. \end{aligned}$$

□

Definition 2.7 allows for broader assumptions about a complex's edge and angle assignments, and so is a generalization of branch structure. The machinery and setting have been put into place. Now we can begin showing that a set of unique radii can be found meeting the requirements of a decorated complex. So a motif can actually exist.

2.4 Existence and Uniqueness of Labels for Decorated Complexes

In this section we will be assuming that all complexes have at least one boundary vertex and are admissible with their respective decorations. We use ∂K to denote the set of boundary vertices of K, and $\lambda(K)$ for the Euler number. For the following statements recall that radii are assumed to be finite in $\mathbb{C}$.

Lemma 2.9. *Let $K(I, A)$ be an admissible flower with nexus v_0 and petals of fixed radii $\{R(v_1), R(v_2), \ldots, R(v_n)\}$. There exists a unique nexus radius r_0 such that $\theta(r_0) = A(v_0)$.*

Proof. By Lemma 2.4,

$$\lim_{r_0 \to 0^+} \theta(r_0) = |F|\,\pi - \sum_{F_i \in F} \sum_{j=1..3} \cos^{-1}(F_i(\sigma_j)) \text{ and } 0 = \lim_{r_0 \to \infty} \theta(r_0).$$

Because $K\,(I, A)$ is admissible

$$\lim_{r_0 \to \infty} \theta(r_0) < A(v_0) < \lim_{r_0 \to 0^+} \theta(r_0).$$

Monotonicity then guarantees that there exists an r_0 such that $\theta(r_0) = A(v_0)$, and that it is unique. □

Definition 2.10. Given a label R, define a **relaxation operator** $\mathfrak{R}$ as a function that assigns the radius $\mathfrak{R}(R(v_i))$ to each $v_i \in \text{int}K$ with petals $\{C(v_0), C(v_1), \ldots, C(v_n)\}$ as follows:

$$\mathfrak{R}(R(v)) = \begin{cases} r \geq 0 \text{ such that } \theta(r; R(v_0), \ldots, R(v_n)) = A(v) & \text{if } v \in \text{int}K \\ R(v) & \text{if } v \in \partial K, \end{cases}$$

i.e., $\mathfrak{R}$ assigns the unique radius from Lemma 2.9 to each flower's nexus such that the angle sum meets its prescribed angle assignment (assuming its petals are unchanged). Denote repeated applications of the operator with $\mathfrak{R}^{k+1}(R) = \mathfrak{R}(\mathfrak{R}^k(R))$ for a positive integer $k \geq 1$.

This type of numerical relaxing algorithm has often been used for finding circle packings. Charles Collins and Stephenson used a similar method in [14]. The method here follows most closely that of Brett Garret [23]. Both are based on concepts of William Thurston. The basic idea being that local impact of radii changes will outweigh the global impact. By repeatedly adjusting radii to meet their local requirements the label will converge towards its global aims as well.

Lemma 2.11. *If R' and R are two labels for an admissible $K(I, A)$ such that $R' \leq R$ then $\mathfrak{R}(R') \leq \mathfrak{R}(R)$.*

Proof. Recall that by $R' \leq R$ we mean that $R'(v_i) \leq R(v_i)$ for every $v_i \in K$. Suppose we have two labels R' and R such that $R' \leq R$ but $\mathfrak{R}(R'(v)) > \mathfrak{R}(R(v))$ for some $v \in K$. If $v \in \partial K$ then its radius is fixed so we can assume that v is an interior vertex with a flower. Let $\{a_0, \ldots, a_n\}$ and

$\{b_0, \ldots, b_n\}$ be v's petal radii given by labels R' and R, respectively. By assumption $a_i \leq b_i$ and $\mathfrak{R}(R'(v)) > \mathfrak{R}(R(v))$. A flower is the sum of its face angles so by Lemma 2.4

$$A(v) = \theta(\mathfrak{R}(R'(v)); a_0, \ldots, a_n) \leq \theta(\mathfrak{R}(R'(v)); b_0, \ldots, b_n) < \theta(\mathfrak{R}(R(v)); b_0, \ldots, b_n) = A(v),$$

but this is a contradiction. □

Lemma 2.12. *Given a label R and flower $\{v; v_0, \ldots, v_n\}$ on an admissible $K(I, A)$ the following are equivalent.*

1. $\mathfrak{R}(R) \leq R$.
2. $\mathfrak{R}^{k+1}(R) \leq \mathfrak{R}^k(R)$ *for each* $k \geq 0$.
3. *For* $v \in intK$, $\theta(R(v); R(v_0), \ldots, R(v_n)) \geq A(v)$.
4. *For* $v \in intK$, $\theta(\mathfrak{R}^k(R(v)); \mathfrak{R}^k(R(v_0)), \ldots, \mathfrak{R}^k(R(v_n))) \geq A(v)$.

Proof. (1) $\iff$ (2). This follows by applying Lemma 2.11 k times. (1) $\iff$ (3) follows from Lemma 2.4, $\mathfrak{R}$ decreases the radius if and only if v's angle sum is too small. (2) $\iff$ (4) follows similarly. □

Theorem 2.13. *Suppose that $K(I, A)$ is a decorated complex with at least one border vertex, and let B be a set of radii bijectively assigned to the border vertices of K. Then if K is admissible there exists a label R such that $\theta(R(v_i)) = A(v_i)$ for each $v_i \in intK$ and $\{R(v_i) \colon v_i \in \partial K\} = B$.*

Recall that $I \leq 1$ means $\sigma_{ij} \leq 1$ for every edge assignment $\sigma_{ij} \in I$. This theorem shows that admissibility is a sufficient condition for the existence of labels.

Proof. By Lemma 2.9 $\mathfrak{R}$ is well defined for $K(I, A)$. There exists a label, say R_∞, with sufficiently large radii such that $\mathfrak{R}(R_\infty) < R_\infty$. Since for any interior vertex v_i neighboring a border circle,

$$\lim_{R(v_i) \to \infty} \theta(R_\infty(v_i)) = \min \theta(v_i).$$

By Lemma 2.12, $\mathfrak{R}^{k+1}(R_\infty) \leq \mathfrak{R}^k(R_\infty)$; each radius is assigned a real radius so then $\mathfrak{R}^k(R_\infty)$ is a non-increasing sequence bounded below. Hence $\mathfrak{R}^k(R_\infty)$ converges to some label $S \geq 0$ with $\theta(S(v_i)) = A(v_i)$ for each $v_i \in \text{int}K$. Now we must show that this label is not degenerate, i.e., that $S(v_i) \neq 0$ for any $v_i \in \text{int}V$.

Suppose that $V_0 = \{v_i \in \text{int}V \mid S(v_i) = 0\} \neq \emptyset$. If V_0 is not a simply connected sub-complex of K then choose some subset of V_0 such that it is, and call this subset V_0. As none of the boundary vertices can be 0 we can further assume that V_0 is a subset of the interior vertices. Following [34], we classify angles at each $v_i \in V_0$ into one of three types. Each angle at v_i is in a face that has either 1, 2, or 3 vertices in V_0. Denote vertices not in V_0 with x and y.

Case 1: Suppose the face has 1 vertex in V_0, say v_i. This angle is of the type

$$\theta(\mathfrak{R}^k(R_\infty(v_i)); \mathfrak{R}^k(R_\infty(x)), \mathfrak{R}^k(R_\infty(y))).$$

By monotonicity, Lemma 2.4, this angle tends to $\pi - \cos^{-1}(\sigma_{xy})$ as $k \to \infty$ (and $\mathfrak{R}^k(R_\infty(v_i)) \to 0^+$) in both $\mathbb{C}$ and $\mathbb{D}$.

Case 2: Suppose the face has 2 vertices in V_0, say v_i and v_j. The angle at x in the triangle $\{v_i, v_j, x\}$ tends to 0 as $v_i, v_j \to \infty$. In $\mathbb{C}$ the sum of the angles at v_i and v_j then must be π. The area of the triangle must also vanish. A hyperbolic triangle's area is the difference between π and the sum of its angles. So then these angles must sum to π in $\mathbb{D}$ as well.

Case 3: Suppose that the face has 3 vertices in V_0. In $\mathbb{D}$ as $k \to \infty$ the area of this face tends to 0 so then the sum of the three angles must tend to π. In $\mathbb{C}$ the sum is always π. In $\mathbb{D}$ an area of 0 implies that the sum of the angles is π.

The sum of angles on all of these faces from cases 2 and 3 will be $\pi\,|\text{int}F|$. The sum of angles from faces in case 1 will be

$$\pi(|F| - |\text{int}F|) - \sum_{F_i \in F \setminus \text{int}F} \left(\sum_{j=1\ldots3} \cos^{-1}(F_i(\sigma_j)) \right).$$

So from these three cases we can see that as $k \to \infty$,

$$\sum \theta(\mathfrak{R}^k(R'(v_i))) = \sum \theta(S(v_i)) > \pi\,|F| - \sum_{F_i \in F} \sum_{j=1\ldots3} \cos^{-1}(F_i(\sigma_j)),$$

for the sub-complex $K_0 \subset K$. $K(I, A)$ is admissible and thus so is $K_0(I, A)$; so this is a contradiction. It follows that $V_0 = \emptyset$. □

This theorem shows that admissibility is a sufficient condition for a motif to exist. Part 1 of admissibility ensures that any computed label can form triangles for the given edge assignments. Part 2 guarantees that monotonicity holds for these labels. Together they allow the relaxation operator to converge.

The third part of admissibility is in fact a necessary condition. A motif is defined to have angle sums matching its angle assignments, and the angle sums will lie in the bounds of part 3. Next we show that the label for $K(I, A)$ is unique using a standard maximal argument.

Theorem 2.14. *Let $K(I, A)$ be an admissible decorated complex. If $K(R, I, A)$ and $K(R', I, A)$ are both motifs in $\mathbb{C}$ or $\mathbb{D}$ with identical border radii then $R' = R$.*

Proof. First the Euclidean case. If $R \neq R'$ then without loss of generality we can assume that there exists an interior vertex $v_M = \{v_i \colon \frac{R(v_j)}{R'(v_j)} \leq \frac{R(v_i)}{R'(v_i)} = m \,\forall\, v_j \in \text{int}V\}$. Scale all the circles of v_M's flower in $K(R', I, A)$ by m so that $R(v_m) = mR'(v_m)$. By similar triangles this also means that $\theta(R(v_M)) = \theta(mR'(v_M))$. Now we must have $\frac{R(v_j)}{R'(v_j)} = m$ for each of v_M's petals. Else $R(v_j) < mR'(v_j)$ for one of v_M's petals, and by monotonicity

$$A(v_M) = \theta(R(v_M); R(v_1), \ldots, R(v_n)) > \theta(mR'(v_M); mR'(v_1), \ldots, mR'(v_n))$$

which is a contradiction. So then $\frac{R(v_j)}{R'(v_j)} = m$ for each v_j tangent to v_i and each of their petals as well. We can repeat this argument until eventually we reach a vertex neighboring a border circle where the labels must agree implying that $R = R'$.

Now the hyperbolic case. Hyperbolic points in the disc can be located by complex numbers on or inside the unit disc. The formula

$$D_{\mathbb{D}}(z,w) = 2\tanh^{-1}\left|\frac{z-w}{1-z\bar{w}}\right|$$

relates the Euclidean distance of z from w (for $|z|$, $|w| < 1$) to its hyperbolic distance in the disc [5].

Let $z_{\mathbb{C}}$, and $r_{\mathbb{C}}$ represent the Euclidean center location and Euclidean radius, respectively, of a hyperbolic circle $C(z)$. Apply a Möbius transformation which rotates the circle such that $z_{\mathbb{C}}$ is a real number. This also makes the point on $C(z)$ furtherest from the origin equal to $r_{\mathbb{C}}$.

$$\frac{d}{dr_{\mathbb{C}}} D_{\mathbb{D}}(z_{\mathbb{C}}, r_{\mathbb{C}}) = \frac{2}{1-r_{\mathbb{C}}^2} > 1 \tag{2.13}$$

since $0 < r_{\mathbb{C}} < 1$. This means that changing the associated Euclidean radius of a hyperbolic circle has a greater effect on the hyperbolic radius.

Use a Möbius transformation to map v_M's flower in both $K(R,I,A)$ and $K(R',I,A)$ such that v_M is at the origin. Scale the Euclidean circles of v_M's flower by a value $m^\star$ such that $2\tanh^{-1}(m^\star R'(v_M)_{\mathbb{C}}) = R(v_M)$. Because the flower was scaled Euclideanly the angle sum will not be changed, however this is not a hyperbolic scaling. The hyperbolic radii of v_M's flower have been increased too much by Equation 2.13. For this to be a hyperbolic scaling the petals must now be decreased. However by monotonicity, decreasing the hyperbolic radii of the petals also decreases the angle sum at v_M, which is a contradiction. □

Chapter 3

Coherence

A motif's label is made from a recipe of specified patterns, inversive distances, and angle sums. Placing circles for these radii onto one of the standard geometries according to the motif's decorated complex creates a geometric structure. This structure will be called a *layout*, the properties of which are not necessarily independent of the construction method. Consider the structures in Figure 3.1. Here we have two different pictures created from the same set of radii and pattern of contiguousness. Even after a normalization there are multiple ways to place these circles in $\mathbb{C}$ according to its complex, i.e., well-defined locations for the circles do not exist.

We will call this sort of motif *incoherent* and say that it is *coherent* only when it can be "consistently laid out" (formal definitions are provided below) or equivalently when it defines a circle packing. Notice that the flower at v_1 fails to be coherent as a sub-motif; so this motif also lacks coherence at a local level. The label R_1 provided by Theorem 2.13 computationally meets the prescribed angle and edge assignments, but being able to realize them while embedded in $\mathbb{G}$ is another matter.

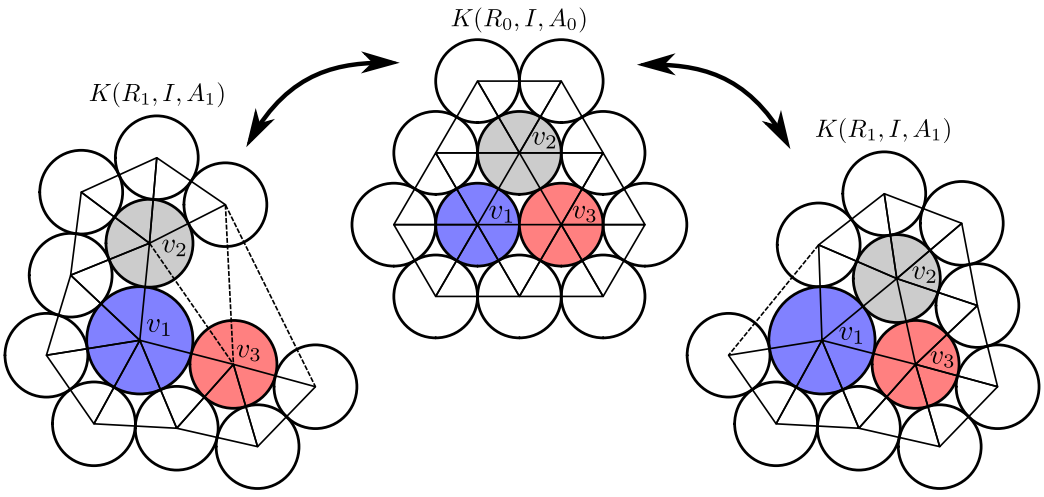


Figure 3.1: Two different layouts of the same motif, $K(R_1, I, A_1)$.

It is not difficult to see that a single flower is coherent in $\mathbb{G}$ if and only if the angle sum of that flower is an integer multiple of 2π (Lemma 3.4); this is commonly known as the *packing condition*. It is a happy consequence of monodromy that a simply connected motif is coherent if only if each of its flowers is coherent. Hence the *packing condition* is well named. However this is most certainly *not* the case for more general complexes. The partnership between local and global coherence works so seamlessly for discs and spheres that the need for distinction when the complexes are non-simply connected can easily be overlooked. Accordingly we will carefully separate our investigation of the global and local properties of labels.

This chapter will first establish some basic language and facts so that a motif can be placed into one of the geometries. Then we give formal definitions for coherent motifs. The rest of the chapter provides some conditions for a motif to be coherent.

3.1 Chains and the Fundamental Group

Paths and loops are key concepts in Topology. As a circle packing analogue, edge paths might seem like the natural choice. However circle packing is about the dance of local geometry with global combinatorics. Using edges ignores too much of the latter; the location of a sequential circle in an edge chain is only restricted by its distance from the last circle. Its placement has a wide range of freedom, and no memory of the geometry from earlier flowers gets carried over and expressed.

Instead we use *face chains* or just *chains*. A chain is a sequence of faces, for example $\Gamma = \{f_0, \dots f_n\}$, where each successive face, $f_{i+1} \in \Gamma$, shares an edge with its predecessor, $f_i \in \Gamma$. If $f_0 = f_n$ then we say that the face chain is *closed*. Once f_i is placed, local geometry (and orientation) then determines the location for f_{i+1}. The location of the first face, called the *base face*, thus determines the location of every face in the chain.

Definition 3.1. Chains of faces can be modified by a finite succession of local modifications called *homotopies*. Take a (face) chain $\Gamma = \{f_0 \dots, f_i, \dots, f_j, \dots, f_n\}$ and a subchain $\gamma = \{f_i, \dots, f_j\}$. A new chain Γ' can be created by replacing γ with some other chain beginning with f_i and ending with f_j. If by performing a finite number of such modifications a chain Γ_1 can be obtained from another chain Γ_0 then we say that that they are *homotopic*, denoted $\Gamma_0 \sim \Gamma_1$.

See Figure 3.2. This example shows two homotopic chains in a circle packing. Chains and homotopies of chains can be considered on the abstract complex, but they come into force on the actual circle configurations. There they will be used to layout motifs into geometries and demonstrate key results about their behavior.

A *boundary element* is a collection of boundary vertices connected by boundary edges. A *border chain* $\partial\Gamma = \{f_0, \dots, f_n\}$ for the boundary vertex b is the closed chain of faces such that each face $f_i \in \partial\Gamma$ contains at least one border vertex in b's boundary element. Let $\mathfrak{B} = \{\partial\Gamma_i\}$ be the set of border chains.

Our use of chains is analogous to the use of paths in continuous surfaces. These chains can be modified in a number of different ways:

$$\{\dots, f, f, \dots\} \leftrightarrow \{\dots, f, \dots\},$$

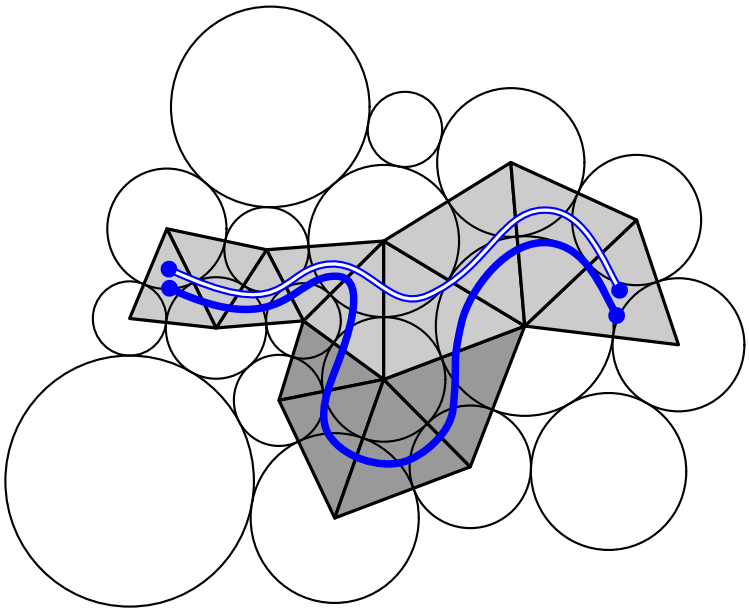


Figure 3.2: Two homotopic face chains. Γ_0 is in white, and Γ_1 is blue; Γ_0 can be obtained from Γ_1 by removing the additional faces (those darkened).

$$\{\dots, f, g, f, \dots\} \leftrightarrow \{\dots, f, \dots\},$$

$$\text{or } \{\dots, f_1, f_2, f_7, f_8, \dots\} \leftrightarrow \{\dots, f_1, f_2, f_3, f_4, f_5, f_6, f_7, f_8, \dots\};$$

a modification that changes the direction in which the chain passes around a vertex (see Figure 3.2).

The collection of closed chains that share a base face f_0 on K forms a group. The elements are the sets of homotopic chains, and the group action is the concatenation of face strings, e.g., if $\Gamma_1 = \{f, \dots, f_1, f_2, \dots, f_0\}$ and $\Gamma_2 = \{f_0, \dots, g_1, g_2, \dots, f_0\}$ then

$$\Gamma_2 \circ \Gamma_1 = \{f_0, \dots, f_1, f_2, \dots, f_0, \dots, g_1, g_2, \dots, f_0\}.$$

The group identity is the *null chain* $\Gamma_0 = \{f_0\}$, a single face. If a chain is homotopic to the null chain we say that it is *null homotopic*.

Denote this group as $\pi_1(f_0, K)$ or just $\pi(K)$; called the *fundamental group of* K. Our complexes will always be assumed to be chain connected; so while the fundamental group depends on the choice of base face, up to isomorphism, this choice makes no difference.

Definition 3.2. Call a collection of closed chains that is a minimal set of generators a *set of generating chains for* K, denoted $\mathcal{G}(K) = \{\Gamma_1, \dots, \Gamma_2\}$. Call a chain $\Gamma \in \mathcal{G}(K)$ a *generator*.

Any closed chain in a complex or motif will either be homotopic to a generator chain in $\mathcal{G}(K)$, or it will be homotopic to a concatenation of generator chains in $\mathcal{G}(K)$. The fundamental groups of the disc and sphere are trivial so a (closed) chain in either is null homotopic. The fundamental group of the annulus is $\mathbb{Z}$ meaning every chain is null homotopic or circumnavigates the annulus an

integral number of times. A chain wrapping itself n-times around the annulus is an n-concatenation of a chain going around once as $\mathbb{Z}$'s (group) generator is 1. The torus has fundamental group $\mathbb{Z} \times \mathbb{Z}$, and so has two fundamental chain homotopy classes.

3.2 Chain Developments and Layouts

Saying that a motif exists assumes that a label also exists for the given inversive distance and angle sum assignments. Without such a label in hand there is no motif. Once a label has been found we can then investigate the structure of its layouts in one of the geometries. This begins by placing circles from the label contiguously in $\mathbb{G}$ with the aim of constructing circle packings; what we will call coherent motifs. Chapter 2 provides methods for finding a motif in $\mathbb{C}$ and $\mathbb{D}$. Below we will assume that the motif has first been found for one of these metrics and use projection to find and place motifs in $\mathbb{P}$.

A motif $K(R, I, A)$ provides a radius for each vertex. Once a circle $C(v_0) = C_0$ has been placed (in $\mathbb{G}$) Equation 2.3 can be used to place one of its neighboring circles, say C_1, such that the distance between them matches their edge assignment. R is assumed to be the label found in Theorem 2.13. Thus a mutual neighbor of C_0 and C_1, say C_2, can be uniquely placed using Equation 2.3, the appropriate Law of Cosines, and orientation.

Whether it is a circle, edge, or face we call an object placed in such a manner as having been *laid*, and the result a *layout*. Laying a face f_0 also lays two circles of any neighboring face, say f_1, and f_1's third circle can be similarly located. The same is true for any faces sharing an edge with f_1. In this way we can use a face chain $\Gamma = \{f_0, \ldots, f_n\}$ (closed or non-closed) to lay the circles for f_n once the *base face* f_0 has been laid. We say that the location of f_n, denoted $\Gamma_{f_0}(f_n)$, was obtained by a *development* along Γ from f_0.

Once a motif has been found, developments along a chain can be used to layout all the circles in the chain's faces. Complexes are assumed to be face connected. Thus after the initial triangle has been laid there is a way to sequentially layout every face in the motif.

3.3 Coherence

Layouts will produce circle configurations from motifs, but are these layouts consistence? Meaning will two different layouts of the same motif be identical up to Möbius transformations? Recall Figure 3.1. Such a configuration will not be of much use in the service of creating discrete functions or conformal maps. Motifs are laid in their geometry with chains, and so layouts will be consistent if the developments along chains are consistent.

Let $\Gamma_1 = \{f_0, \ldots, f_n\}$ be a closed chain ($f_0 = f_n$), and let Γ_0 be the null chain. $\Gamma_0(f_0)$ and $\Gamma_1(f_n)$ are placed using the same label and orientation and are thus similar triangles. Using the location of corresponding edges in both triangles, a Möbius map $\phi_{\Gamma_1} \in \mathrm{Aut}(\mathbb{C})$ (also written $\phi(\Gamma_1)$) can be found such that $\phi_{\Gamma_1}(\Gamma_0(f_0)) = \Gamma_1(f_0)$. ϕ will always be trivial if its motif is coherent. In

which case the associated ϕ_Γ will be the identity transformation

$$\begin{bmatrix} 1 & 0 \\ 0 & 1 \end{bmatrix} = \phi_{\mathrm{id}}.$$

These developments are how motifs are placed in their geometry. Furthermore using local modifications we can see that for locally coherent motifs ϕ_Γ depends only on the homotopy class of Γ (by monodromy, see Theorem 3.9 below). Thus a necessary and sufficient condition for coherence is that $\phi_\Gamma = \phi_{\mathrm{id}}$ for every generator chain $\Gamma \in \mathcal{G}(K)$ [44]. Call the map ϕ_Γ the *holonomy* of Γ, and we say that Γ has *trivial holonomy* if $\phi_\Gamma = \phi_{\mathrm{id}}$.

Holonomies will come into use in Chapter 4 to demonstrate incoherence, in Chapter 8 as a tool for measuring and optimizing motifs, and here as a basic tool for proving results about motifs.

Definition 3.3. $K(R, I, A)$ is locally coherent at an interior vertex v if any two layouts of the flower of v are Möbius images of one another.

Lemma 3.4. *A motif $K(R, I, A)$ in $\mathbb{G}$ is locally coherent at an interior vertex v if and only if $\theta(v) = 2\pi n$ for $n \in \mathbb{Z}^+$.*

Proof. Let Γ be the closed chain of faces that is v's flower. Γ fixes v so then $\phi(\Gamma_f)$ is rotation, and Γ is null homotopic if and only if this rotation is an integer multiple of 2π. The total rotation is determined by the sum of angles at v which is its angle sum, $\theta(v)$. □

Maybe expectedly, this is the first criteria for having coherence for the entire motif. Requiring angle sums to be set to integral multiples of 2π is commonly known as the *packing condition*. A name which was first applied here [7], and motivates the following definition.

Definition 3.5. A motif that is locally coherent at every vertex is a *branched motif*.

Observe that the branch set from Definition 2.6 may be empty. The term "branching" has traditionally been reserved for circle packings with a non-empty branch set, however in this thesis the term is used more generally.

Definition 3.6. If any two layouts of the same motif $K(R, I, A)$ are Möbius images of one another then the motif is called *globally coherent* or *coherent*.

Remark 3.7. By homotopy, a motif $K(R, I, A)$ will be coherent if and only if the holonomy of $\phi(\Gamma)$ is trivial for every $\Gamma \in \mathcal{G}(K)$.

Theorem 3.8. *A layout of a coherent motif is a circle packing.*

Proof. ($\Rightarrow$) From Definition 1.2, parts 1 and 3 follow immediately from the definition of a layout. The fact that any two layouts are isomorphic ensures that each circle is properly contiguous to all its neighbors, not just the ones used to place it. Otherwise a development based at the face with the non-contiguous circles would immediately yield a non-isomorphic layout.

($\Leftarrow$) By definition every circle and thus every face is laid such that their assignments are met. So the development along any closed chain $\Gamma = \{f_0, f_1, \ldots, f_n, f_0\}$ is identical to how the faces are laid in P. This includes f_n and f_0 as located from f_n. □

If $K(R, I, A)$ is a coherent motif denote its layout with $P_{K(R,I,A)}$ or just P_K when K's decorations are understood. We now state an important theorem regarding simply connected complexes.

Theorem 3.9. (Monodromy Theorem) *Let K be a simply connected complex. $K(R, I, A)$ is a branched motif if and only if $K(R, I, A)$ is coherent.*

Proof. If $K(R, I, A)$ is coherent then it also must be locally coherent since any layout that begins with an incoherent flower will not be unique (up to isomorphisms).

It needs to be shown that a layout will be independent of the developments used to locate its circles. The complex is connected, so any order of placement can be traced back to an arbitrary placement of f_0. Any two developments with base face f_0 used to place a face g, say $\Gamma' = \{f_0, \ldots, g\}$ and $\Gamma'' = \{f_0, \ldots, g\}$, can be merged into

$$\Gamma = (\Gamma'')^{-1} \circ \Gamma' = \{f_0, \ldots, g, \ldots, f_0\}$$

(where $(\Gamma')^{-1}$ is the reverse ordering of Γ') by translating and rotating Γ' as necessary. Γ' and Γ'' will find identical placements for g if and only if $\phi(\Gamma(f_0))$ is the identity. Thus we need only prove that all closed chains with base face f_0 have trivial holonomy.

Let Γ', Γ'', and Γ be as described above. Because K is simply connected Γ is null homotopic. Consider a flower $F \in K$ such that F shares faces with Γ. Because F is locally coherent, local modifications of $\Gamma \subset K'$ using sub-chains from F will not affect the development $\Gamma(f_n)$. By repeatedly using sub-chains from neighboring flowers, Γ can be modified down to its base face without affecting the development, where it is clear that $\phi(\Gamma(f_0))$ is the identity. □

The statement and proof are for the most part as they appear in [44].

Remark 3.10. If a motif is coherent then it is a branched motif regardless of the complex, i.e., local coherence is always necessary for global coherence.

Proof. If a motif is coherent then it is the disjoint union of simply connected sub-motifs. Each of which is coherent and thus locally coherent at each vertex by Theorem 3.9. □

All closed chains in simply connected complexes are null homotopic. This is not true for non-simply connected complexes, and thus it should not be expected that Theorem 3.9 would hold. Consider the simple example shown in Figure 3.3; the pictured layout of a motif is locally coherent at every vertex. A development that walks around the inside (or outside border) clearly has non-trivial holonomy. Another example is shown in Figure 3.4. This motif also is locally coherent, and a branch point has been added. These examples demonstrate the sometimes overlooked fact: local coherence does not imply global coherence.

Definition 3.11. Let $K(R, I, A)$ be a motif and $\partial\Gamma \in \mathfrak{B}(K)$ with boundary element $\{b_1, \ldots, b_n, b_1\}$ denoted $\overline{\partial\Gamma}$. Then the *turning angle at the vertex* $b_i \in \overline{\partial\Gamma}$ is

$$t(b_i) = \pi - \theta(b_i) \text{ for } b_i \in \overline{\partial\Gamma}.$$

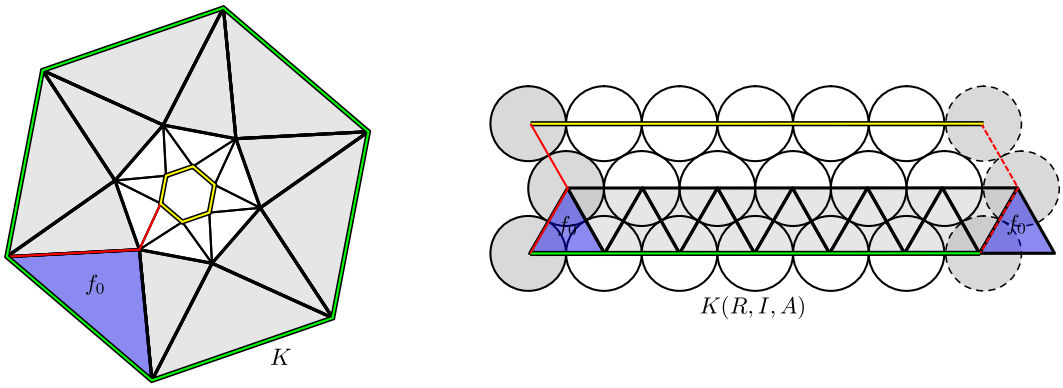


Figure 3.3: A locally coherent but globally incoherent motif. The complex K for an annulus is on the left. The two border edges are colored yellow and green; the red is an interior edge. On the right is a layout of a locally coherent but globally incoherent motif for the same K.

The *turning angle of a border chain* $\partial\Gamma$ is

$$T(\partial\Gamma) = \sum_{i=1}^{n} t(b_i),$$

where each $b_i \in \overline{\partial\Gamma}$. Finally we say that $K(R, I, A)$ has *(total) turning angle* $\sum_{\partial\Gamma_i \in \mathfrak{B}} T(\partial\Gamma_i)$ where all angles are measured Euclideanly.

Turning angle will be measured in the plane where angle is invariant under isometries. (see Figure 3.5). Möbius transformations take circles to circles and preserve inversive distances. So motifs are coherent/incoherent if and only if they are coherent/incoherent in all three geometries. Results evaluating coherence in the plane can then be carried over to the other geometries. If $\mathbb{G} = \mathbb{D}$ then turning angle can be measured by using the associated Euclidean circles, and if $\mathbb{G} = \mathbb{P}$ then the motif can be projected to the disc and then measured using the associated Euclidean circles.

Theorem 3.12. *Suppose we have a branched motif $K(R, I, A)$ in $\mathbb{D}$ or $\mathbb{C}$ with branch set $\beta(K)$ (see Definition 2.6) and at least one boundary element. Let $\lambda(K) = 2-|\mathfrak{B}|$ where $\mathfrak{B}$ is the set of boundary elements in K. $\sum A(v) = 2\pi(intV + |\mathfrak{B}|)$ if and only if the total turning angle of $K(R, I, A)$ is*

$$\sum_{\partial\Gamma \in \mathfrak{B}} T(\partial\Gamma) = 2\pi(|\beta(K)| + \lambda(K)).$$

Note that a development with trivial holonomy must have a turning angle that is a multiple of 2π.

Proof. Recall that *int* and ∂ denote interior and border subsets of F, E, and V. Let $v_i \in \text{int}V$. There are 3 edges per face. Excluding the border edges, this double counts the number of edges. Noting that $\partial V = \partial E$ this gives,

$$E = \frac{1}{2}(3F - \partial V) + \partial V = \frac{3}{2}F + \frac{1}{2}\partial V.$$

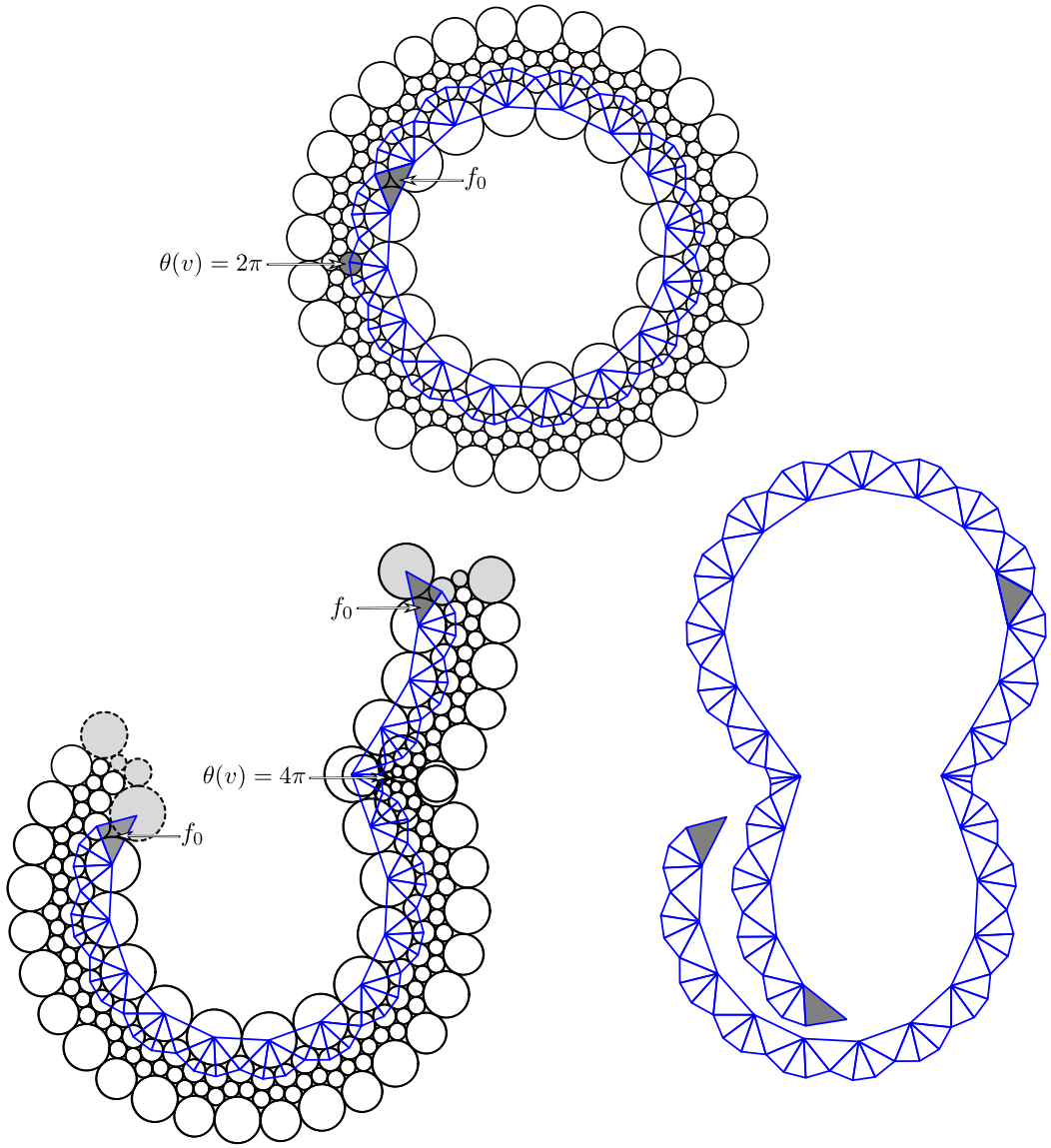


Figure 3.4: Another locally coherent but globally incoherent annulus. On the bottom is a layout of the motif. It has been rendered from the circle packing above by setting $A(v) = 4\pi$. A development for the darkened face is laid out twice on the bottom-right.

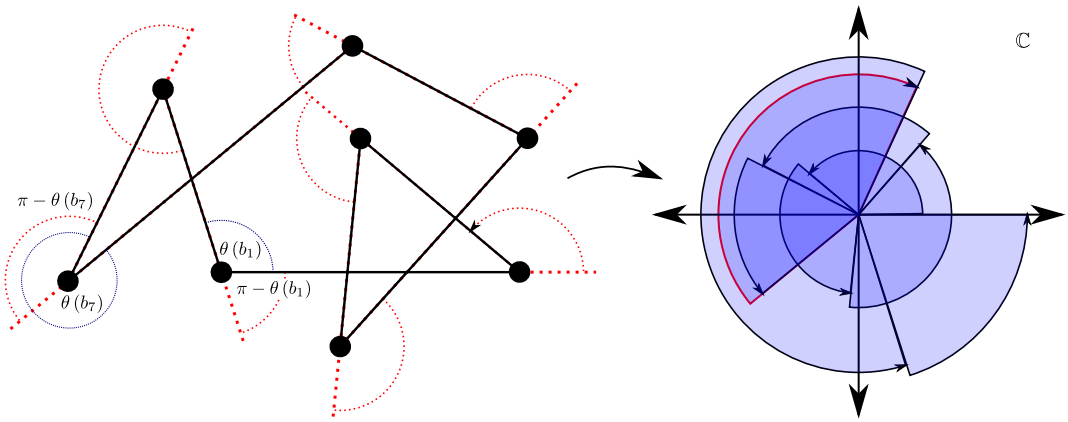


Figure 3.5: Turning angle of a non-simple polygon. Turning angle is in red with a selection of interior angles colored blue. Note the negative turning angle at b_7. On the right, this angle is colored red on the translation of the turning angles.

Substituting this value into the Euler characteristic, we derive that $\pi F = 2\pi(\text{int}V - \lambda(K)) + \pi\partial V$; πF is the total amount of (Euclidean) angle on K so then the sum of the border angles, $\theta(b)$ for $b \in \partial V$ is the difference between this and the sum of the interior angles:

$$\begin{aligned} \sum \theta(b) &= \pi F - 2\pi(\text{int}V + |\beta(K)|) \\ &= \pi(\partial V - 2\,|\beta(K)| - 2\lambda(K)) \end{aligned}$$

which implies that the turning angle is then

$$\begin{aligned} \pi\partial V - \sum \theta(b) &= \pi\partial V - \pi(\partial V - 2\,|\beta(K)| - 2\lambda) \\ &= 2\pi(|\beta(K)| + \lambda(K)). \end{aligned}$$

The other direction follows similarly. □

Admissibility serves as a generalization for branch structure (Definition 2.6) in our setting, but as mentioned before there are non-admissible decorated complexes for which labels do exist. For these labels turning angle provides another necessary condition for coherence. Coherent motifs must have turning angles that are non-zero integral multiples of 2π. This can easily be seen by replacing the interior of coherent motif's border chain with an exterior face.

The turning angle at a border vertex is the difference of π and the petal angle. So then by Lemma 2.4,

$$\pi - \pi\,|F| \leq \pi - \sum_{e \in E_i} \psi_e < t(v_i) < \pi$$

where E_i is the set of border edges of v_i's flower, and $\psi_e = \pi - \cos^{-1}(\sigma_e)$. Using this fact we get the following corollary.

Corollary 3.13. *Suppose that $K(R, I, A)$ is a coherent motif in $\mathbb{C}$. Let $|\partial V|$ be the number of border vertices in a border chain $\partial\Gamma$. If $T(\partial\Gamma) = 2\pi n$ then $|\partial V| > 1 + 2n$. Furthermore, if K is simply connected then $|\partial V| > 2 + 2\,|\beta(K)|$.*

Proof. Following the above remarks, the first part is clear. To see the second part puncture all the branch circles of a coherent motif. Each branch circle's flower is replaced by a border chain with negative turning angle. The sum of which will be $-2\pi\,|\beta(K)|$. So then $\partial\Gamma_i$ must having a turning angle of $\pm 2\pi\,|\beta(K)|$. □

Theorem 3.14. *Let $K(I, A)$ be an admissible combinatorial sphere with half of the branching at a single externally tangent flower. That is, there is a single vertex v_∞ such that*

$$A(v_\infty) = \sum_{v_j \in v_\infty \backslash V} A(v_i) - 2\pi\,|V - 1|\,,$$

and $\sigma_{\infty,i} = 1$ for every petal in v_∞'s flower. Then there exists an essentially unique $P_{K(R,I,A)}$ in $\mathbb{P}$.

Proof. Essentially unique means that if $K(R, I, A)$ and $K(R', I, A)$ are coherent motifs on the unit sphere then there is a Möbius map φ such that $\varphi(P_{K(R,I,A)}) = P_{K(R',I,A)}$.

Let $B = \{v_1, ..., v_n\}$ be v_∞'s petals. Remove v_∞ from K creating the sub-complex K'. By Theorem 2.13 and 3.9 there exists a coherent motif $K'(R_{\mathbb{D}}, I, A)$ on the disc such that each $v_i \in B$ is a horocycle, i.e., it is a branched maximal packing. By Theorem 3.12 the boundary chain of the motif has a turning angle of

$$\sum_{v_j \in v_\infty \backslash V} A(v_i) - 2\pi\,|V - 1|\,,$$

or equivalently the boundary circles wrap around the boundary of the disc $\frac{1}{2\pi}A(v_\infty)$ times.

Via stereographic projection, take $P_{K'(R_{\mathbb{D}},I,A)}$ to the sphere. The boundary is mapped to a hemisphere. Calling this circle $C(v_\infty)$ gives us a spherical label R for the motif $K(R, I, A)$. Since $K'(R_{\mathbb{D}}, I, A)$ was coherent so is its projection. Local coherence of v_∞'s flower then gives us coherence of $K(R, I, A)$. Essential uniqueness then follows by standard arguments from the uniqueness of $P_{K'(R_{\mathbb{D}},I,A)}$. □

The incoherence in Figures 3.3 and 3.4 can most easily be seen in the holonomy of their border chains. It is clear that a motif is coherent only if the holonomy of every generator chain is trivial, however the converse is not true. An interesting example of such a motif is Figure 3.6. The lower half of the figure is an example of a fractional branched motif, the subject of Chapter 6. The two motifs differ only in their angle assignments and resulting labels. Visually it is easy to check that the border chain (Γ_0) has trivial holonomy, but a closer inspection reveals that the three interior vertices fail to be locally coherent. A chain passing (Γ_1) through the interior face will have a non-trivial holonomy.

Though the interior vertices are each locally incoherent, the cumulative effect of their rotational holonomy causes the border chain to have no holonomy. Non-locally coherent angle sums would generally not "correct" the holonomy on the exterior chain, so this is not typical. A notable feature of this example (Figure 3.6) is that the interior incoherence can be ignored if it is avoided. Such

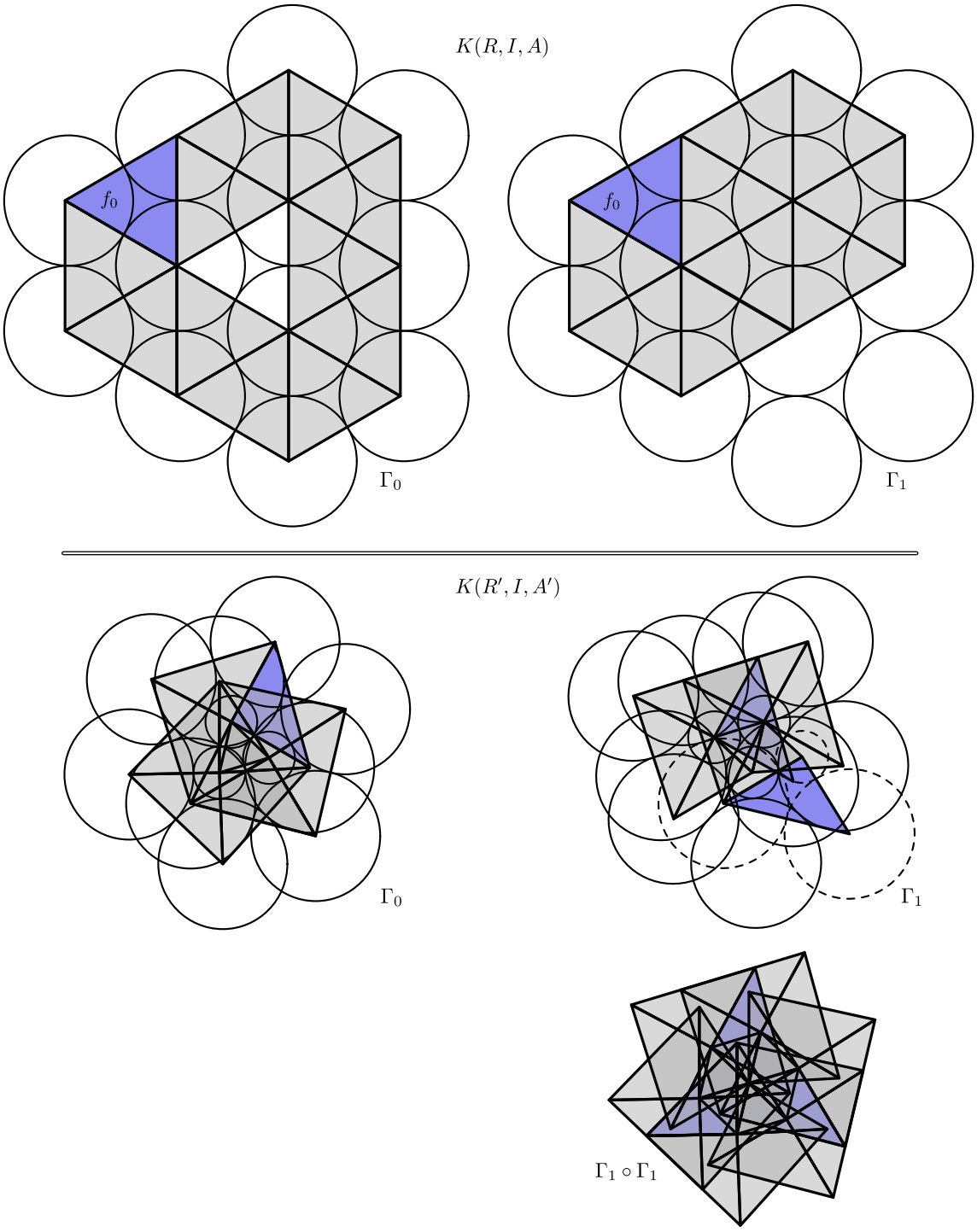


Figure 3.6: Chains passing through and around an incoherent sub-motif. Γ_0 and Γ_1 are closed chains with similar base face f_0 (in blue) in layouts of the coherent motif $K(R, I, A)$ and the incoherent motif $K(R', I, A')$.

configurations within larger motifs can allow coherence outside singular type areas of incoherence. If the boundary element of an incoherent sub-motif has trivial holonomy than the sub-motif can behave like a singular structure bringing rigidity to the super-motif. We formalize this idea in Chapter 5 where it is called *generalized branching*.

Chapter 4

Discretization Issues

Developing discrete analogues of classical functions has been a central focus of circle packing. Thurston conjectured that the Riemann mapping function from a simply connected region onto the unit disk can be approximated by a regular hexagonal pattern (flowers with six petals) [46]. First proved by Burt Rodin and Dennis Sullivan [37] it has since been much generalized and improved (see [6, 42, 27, 28, 25] and others). For instance the hexagonal requirement turned out to be a mere convenience not a crucial assumption. The fundamental property can be summed up by the often repeated adage: *an analytic function is one which maps infinitesimal circles to infinitesimal circles.* So circle packings dense with vertices should be expected to behave like their classical counterparts. What may be surprising is how well the geometric properties of the classical functions are replicated regardless of refinement.

This suggests that the properties of the classical are inherited from the discrete. Since its emergence circle packing has embraced this perspective. Not just as a tool for modeling, circle packing has evolved into a deep and rich independent theory. However circle packing's connection to classical theory is not perfect. This is particularly so when multi-connected decorated complexes are introduced which fail to have coherent motifs. These failures provide evidence of inherent fundamental differences between the discrete and the continuous. Thus refinement may overwhelm these differences, but it should not be expected to extinguish them.

In this chapter we explore some important classical examples which exhibit these failures. As prime specimens we have the Ahlfors function on an annulus and the Weierstrass function on the torus. Both are branched functions from multi-connected surfaces, the annulus and torus, respectively. Specific examples below fail to allow a coherent label to exist, and help justify our exploration of alternative circle packing methods in the following chapter. We also discuss a discrete quadratic polynomial, a simpler example on the plane which fails to exhibit the key behavior of the classical version.

4.1 A Measure of Incoherence

Recall from Section 3.3 that non-trivial Möbius maps defined by a closed chain Γ can be used to demonstrate a motif's incoherence. Here they will also as be used to measure incoherence. Something that will be of more importance in Chapter 8.

A Möbius transformation, $f(z) = \frac{az+b}{cz+d}$, can be associated with an invertible 2 by 2 matrix

$$\phi = \begin{pmatrix} a & b \\ c & d \end{pmatrix} \text{ where } \det(\phi) = ad - bc \text{ and } \operatorname{tr}(\phi) = a + d.$$

Without loss of generality it be will assumed that ϕ has been normalized such that $\det(\phi) = 1$. Both the determinant and trace of ϕ are conjugate invariants, i.e., for any other Möbius transformation φ, $\det(\varphi\phi\varphi^{-1}) = \det(\phi)$ and $\operatorname{tr}(\varphi\phi\varphi^{-1}) = \operatorname{tr}(\phi)$. It can be shown that these conjugates form classes which geometrically result in different types of transformations, and a transformation's class can be identified by the square of its trace function [41]. These classes are commonly labeled as parabolic, elliptic, hyperbolic, and loxodromic.

Given a ϕ_Γ (the Möbius transformation defined by Γ) we can find its Frobenius norm. The Frobenius norm (or Euclidean norm) is a matrix norm,

$$\|\phi_\Gamma\|_F = \sqrt{a^2 + b^2 + c^2 + d^2}, \text{ where } a, b, c, d \text{are the entries of } \phi_\Gamma. \tag{4.1}$$

It is the square root of the sum of the squares of its elements. Alternatively it can be written as,

$$\sqrt{\operatorname{tr}(\phi_\Gamma^H \phi_\Gamma)}, \text{ where } \phi_\Gamma^H \text{ is the Hermitian transpose.}$$

Recall that $\phi_{\mathrm{id}} = \begin{bmatrix} 1 & 0 \\ 0 & 1 \end{bmatrix}$ and that $\mathcal{G}(K)$ is a set of fundamental chains K (see Definition 3.2). Call the following function the *total holonomy error:*

$$E_{K(R,I,A)} = E_K = \sum_{\Gamma \in \mathcal{G}(K)} \|\phi_\Gamma - \phi_{\mathrm{id}}\|_F . \tag{4.2}$$

When comparing the total (holonomy) error of two motifs $K(R, I, A)$ and $K'(R', I, A)$ it will be assumed the same $\mathcal{G}(K)$ and layout order are being used. As a matter of convenience border chains will be used when available. It has been shown in Chapter 3 that a motif $K(R, I, A)$ is coherent if and only if its total error is zero. ϕ_Γ is invariant with respect to homotopy; so E_K provides a reliable measure of incoherence for the Ahlfors and Weierstrass functions below.

4.2 Methods

All our experiments, examples, and pictures are conducted or created using an extended version of the open source program `CirclePack`. This free Java software has been created, copyrighted, and maintained by Ken Stephenson. Now in its sixteenth year of development its ease of use and

versatility are ideal for these type of experiments. Not only does `CirclePack` allow us to compute the labels; it brings the packings to life with vivid and beautiful pictures.

The extended version we work with includes methods for computing fractional branched motifs, coherent shift-points, and experiments implementing these ideas. The source code for the extended version is not yet available with the main `CirclePack` package, but will be provided upon request from Stephenson or the author.

4.3 A Quadratic Polynomial

The ratio function serves as our discrete analogue for the modulus of the derivative in the continuous setting. Suppose that K is a simply connected complex such that $K(I, A')$ and $K(I, A)$ are admissible. Let $K(R', I, A')$ and $K(R, I, A)$ be two motifs where the border radii of R are set by the ratio function $f^{\#}(v) = \frac{R(v)}{R'(v)}$.

By Monodromy, we need only choose an A and A' so that both motifs are branched to ensure that they are coherent. A map $f\colon P_{K(R',I,A')} \to P_{K(R,I,A)}$ between the layouts is then a discrete analytic function. Like many discrete analogues in circle packing the main interest is the behavior of the motif's border.

Consider the function $g(z) = (z - \frac{1}{4})^2$ which has a branch point at $\frac{1}{4}$. Manipulating $f^{\#}$ gives us a method to emulate this classical function. Let $K(\mathcal{R}, I, A') = K_{\mathrm{M}}$ be the maximal motif and R' the Euclidean label for K_{M} when the boundary is the unit disc. By setting $f^{\#}(v) = |g'|$ for a border vertex v we control boundary adjustments of f to mimic those of g. As $g(z)$ has a branch point at $\frac{1}{4}$ we also need to mimic this behavior. However discreteness provides limited options; so we choose the circle center in $P_{K(R',I,A')}$ closest to $\frac{1}{4}$.

Figure 4.1 shows an example of a circle packing with a circle close to the desired point. The blue circle's center (on the left) is at about 0.2551. The blue path on the right indicates the image of the unit circle under g, $(e^{2\pi it} - \frac{1}{4})^2$ for $t \in [0, 1]$. We can see that the boundary of the discrete result follows the classical quite well. A shift via the Möbius transformation $z + \frac{1}{16}$ is the only adjustment which has been made to the image packing. It should be noted that this analogue is not quite as nice on the interior. While the branch circle is very nearly mapped to 0, the vertex v_{138} (marked in pink) has a difference of $|g(v_{138}) - f(v_{138})| \approx 0.628$.

A more coarse example does not fair as well. See Figure 4.2. The circle center at 0 is our best choice to locate the branching. As can be seen, the border circles in the image packing are not anywhere close to where they need to be.

4.4 The Ahlfors Function

The Ahlfors mapping of an annulus is a proper multi-sheeted analytical map onto $\mathbb{D}$. Thus it serves the role of the Riemann map for non-simply connected surfaces. In this section we demonstrate that traditional circle packings cannot provide a fitting discrete analogue of this important class of complex functions. The discrete analogue of the Riemann map, the Maximal packing, was one

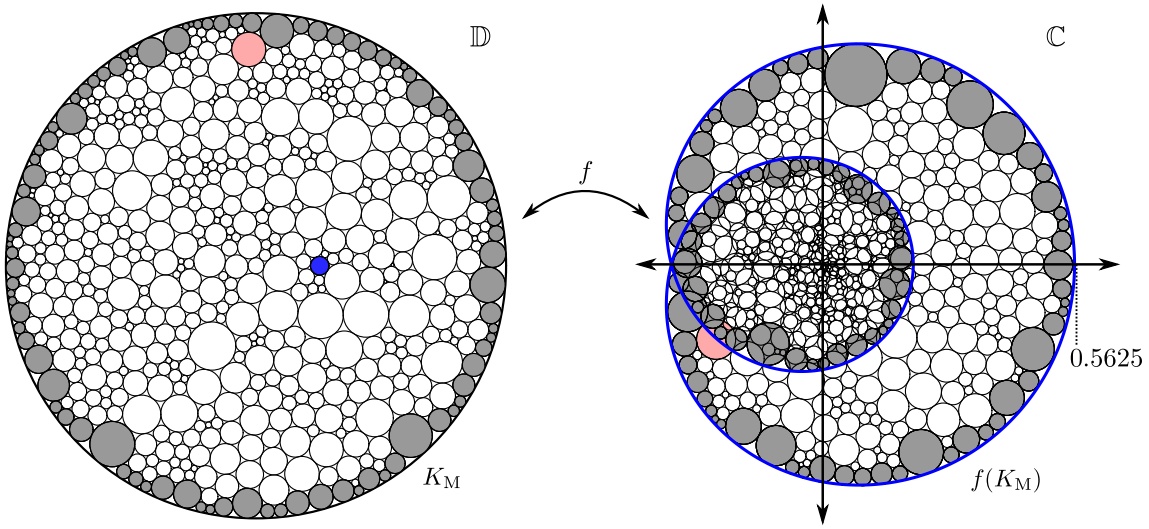


Figure 4.1: A discrete quadratic polynomial. The border circles have been shaded and the branch circle has been colored blue. Because it has become so small the branch circle is not easy to see in $f(K_M)$, but it is very close to the origin.

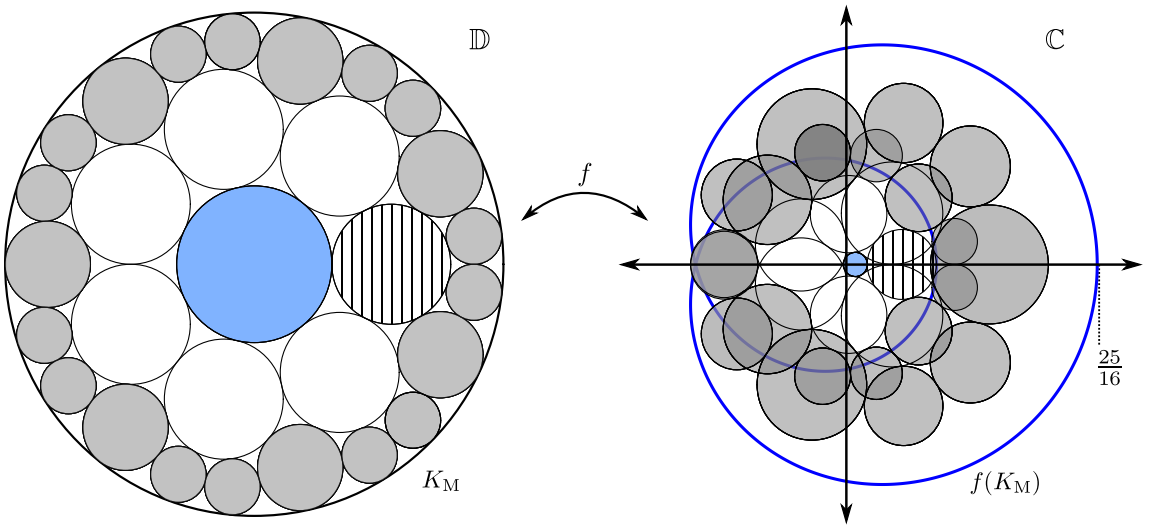


Figure 4.2: A coarse discrete polynomial. The border circles have been shaded and the branch circle has been colored blue. One of the mapped circles has been striped.

of the founding results in circle packing. Its existence and uniqueness are a result of the Discrete Uniformization Theorem as proved by Alan Beardon and Stephenson [6].

First the classical Ahlfors function is defined and discussed. A proof of its existence is outlined below using normal families and Montel's Theorem.

Theorem 4.1. (Montel's Theorem) Let $\mathscr{F}$ (or $\mathscr{F}(\Omega)$) be the family of analytic functions on a plane domain Ω. $\mathscr{F}$ is uniformly bounded on each compact subset of Ω if and only if every subsequence in $\mathscr{F}$ has a subsequence that converges uniformly on each compact subset of Ω, i.e., $\mathscr{F}$ is a normal family.

For a proof see [15]. One can apply Montel's theorem to guarantee the existence of extremal functions for extremal problems. For instance, consider the problem of maximizing the derivative at a prescribed point over a family $\mathscr{F}$ of (analytic) functions $f(z)$ on a domain Ω such that $|f(z)| \leq 1$ in Ω. Now fix a point, say z_0, in Ω and determine the maximum $|f'(z)|$ over all functions in $\mathscr{F}$. The *extremal value* or *analytic capacity* of $\mathscr{F}$ is

$$\mathscr{A} = \sup\{|f'(z_0)| : \ f \in \mathscr{F}, \ |f(z)| \leq 1, \ f(z_0) = 0\}.$$

Functions $f \in \mathscr{F}$ are uniformly bounded. So their derivatives are also uniformly bounded at z_0, and thus so is $\mathscr{A}$. A function $A \in \mathscr{F}$ such that $|A'(z_0)| = \mathscr{A}$ is an *extremal function*. A sequence $\{f_n(z)\}$ of functions in $\mathscr{F}$ such that $|f_n'(z_0)| \to \mathscr{A}$ must have a subsequence that converges normally on Ω to a function $A(z)$ by Montel's theorem. The convergence is normal so then $|A(z)| \leq 1$ and $|A'(z_0)| = \mathscr{A}$.

The function $A(z)$ is called the *Ahlfors function*, named after Lars Ahlfors who showed the existence and uniqueness of such functions when he first introduced the concept; with some modesty he later described this honor as undeserving [22, 1]. When Ω is simply connected the Ahlfors function is a conformal map onto the unit disc. Analytic capacity is a generalization of Schwarz's Lemma for multiply connected domains. This is exactly what motivated Ahlfors to study the notion [22].

Recall that the ratio function is the analog of the modulus of the derivative for discrete analytic functions.

Lemma 4.2. ***Discrete Schwarz Lemma.*** *Let $K(R, I, A)$ be the motif in $\mathbb{D}$ for an admissible decorated closed disc. If $K(\mathcal{R}, I, A)$ is the maximal motif then $R(v) \leq \mathcal{R}(v)$ for every vertex v in K; equality for any interior v implies $R \equiv \mathcal{R}$.*

For a proof when $I \equiv 1$ see [44]. Because Monotonicity holds the proof can easily be adapted for admissible decorated complexes.

Thus by the discrete Schwarz Lemma for simply connected complexes, the image of a *discrete Ahlfors function* (DAF) is the Maximal packing of a decorated complex. Existence and uniqueness of this function comes by the Discrete Uniformization Theorem. The only limitations introduced by discretization can be easily avoided by introducing some combinatorial prerequisites. These requirements, what we call admissibility, ensure that a label will exist for its decorated complex. They are however not particular to the maximal packing.

The situation is much different for an annulus. In the classical case, for an n-connected planar domain Ω, the Ahlfors function is a branched analytic function mapping K, n-to-one, and onto

the unit disc with $f(z_0) = 0$. If the boundary curves are Jordan curve, the function will extend continuously to the boundary of Ω. The natural analogue is to find a circle packing such that each boundary circle is a horocycle. We will see that generally discretization prevents this from being possible with circle packing. Why this occurs and how we might obtain a discrete version of the Ahlfors function is the subject of this section.

In the classical setting the branch points of an Ahlfors function are uniquely determined by the point z_0. However a complex supplies us with only a finite selection of vertices for branch points. The geometry created in the dance between combinatorics and radii determines their locations, and on the annulus generally one would not expect to be so lucky that any pair would coincide with their needed location. Indeed we will need to rely on symmetry to construct a simple example that is coherent.

Let $K(I, A)$ be an admissible decorated complex such that K is a topological annulus. If $A \equiv 2\pi$ then $K(I, A)$ has an (essentially) unique label filling some round annulus $A(r_{\text{inn}}, r_{\text{out}})$, where $r_{\text{inn}} \leq r_{\text{out}} \leq \infty$. Typically $r_{\text{out}} = 1$, so it equivalently can be thought of as the boundary of $\mathbb{D}$. Call this label R_{A} and this branched motif the *nested annulus* $K(R_{\text{A}}, I, A)$. By simply attaching a vertex to one of K's border elements it can be made into a disc. The existence and uniqueness of the nested annulus follows directly from the existence and uniqueness of the Maximal packing, and $P_{K(R_{\text{A}},I,A)}$ is a circle packing.

Figure 4.3 shows a nested annulus (with $C(r_{\text{out}})$ removed) on the right. The left is the same complex with different border radii. Identified borders have been marked green and blue. The "dashed" pink circles are identified with the "non-dashed" pink circles.

Figure 4.3 currently has no branching. By Theorem 3.12 the sum of its turning angle must be 0. It has two border elements; on the right one with turning angle of positive 2π and the other with negative 2π, and on the left turning angles are both 0.

Definition 4.3. Let $K(\mathcal{R}, I, A')$ be a branched maximal motif. If $K(\mathcal{R}, I, A')$ is coherent then $f\colon P_{K(R_{\text{A}},I,A)} \to P_{K(\mathcal{R},I,A')}$ is a *discrete Ahlfors function* (DAF). $P_{K(\mathcal{R},I,A')}$ is called an *Ahlfors packing* of $K(I)$.

The boundary of $\mathbb{D}$ has an extrinsic curvature of -1, but it can be embedded in $\mathbb{C}$. So if a border chain is tangent to the boundary and has trivial holonomy we can conclude that it's turning angle is a positive multiple of 2π. Furthermore, to preserve the proper analogy we need each border chain of an Ahlfors packing to wrap around the boundary only once. Thus each border chain in the image needs to have a turning angle of 2π. Theorem 3.12 then necessitates that an Ahlfors packing must have two branch points.

As mentioned, discreteness generally prevents such packings from being realizable, and to create a concrete example we must use symmetry. Returning to the example in Figure 4.3 we have such a packing. We set the angle assignments to 4π at each shaded circle, 2π elsewhere in the interior, and the border radii to ∞; `CirclePack` then applies a standard circle packing algorithm and finds the label. The result is shown in Figure 4.4. Do not worry; no circles were harmed in this packing. Because of the symmetry each trivial branch circle has been mapped precisely onto its symmetric partner —border to border circles and interior to interior circles.

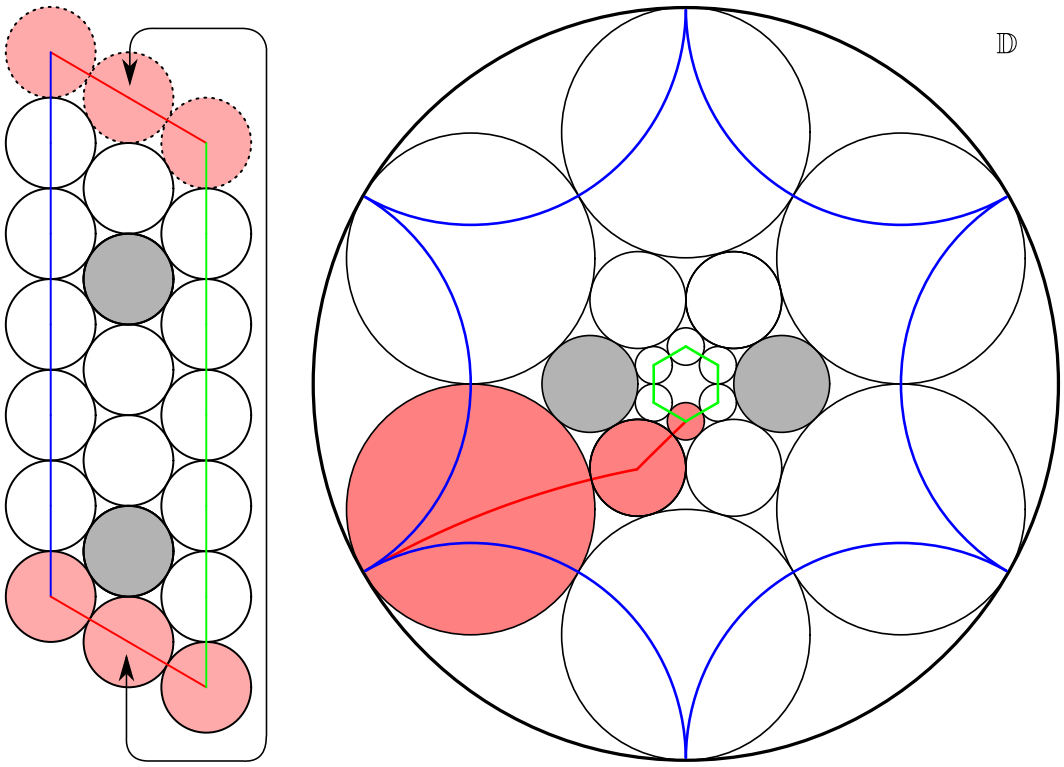


Figure 4.3: Two different motifs and layouts of an annulus. The border elements' edges are marked as green and blue. The gray circles are where the branching will occur in the Ahlfors function.

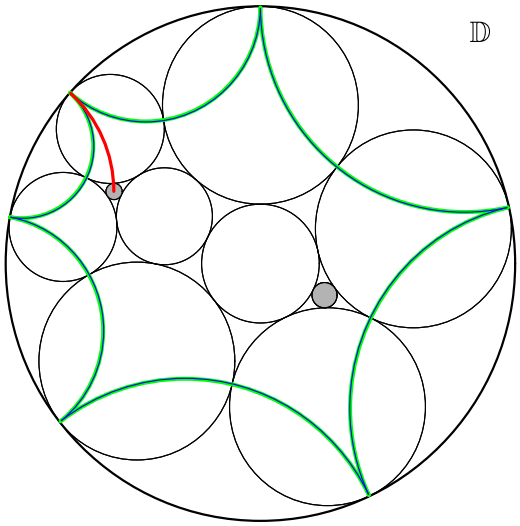


Figure 4.4: The Ahlfors Packing of the example from Figure 4.3. Branching occurs at the shaded circles. The blue and green edged borders have been identically mapped.

We slightly modify the example from Figure 4.3 by applying a *Whitehead move*. As illustrated in Figure 4.5 a Whitehead move replaces one interior edge with another in the union of two edge-sharing faces. Such a modification does not change the global number of faces, edges, or vertices. It only changes the combinatorics locally. These local changes invoke global geometric changes (differing Whitehead moves from *edge flips* which are done strictly in the context of fixed geometric vertices).

We now try to find the DAF of this modified complex. Call the layout of the motif $K(\mathcal{R}, I, A')$, $L_{K(\mathcal{R},I,A')}$. If $K(\mathcal{R}, I, A')$ is incoherent then the map $f\colon P_{K(R_{\mathrm{A}},I,A)} \to L_{K(\mathcal{R},I,A')}$ will be multi-valued. However there are maps of sub-motifs of the nested annulus that are well defined. $K(\mathcal{R}, I, A')$ is a branched motif; so for example, any map of a flower in $K(R_{\mathrm{A}}, I, A)$ will be coherent. Call a map with a coherent image a *function element*, denoted (M, f) where M is a motif. Let (M_1, f_1) and (M_2, f_2) be two function elements. If $f_1 \equiv f_2$ on $M_1 \cap M_2 \neq \emptyset$ then (M_1, f_1) is an *analytic continuation* of (M_2, f_2), written $(M_1, f_1) \sim (M_2, f_2)$. In the case that $K(\mathcal{R}, I, A')$ is not coherent, repeated continuation of a single-valued function element can produce a multi-valued function.

As above, the motif must have a branch order of two. This is where discreteness creates an impasse. Because our selection of branch points is limited to the number of interior vertices, 21 in this case ($\frac{6!}{2\cdot 4!}$ for choosing 2 out of 6 vertices and then +6 for the possibility of placing all the branching at one vertex). The labels for all these possibilities are easily computed with `CirclePack`.

Let $\partial\Gamma$ be the border chain which contains the blue edge illustrated in Figure 4.3. Using `CirclePack` we first compute the labels and then the error E_K for each possible branch set. Figure 4.6 illustrates the incoherence of the motif for the case with branching at vertices 9 and 12. Two different paths Γ_1 and Γ_2 are used to locate the same face (with vertices 4, 10, and 16). Here it can be seen how incoherence is a discrete analogue of an ambiguously defined map.

This label is the unique set of radii which satisfies all the edge and angle sum requirements of the complex, however different layouts result in different locations for these circles. The layout of each of these chains is a function element, and together they form an analytic continuation which gives rise to a multi-valued function, i.e., a layout of an incoherent motif. The E_K for each possible branch pair are easily computed and seen not to produce a coherent label. Each resulting motif lacks well defined circle locations, similar to that illustrated in Figure 4.6.

4.5 The Weierstrass Function

The surface of the three-dimensional torus is a closed (compact and without boundary) 2-manifold of genus 1. So in this sense it is the simplest non-simply connected closed surface, and it plays the progressive role for the sphere that the annulus does for the disc. Perhaps expectedly, attempts to discretize classical branched functions related to this surface encountered similar difficulties.

A standard geometric representation of a two-dimensional torus T is found by opening the torus along any two non-homotopic fundamental curves from some base point. The resulting simply connected sheet can be embedded in $\mathbb{C}$ as a Euclidean parallelogram Ω with identified opposite edges (see Figure 4.7).

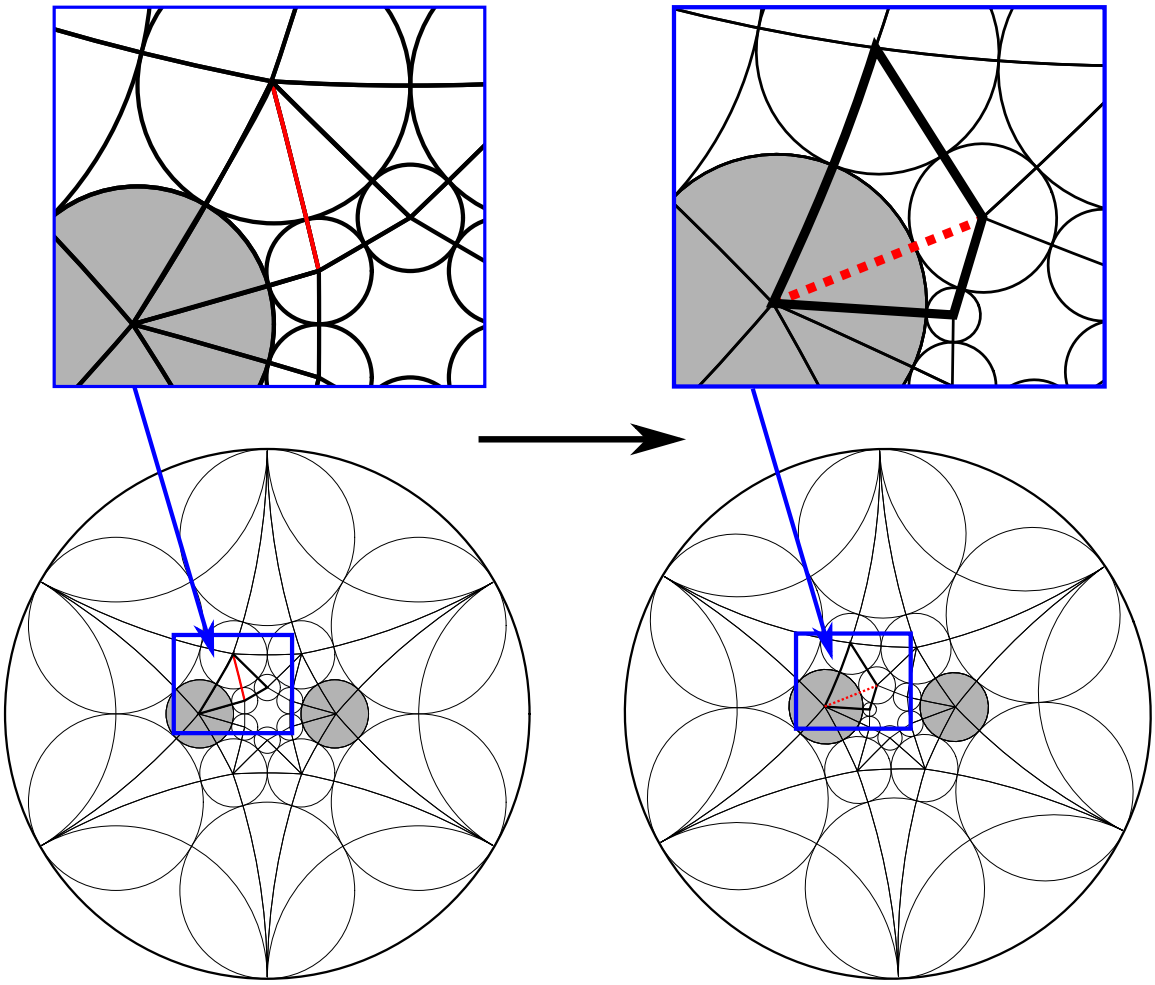


Figure 4.5: The complex is modified with a Whitehead move. The packing before and after the move is illustrated on the left and right, respectively. The solid red edge is replaced with the dashed red edge.

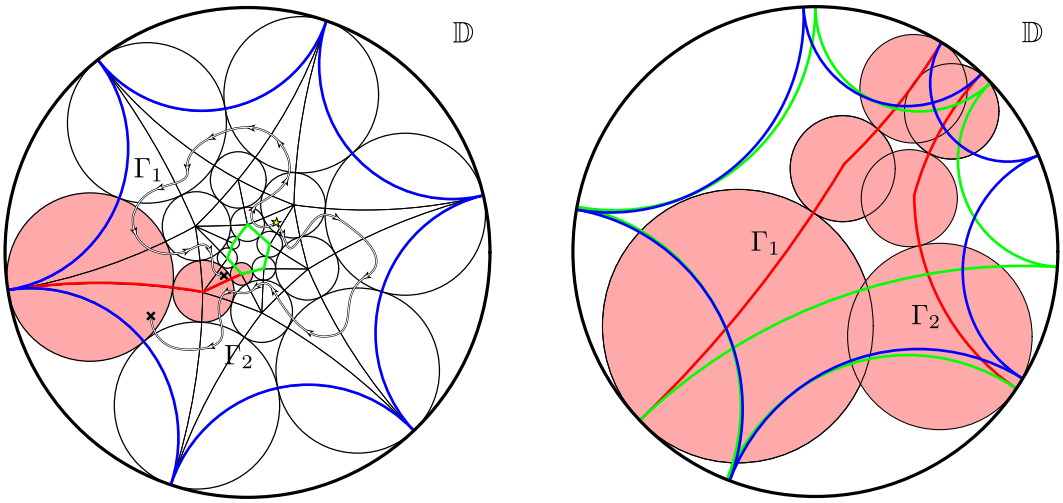


Figure 4.6: Function elements layout the incoherent motif. Using the same label, two different chains, Γ_1 and Γ_2 are used to locate the same three circle (in pink). The label places branching of order 1 at vertices 9 and 12 on the complex from Figure 4.4.

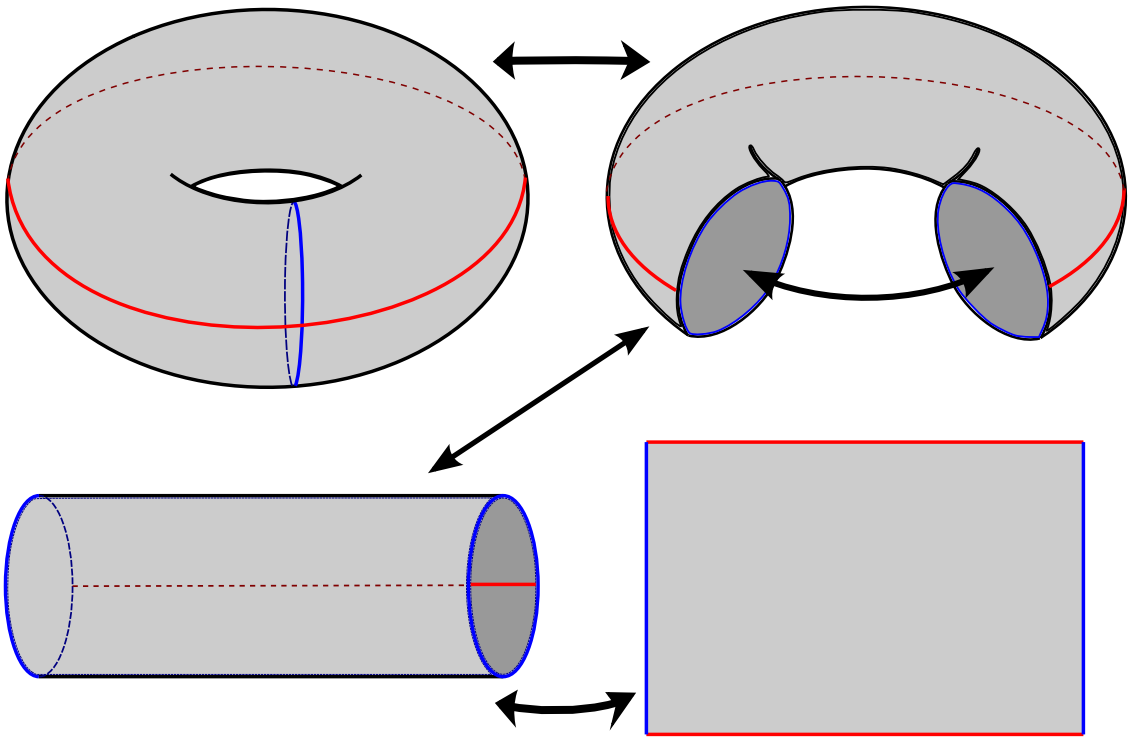


Figure 4.7: The torus "unwrapped".

Repeatedly translating Ω's edges so that edges are identified generates a lattice group

$$\Lambda = \{\phi : z \mapsto z + m\omega_1 + n\omega_2 : \ m, n \in \mathbb{Z}^+\} \subset \mathrm{Aut}\,(\mathbb{C})\,,$$

and copies of Ω tile the plane (see Figure 4.8).

The fundamental group of the torus is the direct product of the fundamental group of the circle with itself, $\pi_1(T) \cong \pi_1(S^1) \times \pi_1(S^1)$ ($\pi_1(X, x_0)$ or $\pi_1(X)$ denotes the fundamental group of X formed by the set of all homotopy classes of loops with base point x_0). The two parts of this product are fundamental groups formed by loops, and the curves we used to open the torus are each homotopic to a different one of these loops. So then the parallelogram Ω is T's fundamental region, and for every orbit, $\mathcal{O}_z = \{\phi(z) : \phi \in \Lambda\}$, on $\mathbb{C}$ there is a unique associated point on T. The collection of these orbits form a topological surface which is equivalent to T, i.e., $T = \mathbb{C}/\Lambda$.

This representation of T provides a geometric structure more accessible than its three-dimensional form. Furthermore, $\mathbb{C}/\Lambda$ inherits the conformal and metric structures of $\mathbb{C}$, and the algebraic properties of an Abelian group. The former properties allow curves on T to be lifted to $\mathbb{C}$ and measured Euclideanly. Thus an angle between curves on T is the angle between the lifted curves. So $T = \mathbb{C}/\Lambda$ is a conformal torus.

It is the lifted torus (of T to $\mathbb{C}/\Lambda$) that we use to create discrete versions of tori. Loops in circle packing are closed chains of faces. Given a triangulation of a torus, K_t, we can find two simple closed chains that are neither homotopic to each other or the null chain. Every other closed chain will be an element in the group generated by these chains. So K_t can be opened similarly to above using these two fundamental chains, and the resulting complex with opposite edges identified, say K_F, is the fundamental region.

Now provide decorations for K_t and compute a label. Will the resulting motif be coherent in $\mathbb{C}$? It would need to be locally coherent at every vertex. Treat K_F as a simply connected disc by assigning identical radii to identically mapped circles. If K_F is admissible then Theorem 2.13

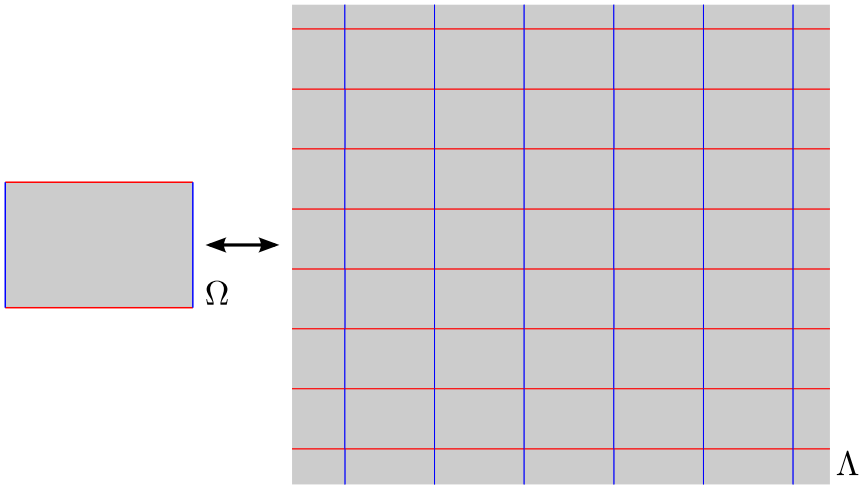


Figure 4.8: The lattice Λ generated by the fundamental region Ω.

guarantees a label, and this label will be coherent as long as each angle sum assignment is locally coherent. However this does not give local coherence at the vertices along the generating chains, all interior vertices of T. If K_F is to be coherent as a fundamental region of T these vertices must have angle sums that are also integral multiples of 2π.

Though it appears we have the necessary tools, a generalization for admissible edge assignments will have to wait. As our primary interested is in branched functions, the univalent case will suffice as a domain. Using this proposition, a circle packing for the universal cover (Λ) of any triangulation of the torus can always be found. It is the functions from these circle packings on the torus to the Riemann sphere ($\mathbb{P}$) which we want to investigate.

Definition 4.4. A meromorphic function $f\colon \mathbb{C} \to \mathbb{P}$ is *elliptic* with respect to a lattice $\Lambda \subseteq \mathbb{C}$ if f is doubly periodic with respect to Λ.

Periodicity is a characteristic that applies equally well to chains as it does for curves. So this classical definition needs no modification for our discrete setting, and from figure 4.9 we easily see that the lattice of T is doubly periodic. Elliptic functions were in fact named for ellipses; albeit the relation is somewhat indirect. Gauss is credited with first discovering (but not publishing) that the length of an ellipse's arc can be expressed as an integral of an elliptic function [29].

Our interest in elliptic functions is a bit more vogue. Elliptic functions are to the torus what rational functions are to the sphere. These functions are by definition doubly periodic. Conversely any doubly periodic function on $\mathbb{C}$ will generate an associated fundamental parallelogram, and so is a function on a torus.

An elliptic function is bounded, so if it has no poles then it is known to be constant by Liouville's Theorem. It also turns out that no elliptic function can have only a single pole. So interesting functions on the torus are meromorphic with at least two poles. Construction of an elliptic function with only two poles is not trivial. The *Weierstrass function* (*$\wp$-function*),

$$\wp(z) = \frac{1}{z^2} + \sum_{\omega \setminus 0 \in \Lambda} \left(\frac{1}{(z-\omega)^2} - \frac{1}{\omega^2} \right),\ z \in \mathbb{C},\ z \notin \Lambda,$$

(associated with Λ) is such a function. The $\wp$-function is a doubly-periodic meromorphic function, and we can see that the poles of order two at its lattice points determine the function.

It is important not only as an example, but because $\wp$-functions can be used to construct all elliptic functions. Every elliptic function f associated with Λ can be written as

$$f = R_1(\wp) + \wp' R_2(\wp),$$

where R_1 and R_2 are rational functions. $\mathbb{C}(\wp, \wp') \subset \mathcal{E}(\Lambda)$ where $\mathcal{E}(\Lambda)$ is the field of all elliptic functions on Λ and $\mathbb{C}(\wp, \wp')$ is the field of rational functions of $\wp$ and $\wp'$. So then $\mathcal{E}(\Lambda) = \mathbb{C}(\wp, \wp')$ [29].

The function f is thus a degree two branched covering map of the sphere. Any degree two cover of $\mathbb{P}$ branched over four points is the image of an elliptic function and thus can be represented with a $\wp$-function up to some Möbius function of $\mathbb{P}$. Edward Crane has constructed a discrete $\wp$-function

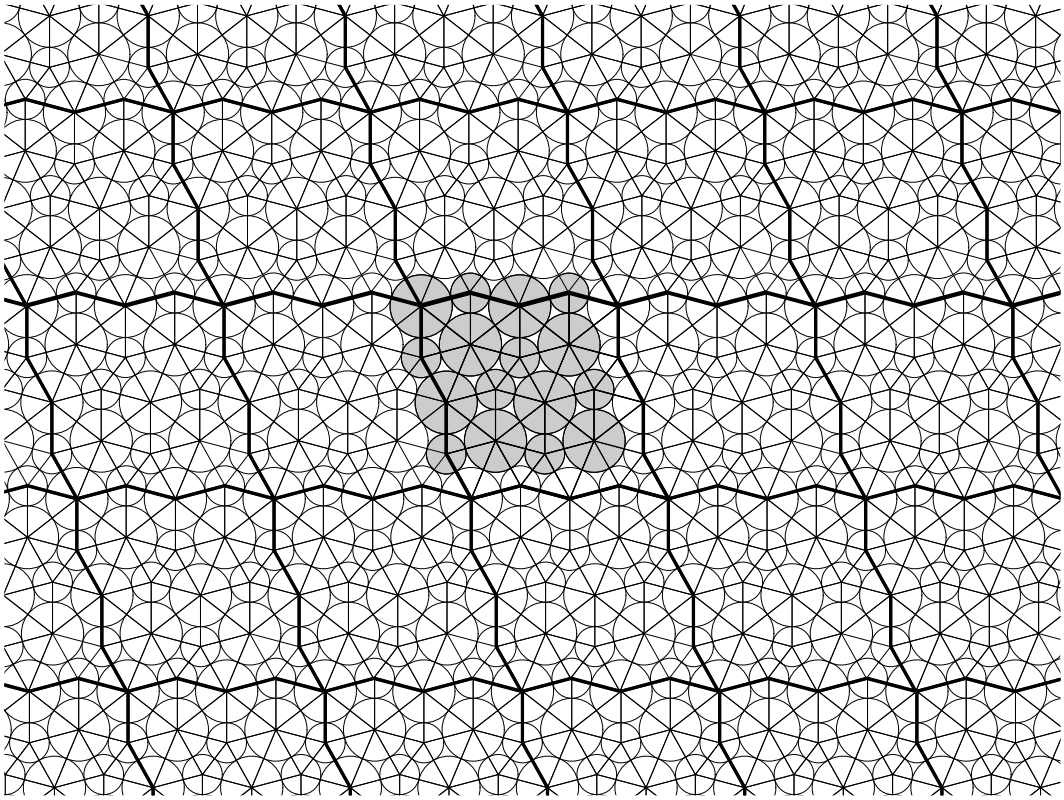


Figure 4.9: A lattice generated by a circle packing of a fundamental region.

using the following method. Using any triangulation of the torus, find the circle packing of its universal cover. Now mark a circle, say b, to be branched, and pull back by $z \mapsto 2z$ to obtain a circle packing with a fundamental region that has four times as many circle. The pull back has four copies of b, say $\{b_1, b_2, b_3, b_4\}$, all in the same orbit of the original fundamental region.

Now puncture one of the branch circles, say b_1, and find the maximal (branched) packing on $\mathbb{D}$ (for this reason we need to assume that the motif has no overlaps on the branch circle b_1) with angle sums of 4π at the remaining three branch vertices. A hyperbolic label for such a packing is guaranteed to exist and be unique. The question is whether it will be coherent.

If the punctured motif is coherent, then a projection onto $\mathbb{P}$ will also be coherent. When projected to the sphere the max-packed punctured torus is a non-bordered multi-connected surface of genus two, and projection preserves coherence. It will be seen that having two non-homotopic fundamental chains with trivial holonomy is a necessary and sufficient condition for this motif to be coherent (Remark 5.2), regardless of whether its geometry is $\mathbb{P}$ or $\mathbb{D}$. Note that this is not a polynomial branched packing which would need to have half its branching at a single vertex (see [12]).

Experimentally, this appears to work. The pull back action creates a symmetry that, similar to what we saw above with the DAF, prevents the combinatorics from getting in the way (exactly why this is so is still unclear). The first example is a simple triangulation with only 16 vertices. It is a pull-back of a 4 vertex torus; 2 vertices have degree 5 and the other 2 have degree 7. Following Crane's method described above an approximate solution is produced (see Figure 4.10).

By approximate solution we mean a coherent motif with an acceptably small holonomy error computed with `CirclePack`. Using a pair of fundamental chains we find that this example has an error of $E_K \approx 0.0$. The resulting branched packing of degree 2 on the sphere has a $S_2 \times S_2$ of Möbius symmetries. The branch points are on a single orbit of the 2-torsion, $(\Lambda/2)/\Lambda$; thus the four branch vertices in each orbit can be mapped to have equal spherical radii [17].

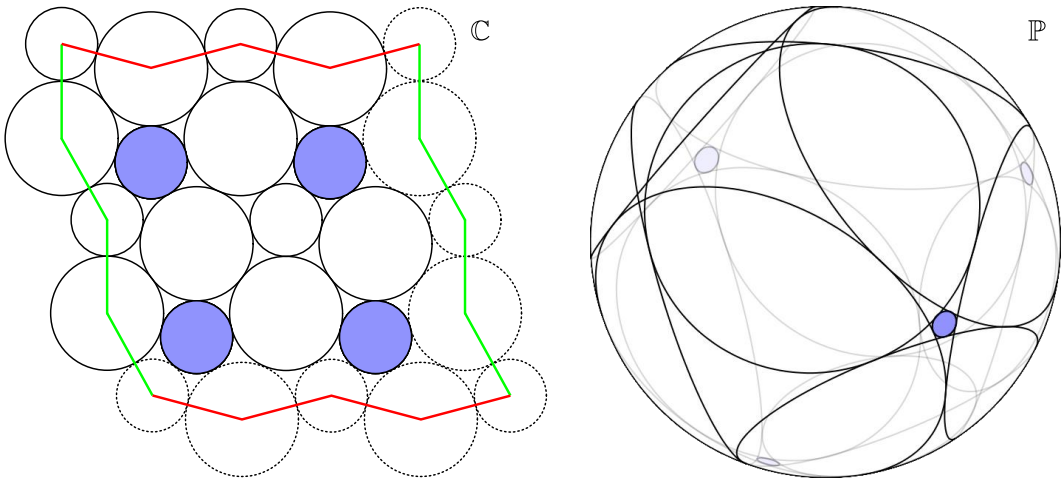


Figure 4.10: The fundamental region of a symmetric 16 vertex torus. On the right is its branched image on the sphere.

Another example is shown in Figure 4.11. A pull-back of a 12 vertex hex torus. Again symmetry provides a coherent branched spherical motif. As in Figure 4.4, trivial branch circles are mapped precisely onto their symmetric partner.

Flipping a single edge in either of these examples breaks the symmetry and we lose the coherence. This can be easily checked by measuring the error of the punctured torus on the disc. It is also easily checked that no other choice of branch circles gives a solution. See Figure 4.12 and 4.13 for illustrations of how the flips break symmetry and cause incoherence. For each example, repeated developments of a face using the same closed chain were laid out. Each successive development finds a different location for the face, demonstrating the incoherence of the different motifs.

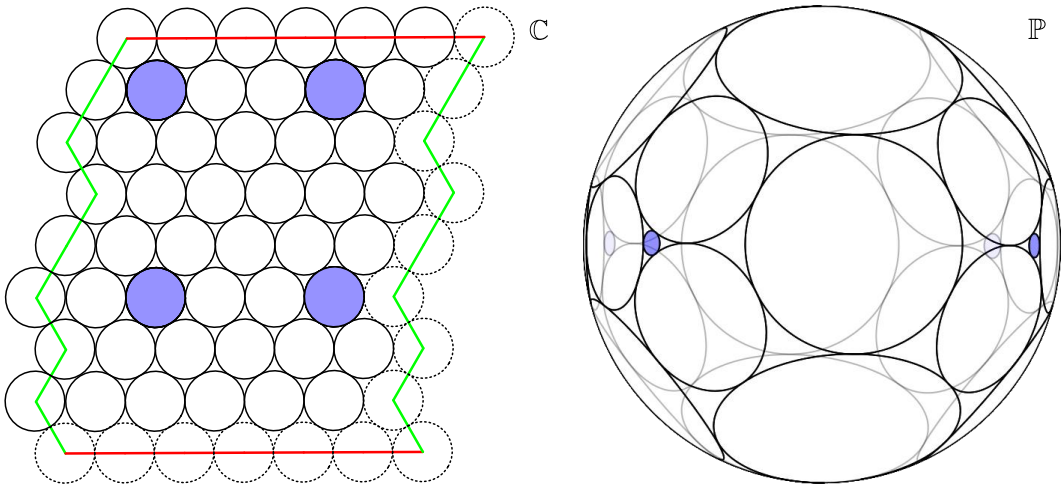


Figure 4.11: The fundamental region of a symmetric 48 hex packed torus. On the right is its branched image on the sphere.

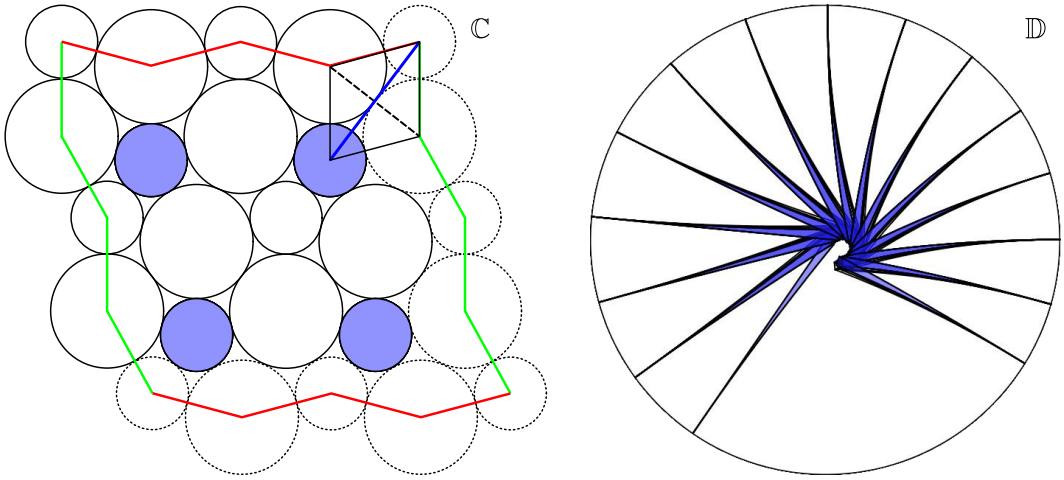


Figure 4.12: Breaking the symmetry of the symmetric 16 vertex torus. The edge created by the flip is colored blue; the dashed edge is removed. For simplicity only the faces of the chain are shown, and the base face is colored blue.

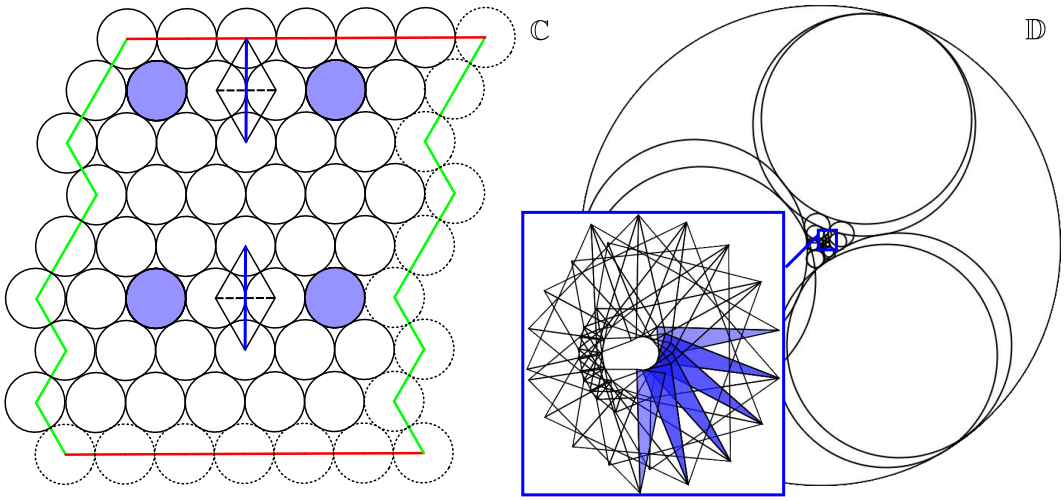


Figure 4.13: Breaking the symmetry of the symmetric 48 hex packed torus. Components are colored as in Figure 4.12.

Chapter 5

Generalized Branching

Chapter 4 demonstrates an intrinsic failure of circle packing to properly model classical functions. These problems are congenital to the discrete characteristics of circle packing, and thus unavoidable without the introduction of some type of flexibility. It would be desirable for such a method to have a controllable parameter. For predictability it should be monotone, and the range of its effect should be broad enough to provide sufficient flexibility. Seasoned circle packers will attest that these properties are also desirable for proving existence and uniqueness results.

Consider the angle sum of a flower parameterized by it's central radius. It is monotone (actually convex); increasing or decreasing the radius always causes the angle sum to decrease or increase, respectively. Furthermore, the end behaviors give the angle sum (with some combinatoric prerequisites) enough scope to guarantee that it can obtain a targeted value (usually some multiple of 2π).

The decorations presented in Chapter 2 are likely candidates for being adjustable parameters. However angle sums are too restrictive because of local coherence conditions, and inversive distance is not monotone (recall Figure 2.6). Another idea is to puncture branch points and manipulate the created border chain. This idea will be explored in Chapter 8, but predictability and retaining admissibility proves difficult.

Chapters 6 and 7 develop some promising alternative methods for inducing branching. Their successes and failures will be demonstrated in Chapter 8. The basic idea is to insert non-traditional structures contained within a sub-complex that is viewed as the branch point. If a closed chain encircling this sub-complex has trivial holonomy and the motif is coherent elsewhere then the compliment is coherent, i.e., it is a circle packing with limited areas that are ambiguous. Formalizing this idea is the subject of this chapter.

Definition 5.1. Let $K(I, A)$ be a decorated complex and R a label for K. A simply connected sub-complex with at least one interior vertex is a *generalized branch point* for the label R if its border chain has trivial holonomy.

A motif will be called a *generalized (branched) motif* if it satisfies conditions for a (branched) motif outside the generalized branch point(s). The nexus and petals of a flower form a border chain

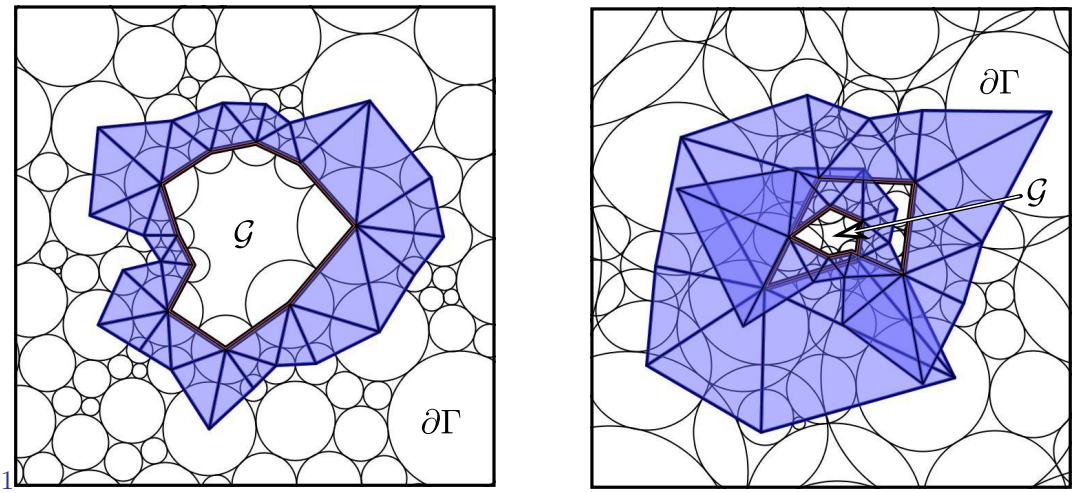
so a coherent flower is a generalized branch point. If additionally the flower is admissible then it fits the mold of our previous definition branch points; call it a *traditional branch point*.

For the border chain to have trivial holonomy it must have a turning angle (with Euclidean data) which is $2\pi n$ for some integer n by Theorem 3.12. This means that generalized branch points express similar geometric characteristics to those of a traditional branch point with the exception that n can be negative. Hence a generalized branch point will coherently express branching regardless of whether its interior is coherent or not. For this reason generalized branch points can be used to "quarantine" areas of incoherence so that the super-motif can elsewhere be treated like a circle packing. Laying out generalized motifs will be done as described in Section 3.2 except that *generalized branch points only have their border chains laid* –the interiors of the generalized branch points are ignored.

Let Γ be the border chain of a generalized branch point. As $\phi(\Gamma)$ is assumed to be trivial, laying out Γ uniquely places (up to isomorphisms) every face in the chain. The neighboring faces not in the generalized branch point then have their positions determined as well. The generalized branch point provides structural properties similar to those given by locally coherent flowers.

Laying out a generalized branch point from a motif can thus be seen as no different than laying a face, and so they can be used in the same way that faces are used for developments and modifications (see Figure 5.2). So the concepts employed in the proof of the Monodromy Theorem (Theorem 3.9) can seamlessly be applied to a generalized motif. It follows that a generalized branched motif with a simply connected complex will be coherent.

Remark 5.2. Faces and generalized branch points can be laid with developments via closed chains that include branch points. A chain can be written as a concatenation using a subchain from the branch point's border chain. So chains can be modified using the border chains of generalized branch points just as if they were traditional branch flowers. Furthermore the minimal set of generating chains in the generalized branched motif can be assumed to be identical to the set for $\mathcal{G}(K)$.



5.1

Figure 5.1: A generalized branched point. The interior of the generalized branch point, $\mathcal{G}$, does not get used in the layout of the generalized branched motif.

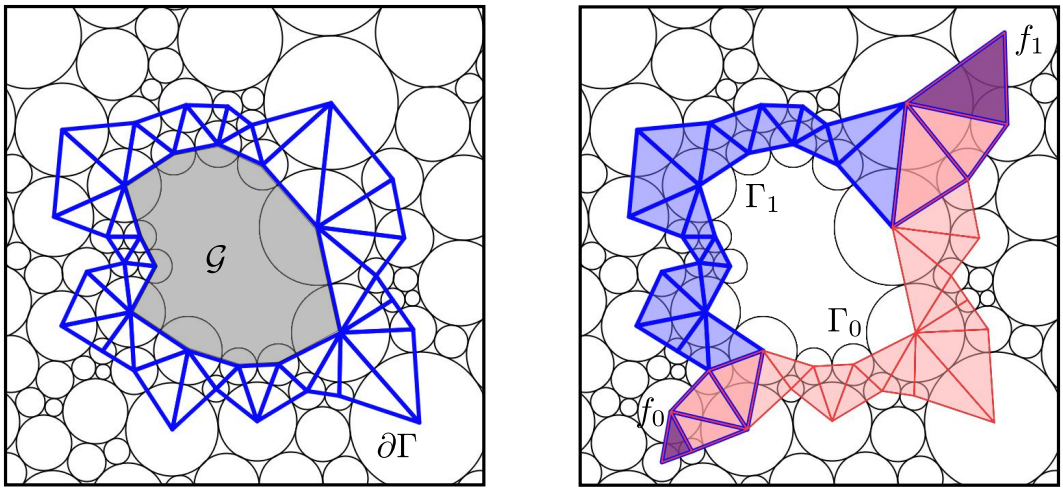


Figure 5.2: Laying out a generalized branched motif. The modifications on the right illustrate how the border of $\mathcal{G}$ behaves similarly to a face.

Definition 5.3. If any two layouts of a generalized branched motif are Möbius images of one another it is called a *branched circle packing*.

Henceforth branched circle packings and motifs will be assumed to possibly include generalized branch points. The notion of branch set (see Definition 2.6) will be extended to include generalized branch point; its elements will now be vertices and sub-motifs. To distinguish when strictly traditional branch points are being used, the packing or motif will be called *traditional*.

Chapter 6

Fractional Branching

Circle packings have an inherent rigidity beyond their classical counterparts. Their discreteness introduces further restrictions like those illustrated in Chapter 4. These limitations have been known hurdles from the beginning, especially for multi-connected complexes. In particular many open and difficult questions involve branched meromorphic functions. Just recently Edward Crane demonstrated the non-uniqueness of branched spheres [17], and there is still no direct method for computing labels on the sphere (branched or unbranched).

As a means to overcome the limitations of discreteness, Ken Stephenson suggested the use of "fractional branching" as a potential method to circumvent these problems [44]. The idea was that a collection of neighbors could represent the branching by sharing the extra angle sum, and that the distribution of this extra 2π might be adjusted to eliminate holonomy and obtain global coherence.

When conceived, Stephenson had meromorphic functions particularly in mind. Elias Wegert and David Bauer have also suggested that fractional branching might be an approach to overcoming issues in discrete Riemann-Hilbert problems [48]. Owing to an evolution via personal communication this concept has also been called "fractured branching".

Traditional branched circle packings are locally coherent and thus each branched flower is on its own a circle packing. However angle preservation is lost at classical branch points in classical maps. Therefore a reasonable discrete analogue of a multi-sheeted function could (or maybe should) include structures which fail to be coherent at a vertex or at a sub-complex.

This is what fractional branching seeks to do; partitioning the extra angle on a chain of vertices instead of a single circle. Setting angle assignments to non-integer values causes the motif to be locally incoherent and thus globally incoherent. However, as discussed in Chapter 5, if a holonomy containing these points is trivial the complementing motif will be globally coherent.

When this happens one can consider the branching to occur on the face or connected faces enclosed by the vertices. In this way the "singularity" can be expressed not on a single vertex as per usual but instead on a sub-motif. The sub-motif will then be a generalized branch point, and the parent motif a branched circle packing.

Fractional branching is an interesting and aesthetically pleasing alternative to traditional branching. In service of introducing flexibility, it will be seen that fractional branching's spectrum

of behavior varies from bad to good. It would be preferable to have an adjustable parameter which has a unique generalized branched circle packing for each value. As seen in Section 6.2, Fractional branching on tangency motifs lack flexibility while potentially lacking uniqueness. Adjusting the edge assignments on the sub-motif allows flexibility but the problem with uniqueness persists. The good news, Theorem 6.8 demonstrates that uniqueness holds when additional assumptions are placed on the edge assignments.

This chapter will explore fractional branching on closed chains of three and four vertices, i.e., singularities expressed on a single or pair of connected faces. A special case of fractional branching on three mutually tangent vertices was studied by the author in [4].

Definition 6.1. Let M_B be a simply connected sub-motif of $K(R, I, A)$ and B the set of interior vertices of M_B's border chain. If $\sum A(v) = 2\pi n$ and $\sum A(v) \bmod 2\pi \neq 0$ for $v \in B$ and $n \in \mathbb{Z}^+$ then $K(R, I, A)$ is a *fractured motif* on B; call B the *fractured points*. (see Figure 6.1).

Alternatively we can start with the fractured points B, and let B define M_B. The requirement that $\sum A(v_i) \bmod 2\pi \neq 0$ means that $K(R, I, A)$ is not locally coherent, making a fractured motif distinct from a branched motif. Following the protocol of Chapter 5, if a fractured motif satisfies the conditions for a generalized branched motif outside of M then it will be called a *fractured branched motif*.

If M's border chain has trivial holonomy then M is a generalized branch point. Moreover, M is a disc so the turning angle of the border chain will be $2\pi n$. Fractional branching is thus an alternative form of branching with which branched circle packings can be constructed. Though a fractured motif is necessarily incoherent this sub-complex may still be coherent, in which case it will be a suitably rigid structure. For example, if $K(R, I, A)$ is a fractured branched motif, M a generalized branch point, and K a simply connected disc then $K(R, I, A)$ is a branched circle packing.

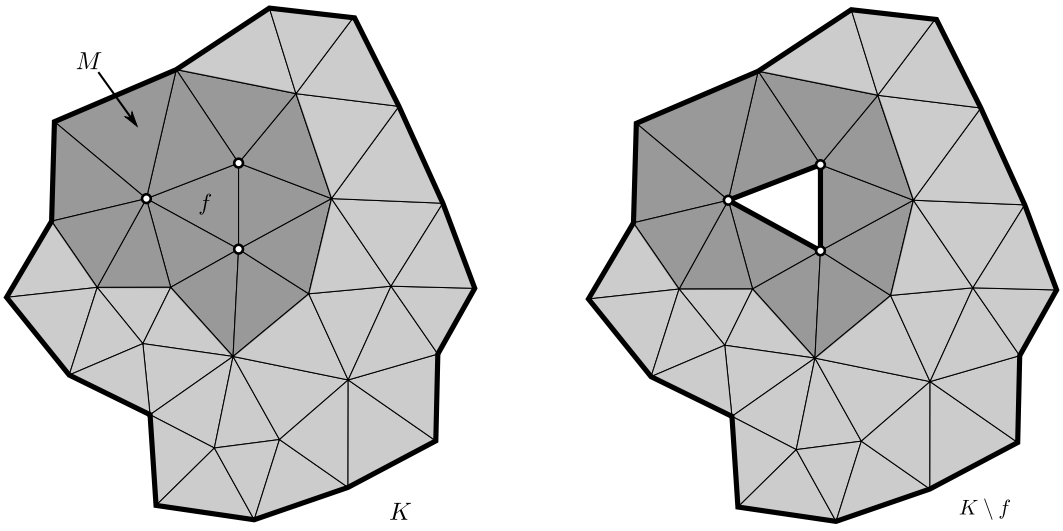


Figure 6.1: Complex of a fractured motif. On the left M is shaded, and the vertices in B are highlighted. On the right the interior of M has been removed leaving its border chain, $\partial\Gamma$.

Definition 6.2. Call a branched circle packing that is fractured on B a *fractured branched circle packing* on B.

Below, M will be a single face or a pair of faces sharing an edge. Possible applications abound, but in keeping with the overall theme of this work we keep the alterations confined to small areas.

6.1 Fractional Branching on Three Vertices

Recall that for a motif $K(R, I, A)$ we denote the angle sum at an interior vertex v with $\theta(R(v)) = \theta(v)$. Below we use the *floor function*, $\lfloor x \rfloor = \max\{n \in \mathbb{Z} \colon n \leq x\}$ for $x \in \mathbb{R}$.

Theorem 6.3. *Let K be a simply connected complex with a strictly interior face $f = \{v_1, v_2, v_3\}$. Then a fractured branched motif $K(R, I, A)$ is a fractured branched circle packing on f if and only if for each bijection $\{1, 2, 3\} \to \{i, j, k\}$.*

$$\theta(v_i) = 2\pi n_i + 2\theta(v_i; v_j, v_k), \tag{6.1}$$

where $\left\lfloor \frac{A(v_i)}{2\pi} \right\rfloor = n_i$.

The following lemma will be needed.

Lemma 6.4. *In Theorem 6.3, $K(R, I, A)$ is not a fractured branched circle packing if $A(v) = 2\pi n$ for any $v \in f$ and $n \in \mathbb{Z}^+$.*

Proof. Let Γ be the border chain for the fractured points' sub-motif (M in Figure 6.1). R and I define a triangle for f in its geometry, say $\mathcal{T}$, associated with f. $K(R, I, A)$ is a branched circle packing if and only if Γ has trivial holonomy, and $\phi(\Gamma)$ will be trivial if and only if any development using Γ fixes $\mathcal{T}$.

The flowers for v_1, v_2, and v_3 are each closed chains in K, and as developments of $\mathcal{T}$ in $K(R, I, A)$ each flower is a rotation. Coherent flowers are trivial rotations, and incoherent flowers are non-trivial rotations. The turning angles of $\partial\Gamma$ are precisely these flowers minus the angles at $\mathcal{T}$. So then Γ will place the edges of $\mathcal{T}$ emanating from a vertex identically to developments of $\mathcal{T}$ at that vertex's flower.

If $K(R, I, A)$ is locally coherent at say v_1 or v_2, but not v_3 then Γ fixes $\mathcal{T}$ at the first two vertices and then rotates it non-trivially. Now suppose that $K(R, I, A)$ is coherent at only one vertex, say v_1. The rotation at v_2 rotates the edge $e(v_2, v_3)$ repositioning v_3. At v_3 the edge is then rotated repositioning v_2, but then there are no rotations left to return v_2 to its original location (see Figure 6.2). □

Now we begin the proof of Theorem 6.3.

Proof. Let $\mathcal{T}$ and Γ be defined as in the previous lemma. Assume that $K(R, I, A)$ is a fractured branched circle packing on $\{v_1, v_2, v_3\}$. By assumption $K(R, I, A)$ is not locally coherent at all three vertices, and by the lemma it cannot be locally coherent at just 1 or 2 vertices. So Γ has nontrivial rotations at each of f's vertices.

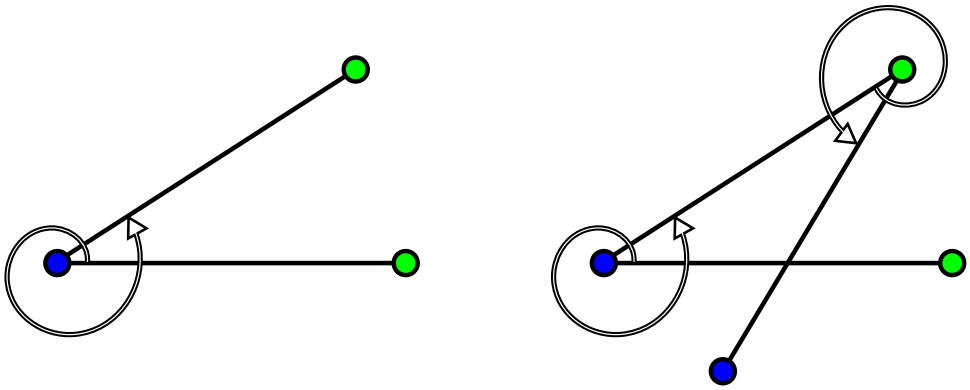


Figure 6.2: Three fractured points are needed. The rotations are done at the blue then the green vertex.

Starting at v_1 we can rotate $\mathcal{T}$ around each of its vertices in sequence such that only the third and final rotation returns $\mathcal{T}$ to its original position. Each rotation produces a copy of $\mathcal{T}$, say $\mathcal{T}_i$ for $i = 1, 2, 3$, each connected at the shared vertex of rotation (see Figure 6.3). The edges of their shared vertices enclose a new triangle $\mathcal{T}'$. Each $\mathcal{T}_i$ shares an edge with $\mathcal{T}'$; $e(v_1, v_2)$ from the first rotation, $e(v_2, v_3)$ from the second rotation, and $e(v_3, v_1)$ from the third. So $\mathcal{T}'$ is a reflection of $\mathcal{T}$, and they have similar angles. Thus the angle of the rotation at vertex v_i is

$$\theta_{\mathcal{T}}(v_i; v_j, v_k) + \theta_{\mathcal{T}'}(v_i; v_k, v_j) = 2\theta_{\mathcal{T}}(v_i; v_j, v_k) \tag{6.2}$$

where v_j and v_k are the other two vertices. Conversely the rotation of $\mathcal{T}$ by $2\theta(v_x; v_y, v_z) + 2\pi n_x$ at each vertex x will return $\mathcal{T}$ to its original location.

Equation 6.1 implies that f's sub-motif is a generalized branch point. Monodromy and Remark 5.2 then imply that $K(R, I, A)$ is a branched circle packing. □

The next theorem shows that given a branched motif $K(R, I, A)$ (with some admissibility assumptions), there exists an angle assignment A' such that $K(R', I, A')$ is a coherent fractured motif on $f = \{v_1, v_2, v_3\}$. In other words, we show that a label meeting the criteria of Theorem 6.3 exists.

Theorem 6.5. *Suppose K is a simply connected complex with a strictly interior face $f = \{v_1, v_2, v_3\}$ and that $K(I, A)$ is admissible with each $A(v)$ an integral multiple of 2π. Furthermore, suppose admissibility holds if the assignment $A(v)$ is replaced by $A(v) + 2\pi$ for $v = v_1, v_2$, or v_3. Then there exists an angle assignment A' such that $K(I, A')$ has a fractured branched circle packing on $\{v_1, v_2, v_3\}$ and $A(v) = A'(v)$ elsewhere.*

Also, the border chain of $K(R, I, A)$ will have trivial holonomy with turning angle $T(\partial\Gamma) = 2\pi(2 + \sum(n_i - 1))$.

Proof. The notation will be the same as in Theorem 6.3. By the same theorem, if such an R exists then $\theta(r_i) = 2\theta(r_i; r_j, r_k) + 2\pi n_i$ for each bijection $\{1, 2, 3\} \to \{i, j, k\}$. Let Λ be a tetrahedron in $\mathbb{R}^3$ with three edges each of length 2π meeting orthogonally at the origin.

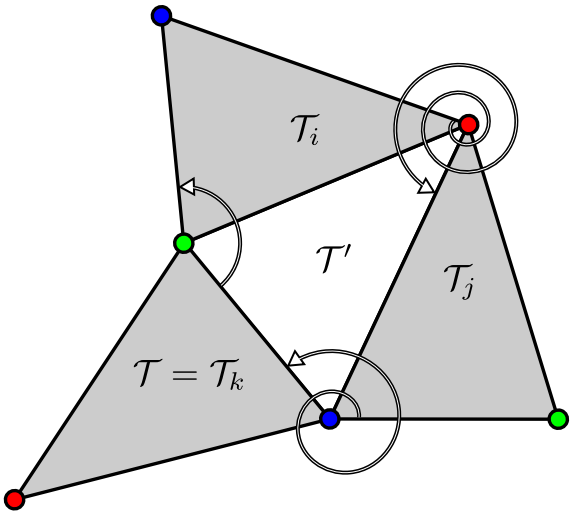


Figure 6.3: The "frac-branch property". $\mathcal{T}$ and its copies for each rotation are shaded gray; the rotations are done in the order of the green, red, and then blue vertex. T' is the enclosed white triangle.

Let $\widehat{A}$ be the collection of angle assignments for K such that for each $A' \in \widehat{A}$,

$$2\pi n_i \leq A'(v_i) \leq 2\pi(n_i + 1) \text{ for } i = 1, 2, 3,$$

and $A'(v) = A(v)$ is an integral multiple of 2π elsewhere. $K(I, A')$ is admissible for every $A' \in \widehat{A}$ because $K(I, A)$ is admissible.

By Theorem 2.13, a unique label exists for each $K(I, A')$, and the angles in $K(R, I, A')$ are a continuous function of A'. Now let $A' \in \widehat{A}$ and $G \colon \Lambda_\theta \to \Lambda_\alpha$ be a map from

$$\Lambda_\theta = \{A'(v_1) - 2\pi n_1,\ A'(v_2) - 2\pi n_2,\ A('v_3) - 2\pi n_3\}$$

onto

$$\Lambda_\alpha = \{2\theta(r_1; r_2, r_3),\ 2\theta(r_2; r_1, r_3),\ 2\theta(r_3; r_1, r_2)\}$$

$2\theta(r_i; r_j, r_k) \in [0, 2\pi]$ so G is a continuous function from the closed compact space Λ onto itself. By Brouwer's fixed point theorem this function must have a fixed point.

A fixed point at one of Λ's vertices would imply that one of f's interior angles would be 0 or π, but this would require R to have a degenerate or infinite radius, something which cannot happen by Theorem 2.13 and assumption, respectively. A fixed point along one of Λ's edges would imply that one of f's vertices was locally coherent which contradicts Lemma 6.4. So the fixed point must be on the interior of Λ, call this angle assignment $A^\star$.

The motif $K(R, I, A^\star)$ is a branched circle packing by Theorem 6.3. As Euclidean angles (projecting to $\mathbb{C}$) if necessary, $\sum_{i=1\ldots3} A^\star(v_i) = 2\pi(n_1 + n_2 + n_3 + 1)$ and $A^\star(v) = 2\pi n$ for some $n \in \mathbb{Z}^+$ elsewhere. So then $T(\partial\Gamma) = 2\pi(2 + \sum(n_i - 1))$ on $K(R, I, A^\star)$ by Theorem 3.12 which completes the proof. □

Figures 6.4 and 6.5 are examples of coherent fractional branched motifs. Figure 6.6 is the same complex used in Figure 6.4.

Any simply connected coherent motif where all border circles are horocycles (a *maximal fractured branched circle packing*) can be projected onto the sphere. The border becomes a traditional branched circle in the spherical image, and as result of its turning angle will have a sum of $2\pi(n_1+n_2+n_3-2)$. This places exactly half the branching at a single vertex; a characterization of polynomial rational maps. So a fractured version of the discrete polynomial functions as seen here [12] can be constructed.

The assumption of $K(R,I,A)$'s incoherence necessitates that it is locally incoherent at each vertex of f , and thus rules out the case when K is a normal branched or unbranched motif. There is one special case that bears mentioning here. If one edge of f has an inversive distance assignment of -1 then $\mathcal{T}$ is degenerate giving $\mathcal{T}$ two face angles that are 0. If such a motif is a branched circle packing then Theorem 6.3 tells us that it is actually coherent at each vertex of f, and is thus by definition not a fractional branching. Structurally though it can still be thought of as one. If the inversive distance assignment is adjusted continuously as a parameter then a fractional branching could be produced from this special case.

6.2 Uniqueness of Fractional Branchings

A fractured branched circle packing could equivalently be treated like an annulus by puncturing the fractured points' face. Equation 6.1 better illustrates the result from the perspective of its original motivation, distributing branching among a collection of vertices. However this equation can be rewritten in terms of turning angle on the boundary of the punctured face.

$$t(v_i) = -\theta(v_i; v_j, v_k) - \pi(2n_i - 1)$$

The angle assignment condition then becomes a turning angle condition. Instead of a simply connected branched circle packing, the motif is treated as a coherent annulus.

Look closely at Figure 6.5; the orientation of f has simply been flipped. For coherence to hold, the face angle at f's vertices must be exactly twice its angle sum in excess of the packing condition. The excess is accounted for half in the positive direction and half in the negative (as faces are laid out). As a rigid structure in $\mathbb{R}^3$ this could be viewed as a fold.

One could say this motif is coherent in three-space, or relax the orientation requirement in the definition of a circle packing and say it is coherent. Call a flower with this property *quasi-coherent*. Implementing these types of "folds" throughout a motif would allow multiple labels to exist for the same decorated disc $K(I,A)$, and allow for a greater menagerie of packing types. While interesting these folds do not mimic classical analytical behavior, and so are not pursued here.

Given an admissible decorated complex Theorem 2.13 provides a unique label. For simply connected complexes with fixed border radii, this label is also coherent as long as the angle assignments are locally coherent. A meaningful uniqueness result for fractured branched circle packings would be that *there is only one way to distribute an additional* 2π *on an interior face of a coherent motif such that the resulting motif is a fractured branched circle packing.*

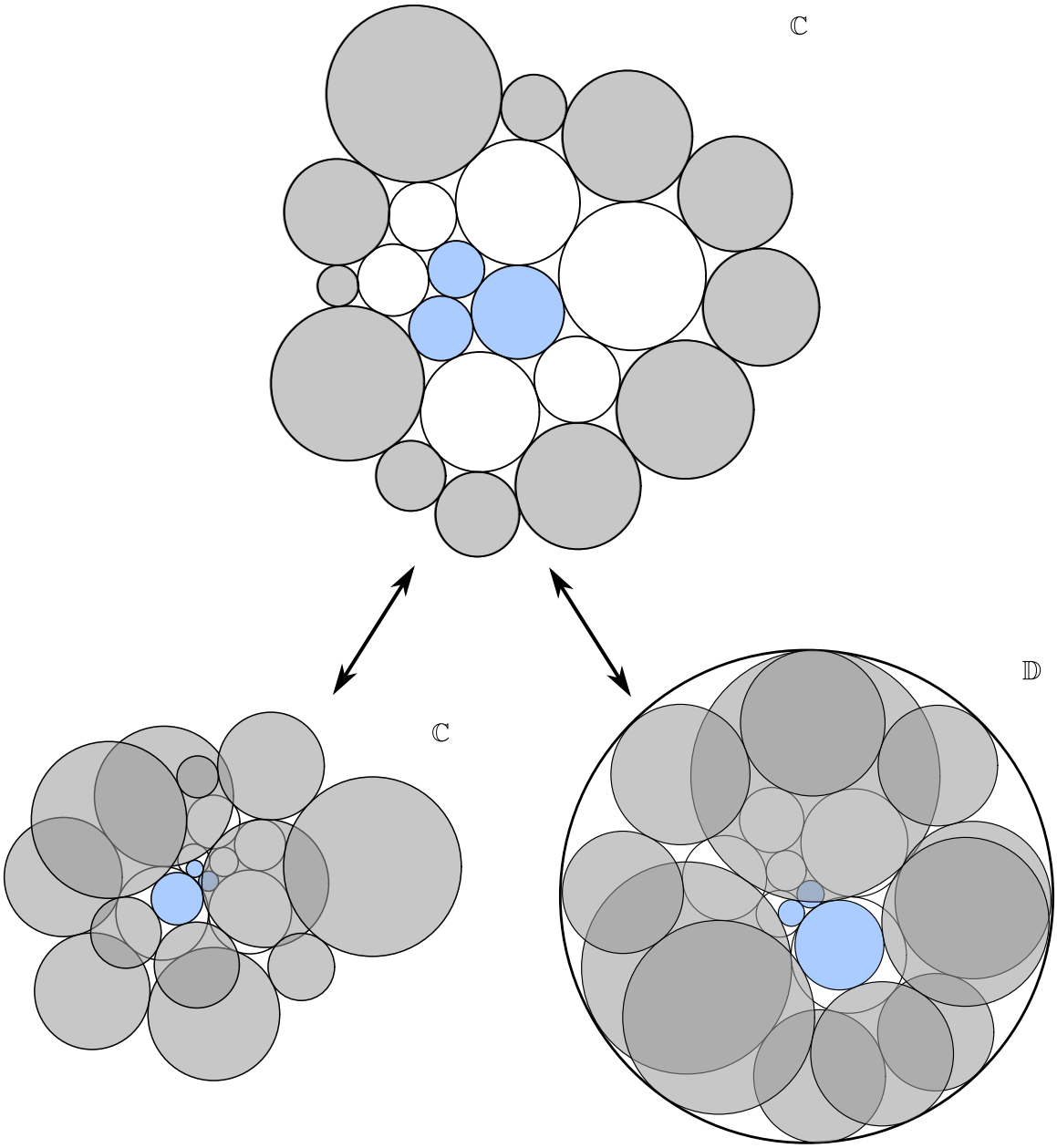


Figure 6.4: Fractured branched circle packings in $\mathbb{C}$ and $\mathbb{D}$. On the bottom-left is a fractured branched circle packing in $\mathbb{C}$, and on the bottom-right is a maximal fractured branched circle packing using the same complex and edge assignments.

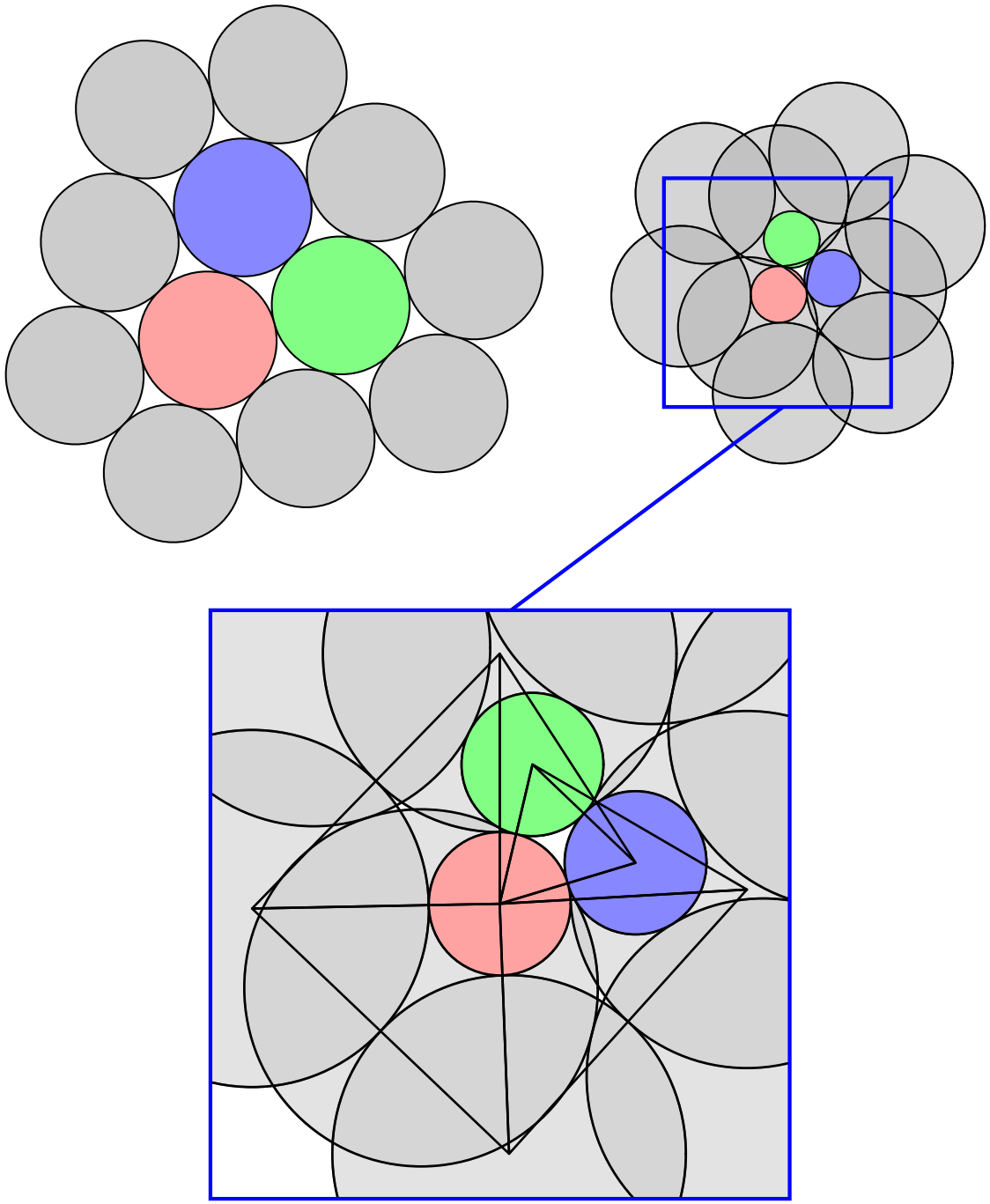


Figure 6.5: Detail of a simple fractured branched circle packing. The upper left is an unbranched circle packing. The upper-right is a fractured branched circle packing using the same complex and border radii. The branching has been distributed on the three colored circles. Note how the face where the fractured branching occurs has its orientation reversed.

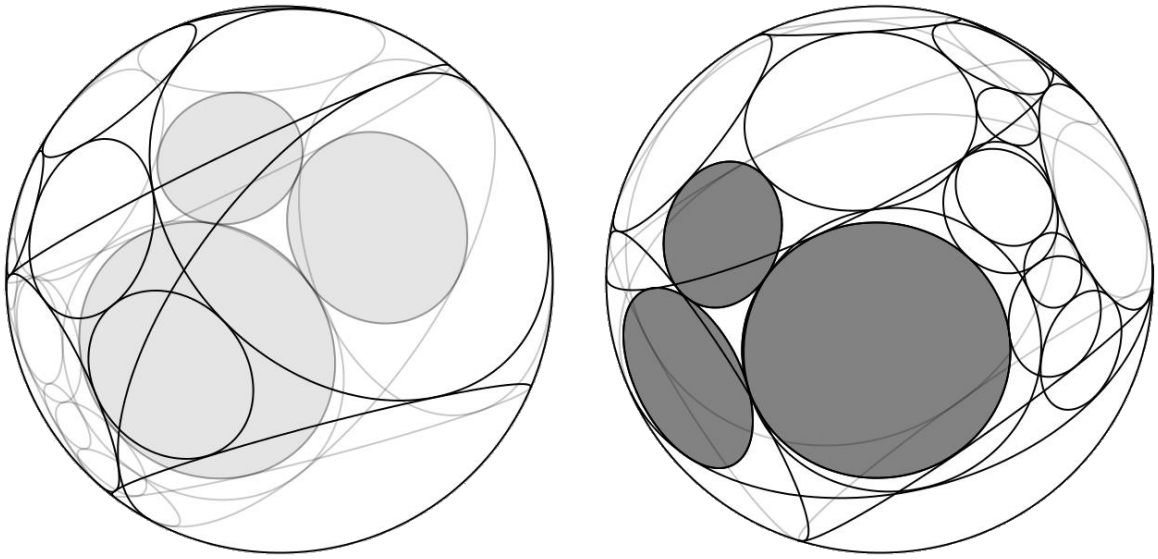


Figure 6.6: Fractured branched circle packing on $\mathbb{P}$. Two different views of the hyperbolic branched circle packing from Figure 6.4 projected to the sphere.

It would be desirable to either have this kind of rigidity, or have a fractured branched label for every distribution in some connected set of distributions. The former would be pleasing to a mathematician's sensibilities, but the latter would be useful for introducing flexibility into branched packings as originally conceived by Stephenson.

In regard to the flower at a fractured point, say $v_1 \in f = \{v_1, v_2, v_3\}$ in $K(R, I, A)$ from Theorem 6.5, this orientation flip causes the angle at $\theta(r_1; r_2, r_3)$ to act antipodally to that of the rest of the v_1's petal angles. Monotonicity dictates that the change in face angles of v_1's flower with respect to the nexus radius, r_1, will be opposite of the change in r_1, e.g., decreasing r_1 will increase $\theta(r_1)$. This is still true for $\theta(r_1; r_2, r_3)$, but because the orientation of f is reversed so is the angle's effect on the flower. So while decreasing r_1 will increase $\theta(r_1; r_2, r_3)$ the flip means that the Möbius map associated with the flower will have its rotation decreased; other face angles in the flower will increase the rotation.

The net effect on the flower is generally uncertain, and dependent on the geometry at the petals. Specifically the number of petals and the ratio of each petal radius to its neighbors. Values which can be quite dynamic inside a motif. Contrast this with the monotonicity of flowers when petal orientation is homogeneous. This property makes these so called quasi-coherent flowers quite different.

In a traditional motif the angle sums are negatively monotone as a function of the central radius. So every flower is also a monotone function of its respective central radius. However because of the flip, local monotonicity of angle sums can be lost where fractional branching occurs. Uniqueness can be shown to hold in some special situations, but unfortunately we can also construct examples where uniqueness appears (computationally) to fail. Consider the following single closed Euclidean flower which illustrates the non-monotonicity of quasi-coherent flowers.

Example 6.6. Let $F(v) = F\{v; 1_a, 1_b, 10^{-4}, H, 10^{-2}, 10^2, H, 10^2, 10^{-2}, H, 10^{-4}, 1_a\}$ be an externally tangent Euclidean lower with center radius r, and with angle sum

$$\theta_F(r) = \theta(r; 1_a, 1_b, 10^{-4}, H, 10^{-2}, 10^2, H, 10^2, 10^{-2}, H, 10^{-4}, 1_a).$$

All other petals have fixed radii; H indicates half-planes, i.e., circles of infinite radius.

This flower will be quasi-coherent precisely when,

$$Q(r) = \theta_F(r) - \theta(r; 1_a, 1_b) - 2\pi = 0.$$

Figure 6.7 (on the left) graphs $Q(r)$. The other graph is of $F(r) = \theta_F(r) - 2\pi$; $F(r)$ is zero when the flower is locally coherent in the traditional sense (i.e., the packing condition is met). $F(r)$ is actually convex, however monotonicity is the key behavior in the proofs of existence, uniqueness, and convergence of traditional circle packings. The loss of this monotonicity whether in fractional branchings, shift-points (Chapter 7), deep overlaps (Chapter 2), or inversive packings is a major hurdle in the attainment of general results, because it introduces unpredictable local characteristics which can be dependent upon specific local combinatorial and geometric conditions.

For Example 6.6, there are at least two values of r for which $\theta(r)$ is quasi-coherent. It is the total rate of change with respect to r that allows multiple solutions to exist. At a single face this derivative is dependent on the ratio of neighboring petals' radii. We amplify the effect of the flip by using very large and small circles. Using hyperplanes is not necessary, but their extremity helps illustrate the point. A similar albeit less visually impactive example can be found using sufficiently large circles.

Example 6.7. Construct a tangency motif with a single interior face and fixed border radii by gluing together three copies of the flower in Example 6.6, $F(v_1)$, $F(v_2)$ and $F(v_3)$, as follows. Make

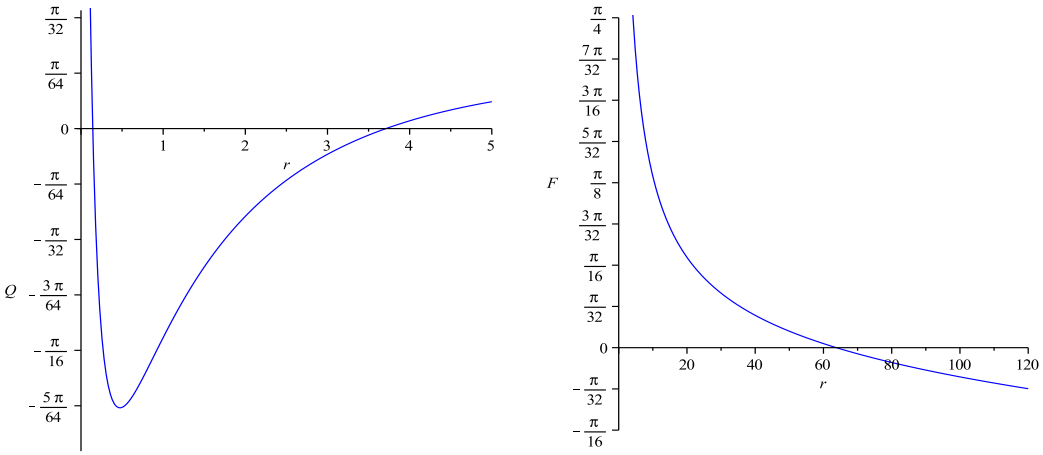


Figure 6.7: Non-uniqueness of a quasi-coherent flower. $Q(r)$ is pictured on the left. For comparison the same flower without a flipped face is pictured on the right.

v_1, v_2, and v_3 the interior face by setting $F(v_1; v_2, v_3, \dots\}$, $F(v_2; v_3, v_1, \dots\}$, and $F(v_3; v_1, v_2)$. The two petals of radii 10^{-4} in each flower will then be shared by two interior vertices. The result is a combinatorially closed disc with three interior circles (r, 1_a, and 1_b from one flower) and 24 border circles with fixed radii.

The symmetry of our construction appears to allow the non-monotonicity of Example 6.6 to carry over. Call this complex K with three interior vertices $\{v_1, v_2, v_3\}$. There is a unique label for K when interior angle sum assignments are 2π, and this is the only trivially branched label for which this motif is coherent. The situation appears to be quite different for fractional branching. Randomly distributing an extra 2π among the three interior vertices, there is (computationally) to a total of 7 different angle assignments which give solutions (see Figure 6.8; error is measured as $|\theta(v_i) - 2\pi n_i + 2\theta(v_i; v_j, v_k)|$).

Figure 6.8 plots the data with the angle distribution on two vertices represented by the x and y-axis and the error on the z-axis. The error is measured using Equation 6.1. These are Euclidean motifs so the third angle distribution is dependent on the other two.

It appears that additional conditions need to be assumed to get uniqueness, e.g., some sort of local univalence or border conditions. For the case when $K = f \cup \partial\Gamma$, uniqueness can be shown when some of the border radii are sufficiently large [4], or by using lemma 2.3 from [14] when the border radii are equal. Theorem 6.8 shows the uniqueness of fractional branched motifs with an extra assumption on the edge assignments f. Constructing similar auxiliary motifs as done in the proof here might lead to more general uniqueness results.

Theorem 6.8. *Let K be a simply connected complex with a strictly interior face $f = \{v_1, v_2, v_3\}$. Suppose that $K(I, A)$ is admissible with each $A(v)$ an integral multiple of 2π and $\cos^{-1}(\sigma_{12}) + \cos^{-1}(\sigma_{13}) + \cos^{-1}(\sigma_{23}) = \pi$. Furthermore, suppose admissibility holds if the assignment $A(v)$ is replaced by $A(v) + 2\pi$ for $v = v_1, v_2$, or v_3. Then there exists one and only one angle assignment A' such that $K(I, A')$ has a fractured branched circle packing on $\{v_1, v_2, v_3\}$ and $\sum A'(v) - \sum A(v) = 2\pi$.*

Proof. An angle assignment exists by Theorem 6.5; call it A. The $K(R, I, A)$ is coherent so it has a unique layout. First we construct and layout an auxiliary motif for $K(R, I, A)$. The purpose of this motif will be to temporarily realize $K(R, I, A)$ as a traditional branched packing (at least at f), and obtain uniqueness through a typical maximal argument.

Recall from Section 2.2 that because $\cos^{-1}(\sigma_{12}) + \cos^{-1}(\sigma_{13}) + \cos^{-1}(\sigma_{23}) = \pi$, the three circles of f will intersect at a point. Add an interior vertex at this point, say v_0, tangent to v_1, v_2, and v_3. Call the three vertices in faces sharing an edge with f: v_{12}, v_{23}, and v_{31} where v_{xy} is tangent to v_x and v_y. Now add *shepherd* vertices s_{12}, s_{23}, and s_{31} to the edges $e(1, 2)$, $e(2, 3)$, and $e(3, 1)$, respectively making each s_{xy} contiguous to v_0, v_x, v_y, and v_{xy}. Call this the *auxiliary* complex K'_{v_0}; see Figure 6.9.

Using the existing motif $K(R, I, A)$ we make a new motif M' as follows. Using the points v_0, $C(v_x) \cap C(v_{xy})$, and $C(v_y) \cap C(v_{xy})$ in $K(R, I, A)$ (if either of the last two pairs overlap there is an obvious choice of the two available points) define the circle $C(s_{xy})$. For example, s_{31} passes through v_0, the intersection of v_3 and v_{13}, and the intersection of v_1 and v_{13}.

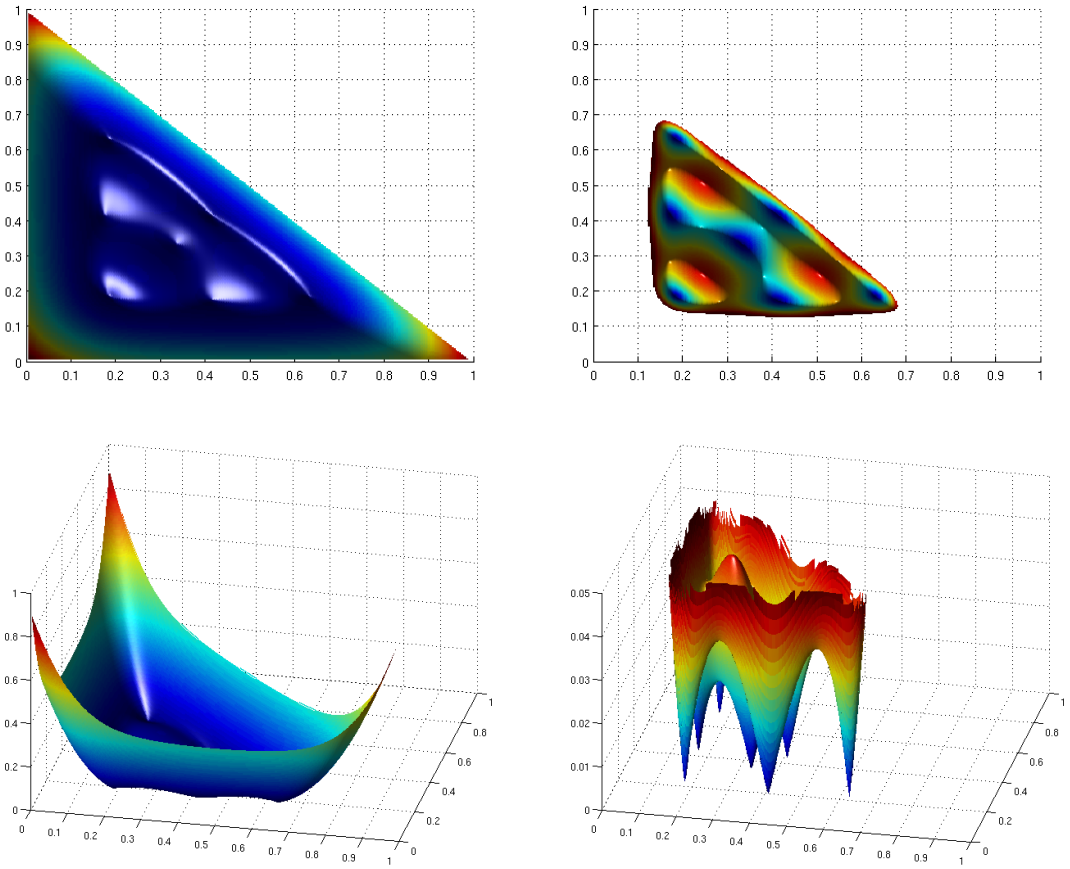


Figure 6.8: Error for different angle assignments on Example 6.6. The images on the right are truncated details of the images on the left. The x are y-axis reflect angle sums $\frac{A(v_i)-2\pi}{2\pi}$ for v_1 and v_2, respectively. The angle at v_3 determined by the remains of the extra 2π. The z-axis is an error value; the sum of Equation 6.1 for each vertex (a necessary condition for coherency).

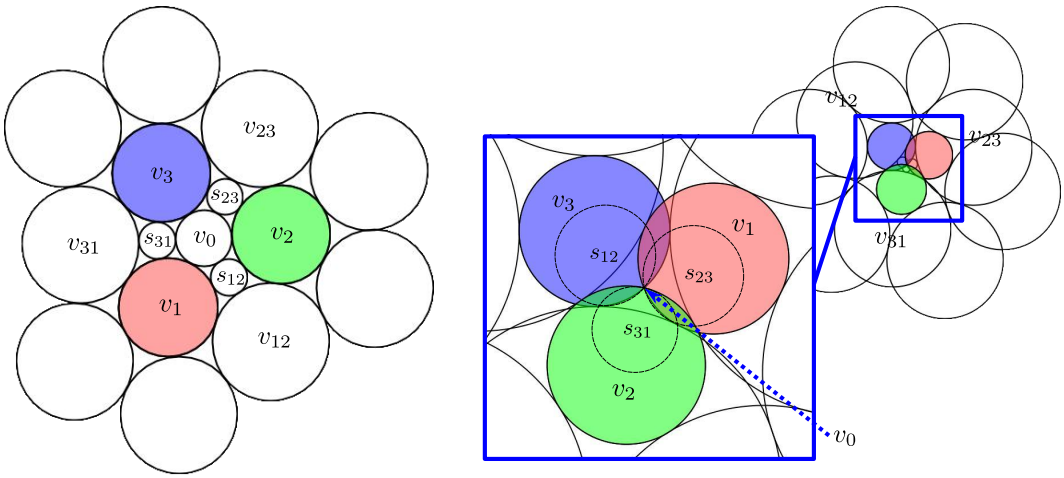


Figure 6.9: A fractured branched circle packing with an auxiliary motif and shepherd circles.

Because the newly created faces

$$\{C(s_{xy}), C(v_x), C(v_{xy})\}, \{C(s_{xy}), C(v_y), C(v_{yx})\}, \{C(s_{xy}), C(v_x), C(v_0)\},$$
$$\text{and } \{C(s_{xy}), C(v_y), C(v_0)\}$$

have no interstice their overlaps must sum to π. This uniquely determines the inversive distances for the edges of each shepherd circle.

Look closely at Figure 6.9. The orientation of f in $K(R, I, A)$ has been flipped. Consider the point v_0 a circle of zero radius with petals $\{v_1, s_{12}, v_2, s_{21}, v_3, s_{32}, v_1\}$. Adding the shepherd circles replaces f with a flower having the proper orientation. The contiguousness for circles of f in $K(R, I, A)$ has become circumstantial placements of this flower.

Let I' have the edge assignments from the construction above for the new edges, let A' be 2π at the shepherd circles, and elsewhere let M' adopt assignments from M. M' was constructed from M so Theorem 2.13 is not used, and the zero circle $C(v_0)$ does not cause any existence issues for M'. Also the edge assignments of v_0's flower necessitate that r_0 is zero regardless of its petal radii.

M' has been constructed so that it is coherent. By Monodromy, M' must be locally coherent, and since it is admissible R' is uniquely determined by M's decorated complex (Theorem 2.14). The complex of M' was created independently of M's angle assignment. So the angle assignment determined by R' and I' then must be identical to A everywhere other than the shepherd vertices. Otherwise the label for $K(I', A')$ would not be unique. □

Global monotonicity of circle packing flowers has been exploited for proving existence and uniqueness of labels using geometric (Garrett [23]), Perron (Stephenson [44]), and variational methods (Alexander Bobenko and Boris Springborn [8]). Different approaches will be required here as we do not enjoy this characteristic. When viewed as an annulus this should not be surprising as the additional border element introduces flexibility. Global coherence no longer automatically

follows from local coherence. The proof of Theorem 2.13 builds on existing labels; we then had to show that one of these would be coherent.

Figures 6.4, 6.5, and 6.6 illustrate coherent fractional branched motifs. These motifs can be generated using `CirclePack` by setting the target angle sum of vertices in f to some non-integer multiple of 2π if the correct distribution of the branching is known. We have a working algorithm for finding this distribution; its method is outlined in [4]. It uses a recursive method, and in practice converges. However it is only proved for a special case. It remains open as to whether this algorithm works in general.

Another open question is whether the angle assignments resulting in a coherent maximal fractured branched circle packing in $\mathbb{D}$ are unique. An affirmative answer would mean fractional branching could provide a pleasingly rigid structure for fractional versions of many marque discrete analogues; discrete Blaschke products and polynomial functions for example. Any condition which ensures that the change in a vertex's angle sum at its non-fractured neighbors outweighs the change at its fractured neighbors will preserve monotonicity. A branched version of the Burt Rodin and Dennis Sullivan's Ring Lemma (see [37, 42, 47]) might be just such a condition for proper mappings. These issues remain to be investigated.

6.3 Fractional Branching on Four Vertices

Call the angle assignments at the fractured points of a fractured motif the *distribution*. Under certain conditions we have seen that a face may support fractional branching with a unique distribution of excess angle. If multiple coherent distributions do exist in the more general case, the experience of experimentation leads us to expect that they are not path connected in the space of distributions. Meaning that there is not enough flexibility to make them of use as an adjustable parameter. Extending the same idea to two adjacent faces is the natural next step.

As a means of introducing flexibility one might try adjusting the distribution of an additional 2π over four vertices on two adjacent faces. However a particular distribution could easily require the two circles in the shared edge to be separated, and it has been seen that such configurations could fail to form triangles.

Whether a separation would occur depends on the label which in turns depends on the decorated complex. This is not easily predicted (perhaps intractable); using angle distribution thus makes existence of the labels problematic. Instead the edge assignment on the shared edge will be used as a parameter on $(-1, 1)$. This allows the decorated complex to be manipulated while always remaining admissible.

We illustrate this with one elementary example. Take a simply connected complex, say K, with two strictly interior faces, $f_0 = \{v_0, v_1, v_2\}$ and $f_1 = \{v_1, v_2, v_3\}$, sharing the edge $e(v_1, v_2)$. Let K be admissible for angle assignments of 4π at either of these vertices. Assign an inversive distance, $\sigma_{12} \in (-1, 1)$, to the shared edge. For simplicity we will assume that all other edge assignments on these two faces are 1, i.e., external tangencies. By Theorem 6.5 there exists a distribution of an extra 2π among the vertices of f_0 such that $K(R, I, A)$ is a fractured branched circle packing in $\mathbb{C}$.

$K(R, I, A)$ is a fractured packing on three vertices. Using this existing label and layout we will create a fractured branched circle packing on $f_0 \cup f_1$. Let $I' = I$ except for the assignment at $e(v_1, v_2)$ which we set to $\sigma'_{12} = 1$. Now let the angle assignments A' be determined by R and I'. By this we mean compute the angle sums resulting from using I' and R with Equation 2.3 and the Law of Cosines, and then set A' equal to these found angle sums. The result is a new motif $K(R, I', A')$.

Claim 6.9. $K(R, I', A')$ is a fractured branched (circle) packing on the four vertices $\{v_0, v_1, v_2, v_3\}$.

Proof. Let $K' = K \setminus \{f_0 \cup f_1\}$ be an annular complex. $K(R, I, A)$ is assumed to be a fractured packing on $f_0 = \{v_0, v_1, v_2\}$, and K a combinatorially closed disc. Thus $K'(R, I', A')$ is a coherent annular sub-motif. The turning angle of $K(R, I', A')$ must then be an integer multiple of 2π, and all interior vertices not in $f_0 \cup f_1$ are locally coherent. Then by Theorem 3.12 the sum of angles on $f_0 \cup f_1$ must also sum to a multiple of 2π.

So we need only show that each vertex in $f_0 \cup f_1$ is locally incoherent in $K(R, I', A')$. v_3 is by assumption locally coherent in $K(R, I, A)$ with an inversive distance of σ_{12} at $\{v_1, v_2\}$. Changing σ_{12} to 1 in $K(R, I', A')$ but keeping the current layout shows that both v_0 and v_3 must be locally incoherent in $K(R, I', A')$. Using an argument similar to Lemma 6.4 it can then be shown that v_1 and v_2 must also be locally incoherent. □

A simple recipe to create a branched circle packing on $f_0 \cup f_1$ for a simply connected complex K:

1. Find a distribution such that $K(R, I, A)$ is a branched circle packing on f_0 and f_0, f_1's shared edge has assignment $\sigma_{12} \in (-1, 1)$.
2. Compute the angle sums, $\{\theta(v)\}$ for $K(R, I, A)$ assuming that $\sigma_{12} = 1$.
3. Set $A'(v) = \theta(v)$ for every $v \in K$, and set $I' = I$ except at $e(v_1, v_2)$ where $\sigma'_{12} = 1$. Now $K(R, I', A')$ is a branched circle packing on $f_0 \cup f_1$.

We begin assuming that $\sigma_{12} \neq 1, -1$ to avoid a fracturing over four vertices where one vertex in $f_0 \cup f_1$ is locally coherent. If we allow $\sigma_{12} \in [-1, 1]$ then this edge assignment can be used to transfer branching from f_0 to f_1.

Let f_0 and f_1 be two faces as in Figure 6.10. Suppose K has external tangencies everywhere except at $e(v_1, v_3)$, and that $\sigma_{13} = -1$. Then the fractured branched packing over $f_0 = \{v_0, v_1, v_3\}$ will be identical to the one over $f_1 = \{v_2, v_3, v_1\}$. The angle $\angle v_0 v_1 v_3 = \angle v_2 v_3 v_1 = 0$ so this comes by Theorem 6.3. Thus by continuously decreasing σ_{13} from 1 to -1 and then back to 1, branching can be transferred continuously from the face f_0 to f_1. See Figure 6.11.

One last note. The choice of pink and blue circles in the last few figures was no accident. The shift-point in Chapter 7 can be viewed as a coherent fractional motif over three vertices. To see this one needs only apply the right edge assignments to a coherent shift-point and adjust the shift-point's flower complex to look like the one seen in Figure 6.10. Conversely any fractured packing might be thought of as a shift-point with overlapping sister circles (see Chapter 7).

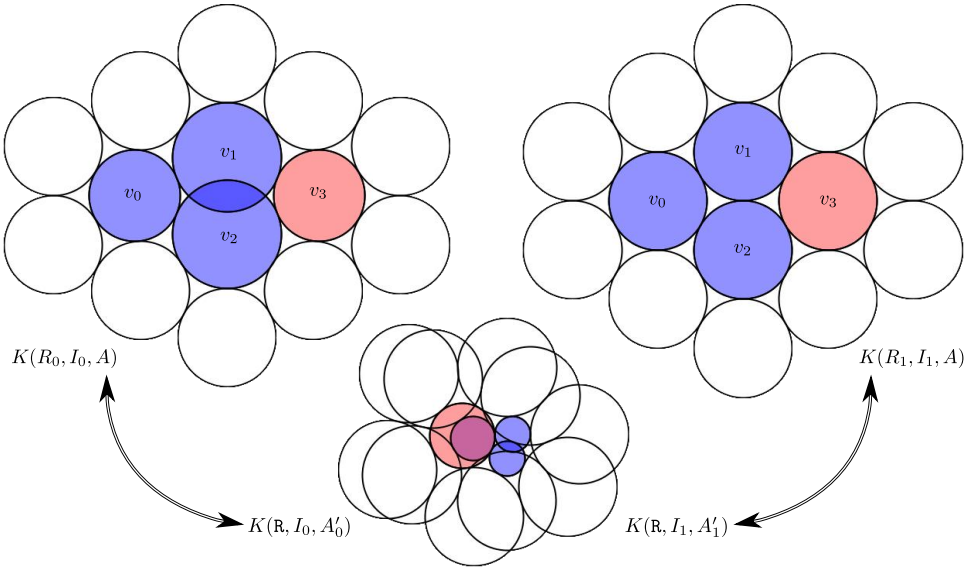


Figure 6.10: Creating a fractured branched packing over four vertices form one with three. Two fractured packings using the same label R. I_0 and I_1 differ only in the one overlapping edge at $e(v_1, v_3)$. $K(\mathtt{R}, I_0, A'_0)$ is fractional branching over 3 vertices with distribution (approximately) $A'_0 = \{2\pi, 2.8\pi, 2.41\pi, 2.8\pi\}$ for $\{A(v_0), A(v_1), A(v_2), A(v_3)\}$, and $K(\mathtt{R}, I_1, A'_1)$ has a distribution on 4 vertices $A'_1 = \{2.07\pi, 2.72\pi, 2.5\pi, 2.72\pi\}$.

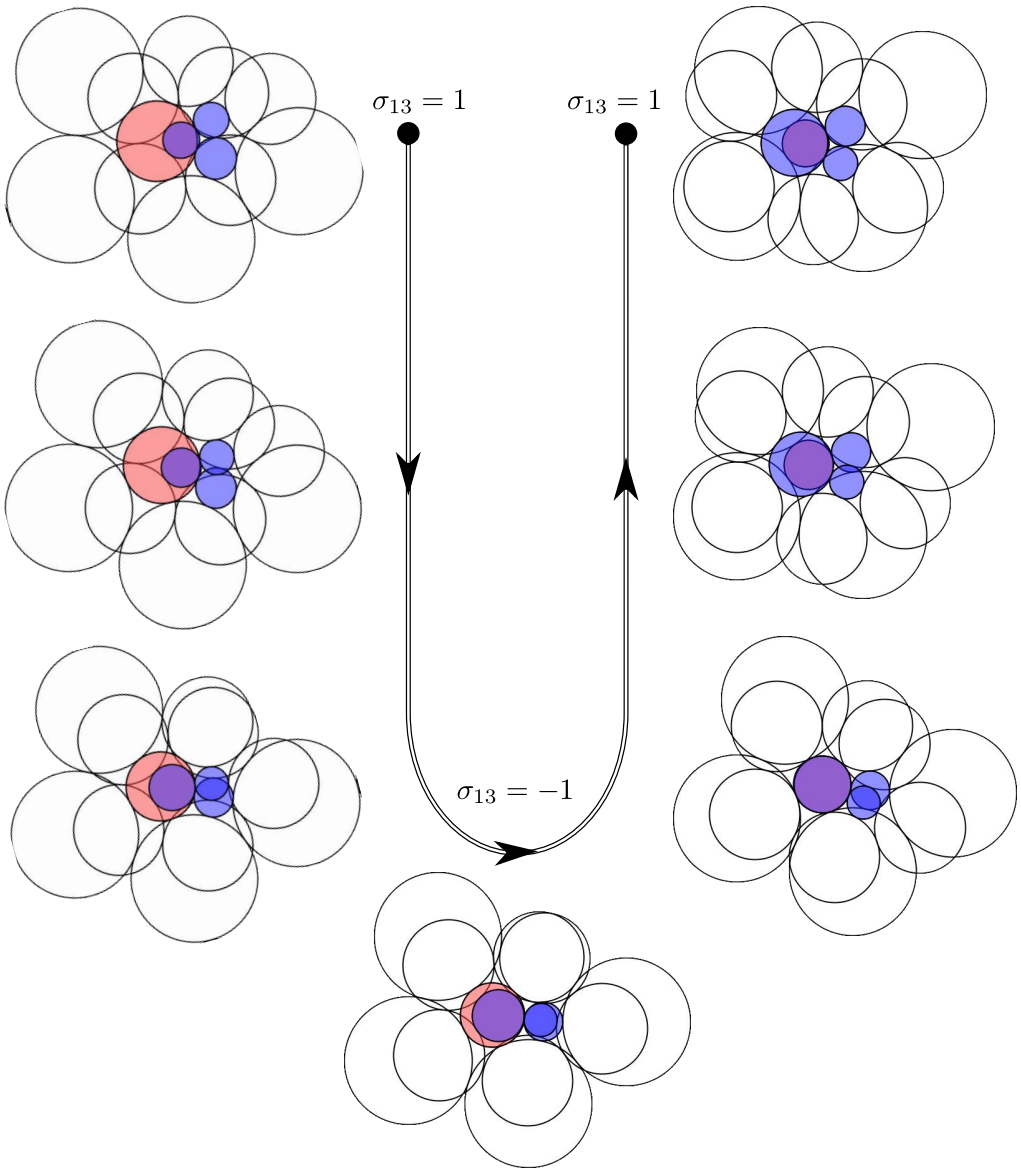


Figure 6.11: The fractional branching is transferred to another face. This is done by continuously adjusting σ_{13} and switching faces at $\sigma_{13} = -1$.

Chapter 7

Shift-Branching

This simple yet elegant idea was generously introduced by Edward Crane via conversation during the 2010 Barrett Lectures at the University of Tennessee. Place a smaller circle, what will be called a sister circle, internally tangent to a branch circle, the two creating a looped curve called a *shift-circle* (see Figure 7.1). Normally the singularity is considered to be at the vertex of the branch circle. Instead consider it to be inside of this smaller circle. The desired branching is created by placing the n-petal circles along the looped curve creating a structure which we call a *shift-point* (see Figure 7.2).

If the petals to the shift-circle can be placed in a consistent manner then the shift-point has the characteristics of a coherent flower. The winding number of a path around this loop is the same as a traditional branch point, a behavior which then is expressed globally via homotopy.

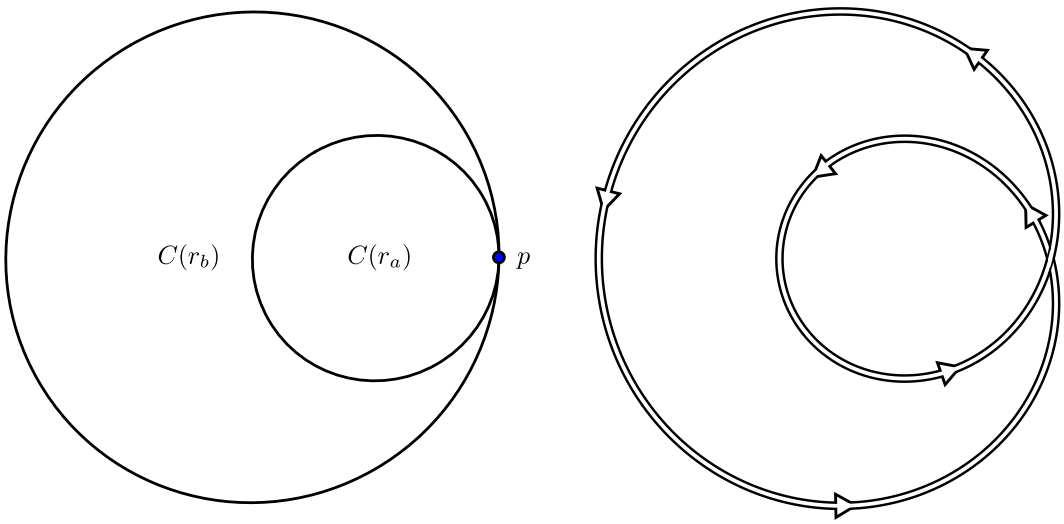


Figure 7.1: The shift-circle, and the direction of its path on the right.

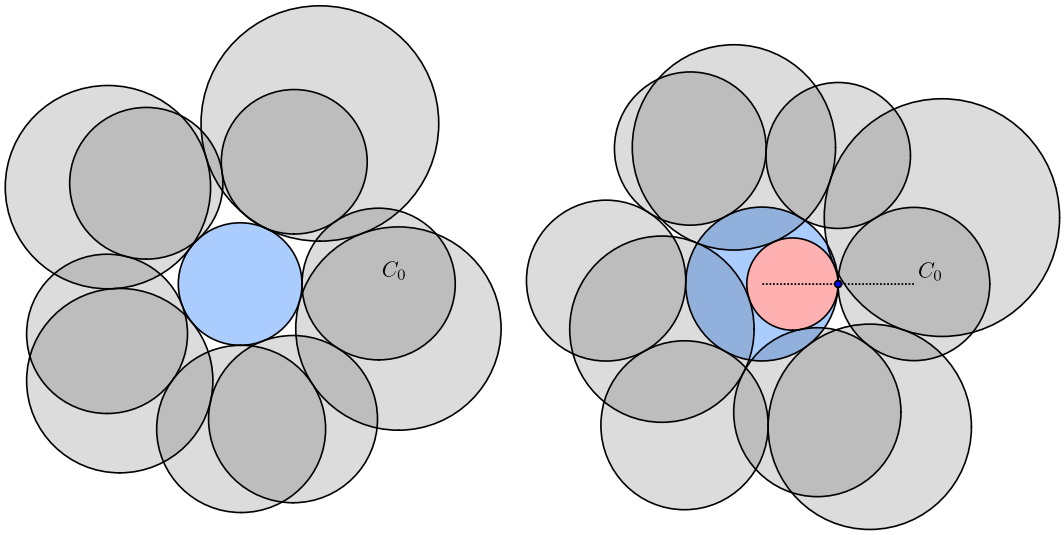


Figure 7.2: A traditional branch point and shift-point. The petals (in gray) are identical in both structures. The little and big sister circles are colored pink and blue, respectively.

Thus shift-points are an alternative method to create branching. It will be shown that shift-points can be classified as generalized branch points. In the service of introducing continuous variables into our discrete setting, shift-points have some nice advantages.

Definition 7.1. Let $F = \{v_0, ..., v_n\}$ where $v_0 = v_n$ be a flower with nexus vertex v. Replace $C(v)$ with two *sister circles* $S(r_\ell) = S_\ell$ and $S(r_b) = S_b$; *v's little sister* and *big sister* circle, respectively, with $r_\ell = x \cdot r_b$ for *shift-ratio* $x \in (0, 1]$. For normalized position, center S_b at the origin and join the two circles so that the little circle is internally tangent to the big circle at a point p on the positive x-axis. Define a path which starts at p and has trace $S_a \cup S_b$:

$$\gamma(\vartheta) = \begin{cases} r_b e^{i\vartheta} & \text{for } \vartheta \in [0, 2\pi) \\ r_\ell e^{i\vartheta} + (r_b - r_\ell) & \text{for } \vartheta \in [2\pi, \infty). \end{cases}$$

Call this structure a *shift-point* and the curve itself a *shift-circle* denoted $\mathfrak{C}(r_b, x)$. The parameter, x, is the shift-point's *decoration*. For both a shift-point and shift-circle we may write $\mathfrak{C}$ when it is understood which is being referenced.

In constructing a shift-point we know the radii $r_0, \ldots, r_{n-1}$ of the n petals. So there are n petal circles $C_i = C(r_i)$ which need to be laid out in $\mathbb{G}$. An additional copy $C_n = C(r_0)$ of the first petal is made; our goal is a coherent shift-point, meaning that this last circle C_n is placed precisely on C_0.

The petals will be laid on the shift-circle at $\mathfrak{C}$ as follows: The *lead-petal* C_0 is placed externally tangent to $\mathfrak{C}$ at $p = \gamma(0)$. Each succeeding petal, say C_k, is then placed (externally) tangent to the preceding petal, C_{k-1}, and to one of the sister circles. Denote the location of a petal C_k's tangency point on a shift-circle with $\gamma(\vartheta_k)$.

If $\vartheta_{k-1} < 2\pi \leq \vartheta_k$, C_k transitions from being placed tangent to S_b to being placed tangent to S_ℓ (see Figure 7.3). Call this transition a *jump*, the petal C_k the *jump-petal*, and $\gamma(2\pi)$ the *jump-point*. Placing petals around a shift-circle in this manner is called a *layout* and the layout a *shift-flower*. If a layout positions the last petal such that $C_n \equiv C_0$ then the shift-point is said to be *(locally) coherent*.

Less formally, we place petals around a sister circle until we would bypass the jump-point. Then we switch, and place petals around the other sister circle. For simplicity, all petal contingencies in a shift-flower are assumed to be external tangencies. Figures 7.2 and 7.3 have examples of a coherent shift-point.

Definition 7.2. The *angle* at a shift-point $\mathfrak{C}$ between two petals $C(r_k)$ and $C(r_{k+1})$ at $\gamma(\vartheta_k)$ and $\gamma(\vartheta_{k+1})$, respectively, is

$$\theta(\mathfrak{C}; r_k, r_{k+1}) = \vartheta_{k+1} - \vartheta_k.$$

If $\{C(r_0), \ldots, C(r_m)\}$ is a string of $m+1$-consecutive petals then the *angle from* C_0 *to* C_m is

$$\theta(\mathfrak{C}; C_0, \ldots, C_m) = \sum_{k=0}^{m} \theta(\mathfrak{C}; r_k, r_{k+1}).$$

If the case that $m = n$ (the chain of circles is closed) then we call this sum the *angle sum of* $\mathfrak{C}$ and write $\theta(\mathfrak{C}(r_b, x))$ or just $\theta(\mathfrak{C})$.

Lemma 7.3. *The layout of a shift-point* $\mathfrak{C}(r_b, x) \in K(R, I, A)$ *is well defined.*

Proof. From Definition 7.1, if $C(r_{j-1}) = C_{j-1}$ is on one of the shift-point's sister circles and C_j is also to be placed on the same sister circle then its location is easily determined by the appropriate Law of Cosines and orientation. So the result is only in question for a jump-petal.

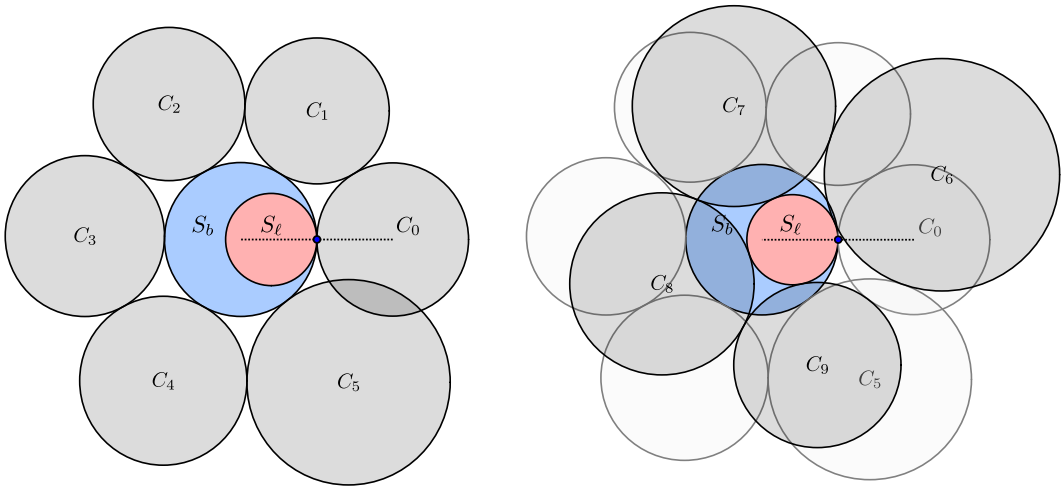


Figure 7.3: Laying out a shift-point. After the lead-petal C_0 is placed, petals are laid sequentially tangent to S_b until the jump-petal C_6 would be placed beyond p. C_6 and the remaining petals are then placed on S_ℓ.

Suppose that C_j is a jump-petal which is placed tangent to the sister circle S_ℓ and the petal $C_{j-1} \sim S_b$. We can assume that the positions of S_ℓ, S_b, and C_{j-1} are all fixed. The distance between C_{j-1} and S_ℓ gives an inversive distance, say σ, using Equations 2.1 or 2.2. Let the edge between C_{j-1} and S_ℓ with distance σ between their centers be the *auxiliary edge* $e_\sigma(C_{j-1}, S_\ell)$.

C_j's position is then uniquely determined if the two edges $e(C_j, S_\ell)$ and $e(C_j, C_{j-1})$ from the shift-point's layout and the auxiliary edge $e_\sigma(C_{j-1}, S_\ell)$ form a triangle T. Because $C_{j-1} \sim S_b$, $\sigma \geq 1$. Let $r_{\min} = \min\{r_j \geq 0 \colon C(r_j) \cap p\}$ (see the left side of Figure 7.4; recall that p denotes the jump-point). $r_{\min}$ exists and $r_{\min} \leq r_j$ or else C_j would not be a jump-petal.

T exists using the $e(C(r_{\min}), C_{j-1})$ in place of $e(C_j, C_{j-1})$ as $C(r_{\min})$ is now tangent to both sister circles. When $\sigma > 1$ the triangle inequality can only fail if

$$e(C_j, C_{j-1}) + e(C_j, S_\ell) < e_\sigma(C_{j-1}, S_\ell).$$

This can only happen when C_j is too small to be simultaneously tangent to both C_{j-1} and S_ℓ, but this cannot happen since $r_j > r_{\min}$. □

Later in this chapter we modify the definition of shift-points to include cases when the jump-petal "jumps" from the little sister to the big sister circle. The above result still holds in this situation as then $-1 \leq \sigma \leq 1$, and the triangle T will exist by Lemma 2.3.

7.1 Monotonicity in Shift-Points

The idea is to have shift-points replace traditional branch points. Most important is that shift-points offer an alternative method which expresses branching while allowing for greater flexibility. However

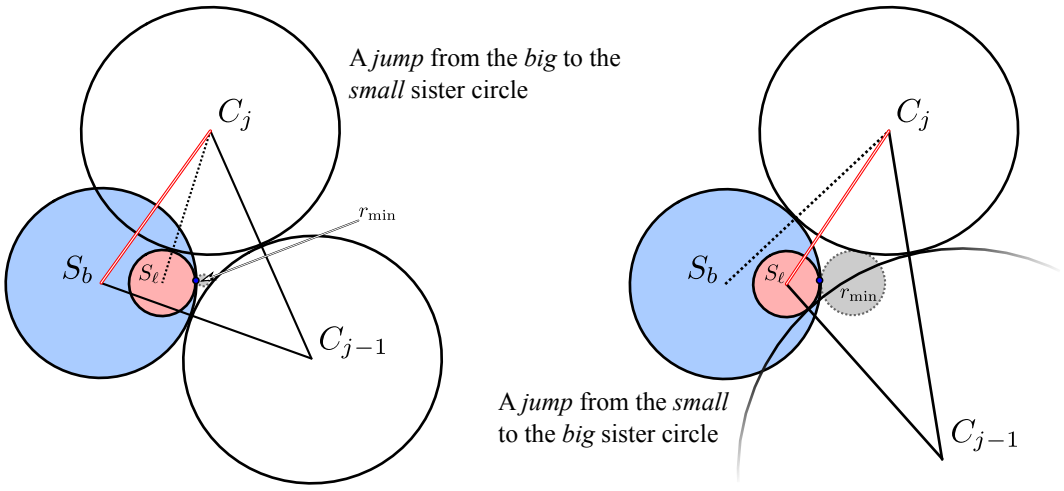


Figure 7.4: Placement of the jump-petal on a shift-circle. The little and big sister circles are colored pink and blue, respectively. The auxiliary edge $e_\sigma(C_{j-1}, S_2)$ is colored in red. On the right, $C(r_{\min})$, is the gray dashed circle.

in order to replace branch points seamlessly, that is without losing any depth of theory, shift-points need to have the key qualities of monotonicity and existence possessed by traditional flowers.

For this section, let $\mathfrak{C}(r_b, x)$ be a shift-circle with petals $F = \{C(r_0), C(r_1), \ldots, C(r_n)\}$, and the location of a petal $C_k \in F$ on $\mathfrak{C}$ will be denoted $\gamma(\vartheta_k)$. Recall that $\theta(\mathfrak{C})$ is the angle sum of the shift-point; it depends on $r_0, \ldots, r_{n-1}$, x, and r_b.

Theorem 7.4. Monotonicity of shift-points. *For $0 \leq k < n$ we have the following:*

1. $\frac{d}{d\vartheta_k}\vartheta_m > 0$ *when* $k < m \leq n$
2. $\frac{d}{dr_k}\theta(\mathfrak{C}) > 0$
3. $\frac{d}{dx}\theta(\mathfrak{C}) > 0$ *for fixed* r_ℓ, *and* $\frac{d}{dx}\theta(\mathfrak{C}) < 0$ *for fixed* r_b *($x = \frac{r_\ell}{r_b}$).*
4. $\frac{d}{dr_b}\theta(\mathfrak{C}) < 0$ *and* $\frac{d}{dr_\ell}\theta(\mathfrak{C}) < 0$ for fixed x.

Normally we will be assuming $r_b = x \cdot r_\ell$. However part 3 treats x not as fixed, but as a function dependent on the big or little sister radius. Part 4 keeps the little circle dependent on the big circle and fixes the shift-ratio x.

Proof. All these claims are fairly clear when the petals are all on the same sister circle. The focus will be on what occurs at the jump-petal.

Part 1. If ϑ_k increases and $\{C_k, \ldots, C_n\}$ are all on the same sister circle the result is clear. So we need only show the result at a jump-petal, say $\theta(\mathfrak{C}_i; r_{j-1}, r_j)$. Let C_{j-1} be the petal with $\vartheta_{j-1} < p$ such that its neighbor C_j is placed on the jump-point, i.e., $\vartheta_j = p$. Lemma 7.3 still holds if circles are placed in the reverse order. That is, C_{j-1} not only uniquely places C_j, but first placing C_j also uniquely places C_{j-1}. Infinitesimally increasing ϑ_{j-1} thus requires a new position for C_j, and it cannot be p. Neither can it be less than p because then it has reverted to the case when both petals share the same sister circle. Proceeding inductively the result follows.

Part 2. Increasing a petal C_k's radii r_k can simultaneously affect its "face" angle (a jump-petal also has a sort of face angle analogous to a normal face angle), the position of itself, and all other petals. We handle this by examining each effect separately. First only increase r_k, keeping both its position and all other petal positions fixed. Now assign new edge assignments to the edges $e(v_k, v_{k+1})$ and $e(v_k, v_{k-1})$ (if C_k is the lead-petal the latter edge can be ignored as its positions is fixed) according to this new layout; call these assignments $\sigma_{k,k+1}$ and $\sigma_{k,k-1}$, respectively. Let the flower temporarily adopt these assignments, but remain tangent elsewhere, see Figure 7.5. These new edge assignments are overlaps, and all other tangencies are external. So by Lemma 2.3 all triangles of concern will exist.

This allows us to increase the assignments in I and obtain the result through part 1. For non-jump-petals we can use Lemma 2.5. When jump-petals are involved the jump-petal's predecessor, say C_{j-1}, will be tangent to a different sister circle, but its distance from the jump-petal's sister circle, say S, is fixed. Using this fixed distance, assign an inversive distance to the auxiliary edge from C_{j-1} to S. Existence of this auxiliary triangle is not an issue, and we can use Lemma 2.5 just as above.

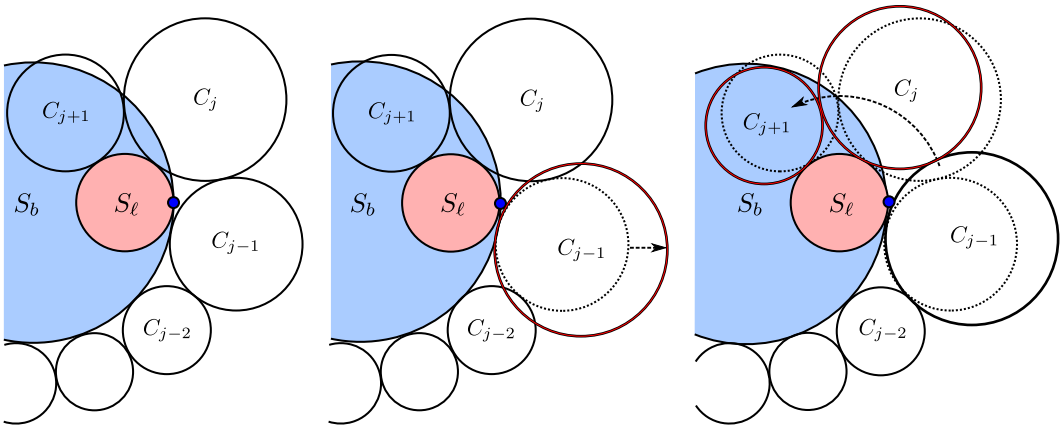


Figure 7.5: Increasing a petal on a shift-point. C_{j-1} is increased and then succeeding petals are moved. Dashed circles indicate petals before a change.

Part 3. We will only show that $\frac{d}{dx}\theta(\mathfrak{C}; r_0, ..., r_m) > 0$ for fixed r_ℓ as the other part can be done similarly. r_ℓ is fixed so then increasing x means r_b must decrease. We have two motions with which to contend, and we employ the same method as above. Keep the positions of each petal fixed, and assign inversive distances accordingly. Beginning with the lead-petal, sequentially decrease the inversive distances back to their original assignment. Again the result follows from Lemma 2.5.

Part 4. This time x is fixed. So increasing r_b also increases r_ℓ, and vise-versa. We can thus use Part 3 first for one sister circle and then again for the other one. □

Recall that Monotonicity at both the flower's center and its petal angles was necessary for us to show the existence and uniqueness of motifs. The relaxation operator used in Theorem 2.13 needed both to converge, and Theorem 2.14 needed both to use a maximality argument.

For traditional flowers, the monotonicity seen in their nexus angle is mirrored in the angles of their petals. The neighbors of traditional flowers are also flowers built from faces; this similarity of construction translates into a similarity of behavior. However shift-points fail to share this characteristic at the jump-point where petals transition from the big to the little sister. Fortunately, the monotonicity of a shift-point's neighboring flowers is retained, but only because our construction eliminates complications with the jump. This issue will be revisited in Section 7.3.

Measure the *petal angle* at a shift-point's petal C_k as $\overline{\theta}(C_k) = \angle v_k v_{k-1} v_{k+1}$ where v_{k-1}, v_k, v_{k+1} are the centers of sequential petals on a shift-flower. The *angle sum* of v_k, $\theta(r_k)$, will now be the sum of $\overline{\theta}(C_k)$ and its other face angles.

Theorem 7.5. *For $0 \leq k < n$ we have the following:*

1. $\frac{d}{d\vartheta_k}\theta(r_k) \leq 0$
2. $\frac{d}{dr_i}\theta(r_k) \leq 0$ for $C_i \in F$ (including $C_i = C_k$).
3. $\frac{d}{dx}\theta(r_k) < 0$ for fixed r_ℓ, and $\frac{d}{dx}\theta(r_k) > 0$ for fixed r_b ($x = \frac{r_\ell}{r_b}$).
4. $\frac{d}{dr_b}\theta(r_k) > 0$ and $\frac{d}{dr_\ell}\theta(r_k) > 0$ for fixed x.

Proof. We mean for $\theta(r_k)$ to represent the sum of face angles at vertices both on the boundary and the interior of K. In either case, only the face shared with the shift-point will be affected. As in Theorem 7.4, there is only anything to prove at $\mathfrak{C}$'s jump-petal, call it C_j. So for all parts we will be assuming that $C_k = C_j$ or $C_k = C_{j-1}$, and we need only show the results for each pair of angles at these two circles. The following claim is needed.

Claim. If $C_k = C_j$ or C_{j-1} with center v_k, and S is the sister circle with center v_S not tangent to C_k then $\frac{d}{d\vartheta} d_{\mathbb{C}}(v_k, v_S) \leq 0$.

Proof. Refer to Figure 7.6. For $C_k = C_j$, we have (after normalization)

$$d_{\mathbb{C}}(v_j, v_b) = \left|(r_j + r_\ell)e^{i\vartheta_j} + (r_b - r_\ell) - 0\right|,$$

and

$$\frac{d}{d\vartheta_j} d_{\mathbb{C}}(v_j, v_b) = \frac{-\sin(\vartheta_j)(r_b - r_\ell)(r_j + r_\ell)}{\sqrt{(r_\ell + r_b + (r_j + r_\ell)\cos(\vartheta_j))^2 + (r_j + r_\ell)^2 \sin^2(\vartheta_j)}} < 0$$

as $\vartheta_j \in (2\pi, 3\pi)$ because $\vartheta_{j-1} < p$.

For $C_k = C_{j-1}$ we have

$$d_{\mathbb{C}}(v_{j-1}, v_\ell) = \left|(r_{j-1} + r_b)e^{i\vartheta_{j-1}} - (r_b - r_\ell)\right|$$

and

$$\frac{d}{d\vartheta_{j-1}} d_{\mathbb{C}}(v_{j-1}, v_\ell) = \frac{\sin(\vartheta_{j-1})(r_b - r_\ell)(r_{j-1} + r_b)}{\sqrt{(r_\ell - r_b + (r_{j-1} + r_b)\cos(\vartheta_{j-1}))^2 + (r_{j-1} + r_b)^2 \sin^2(\vartheta_{j-1})}} \leq 0$$

as $\vartheta_{j-1} \in (\pi, 2\pi]$ because $\vartheta_{j-1} \leq p$. This concludes the proof of the claim. □

Now we continue the proof of Corollary 7.5. Part 1. If ϑ_k changes positively then so must every petal thereafter by Theorem 7.5. There is only the one jump-petal, moving from the big sister circle to the little one. If $\vartheta_{j-1} < p$ and ϑ_{j-1} is increased then $d_{\mathbb{C}}(v_{j-1}, v_\ell)$ decreases or is unchanged by the claim (see Figure 7.6). By the Law of Cosines a non-increase in $d_{\mathbb{C}}(v_{j-1}, v_\ell)$ implies a non-increase in the angle $\angle_j = \angle v_j v_{j-1} v_\ell$. In $\mathbb{D}$ we can use a Möbius transformation to map v_{j-1} to the origin and apply the Euclidean result. The neighboring petal C_{j+1} in the other angle at v_j, say $\angle_{j'} = \angle v_j v_{j+1} v_\ell$, shares the same sister circle as C_j and is thus unaffected. So then $\overline{\theta}(C_j) = \angle_j + \angle_{j'}$ and thus $\theta(r_j)$ does not increase The case for $\theta(r_{j-1})$ can be shown similarly.

Using Part 1, Parts 2, 3, and 4 can now be shown similarly to Parts 2, 3, and 4 of Theorem 7.4 which concludes the proof. □

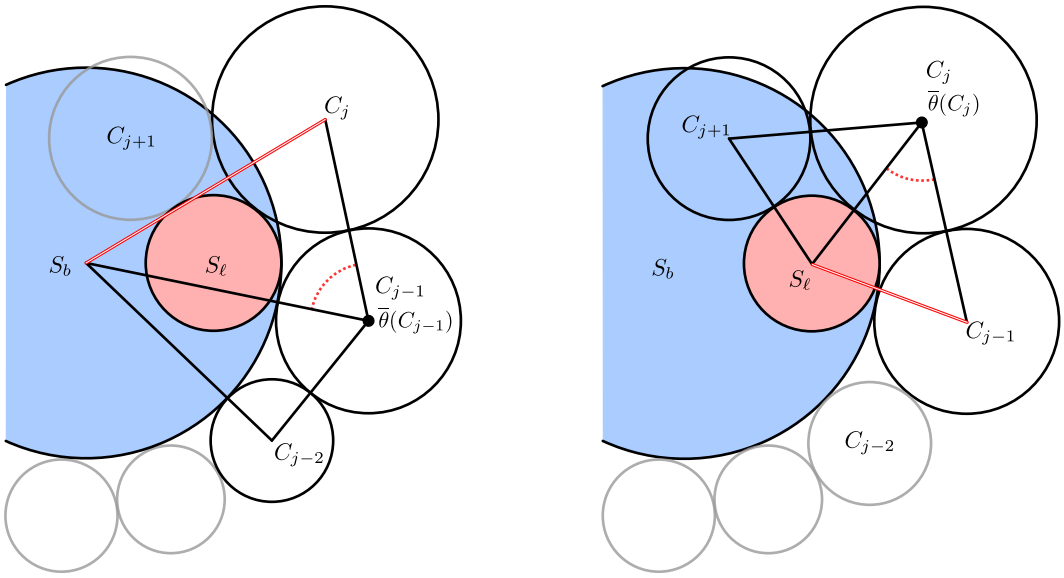


Figure 7.6: Change of the shift-point petal angles. The angles at C_{j-1} and C_j are shown on the left and right, respectively. Black edges are fixed; non-increasing edges are in red.

7.2 Existence and Uniqueness of Motifs with Shift-Points

The preceding lemmas show that computationally, shift-points behave much like traditional branched flowers. This will allow shift-points to be used similarly to traditional branched flowers. Placing coherent shift-points into a packing will create a structure which is a circle packing except within the shift-flowers. This is exactly how generalized branched points were described in Chapter 5. Showing that a shift-point is in fact a generalized branch point is our next step.

Theorem 7.6. *A coherent shift-point is equivalent to a generalized branch point.*

Proof. Let $\mathfrak{C}$ be a coherent shift-point, and K the complex of this flower. Every petal $C_j \sim \mathfrak{C}$ is either externally tangent to $\mathfrak{C}$'s smaller sister circle C_ℓ, or it is separated from C_ℓ by a distance $D_{\ell j} > r_\ell + r_j$ ($D_{\ell j}$ is the distance from the center of C_ℓ to C_j). Each $D_{\ell j}$ determines an inversive distance $\sigma_{\ell j}$ using Equation 2.1 or 2.2. Now consider $K(I, A)$ a separated flower with nexus v_ℓ, $I = \{\sigma_{\ell k}, \sigma_{k,,k+1} = 1 \colon C_j \sim \mathfrak{C}\}$, and $A(v_\ell) = 4\pi$ (see Figure 7.7).

Using the label $R = \{r_\ell\}$, $K(R, I, A)$ is a motif. Because $\mathfrak{C}$ is coherent and the edge assignments were chosen according to $\mathfrak{C}$'s layout, $K(R, I, A)$ will also be coherent. $K(R, I, A)$ is thus a generalized branch point, and any layout of $K(R, I, A)$ can have the petals isomorphically mapped to the petals of any layout of $\mathfrak{C}$. □

In Chapter 2, admissibility was a prerequisite to existence, and a similar assumption is needed here. There are three parts to admissibility. The first two are requirements for the edge assignments less than 1. Only the third part applies, as all edge assignments on shift-points are assumed to external tangencies. For a single flower, part 3 simply states that the angle assignment cannot exceed the flower's maximum angle sum (when $r \to 0$).

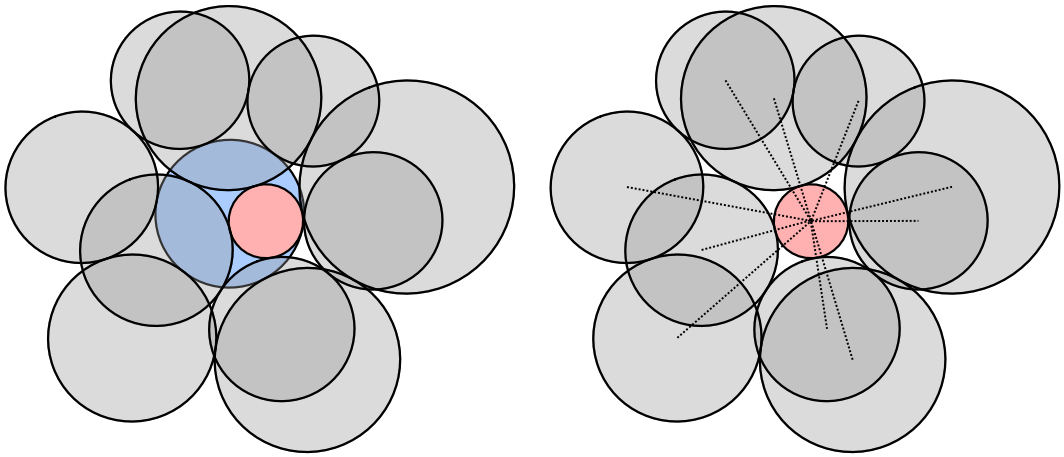


Figure 7.7: Realizing a shift-point as a generalized branch point. The shift-point is converted to a flower with edge assignments $I \geq 1$ using the little sister circle as the nexus.

Lemma 7.7. *If a flower at v is admissible for $I \equiv 1$ and $A(v) = 4\pi$ then for any set of petal radii there exists an r_b such that $\mathfrak{C}(r_b, x)$ is a coherent shift-point.*

Proof. $I \equiv 1$ for shift-points so admissibility is equivalent to Definition 2.6, i.e., the flower is a branch structure meaning that it has at least 5 petals. As in the proof of Theorem, 7.6 realize the shift-flower as a flower with nexus r_ℓ and edges determined by inversive distances greater than or equal to 1. Dynamically assign these edges according to the layout and changes of $\mathfrak{C}$. Call the angle sum of this flower $\theta_\sigma(r_\ell)$.

By Theorem 7.4 decreasing r_b increases $\theta(\mathfrak{C}(r_b, x))$ and thus increases $\theta_\sigma(r_\ell)$. So both these angle sums share the same end behavior, as $r_b, r_\ell \to 0$, $\theta(\mathfrak{C}), \theta_\sigma \to n\pi$ where $n \geq 5$. So there exists a r_b such that $\theta(\mathfrak{C}(r_b, x)) = 4\pi$. □

Definition 7.8. Let $\{\mathfrak{C}\} = \{\mathfrak{C}_i(r_{i,b}, x_i)\}$ be a collection of decorated shift-points on a complex K for interior vertices v_i, and let F_i be the set of petals for a $\mathfrak{C}_\mathrm{i}$. We say that K is *adjusted* with $\{\mathfrak{C}\}$ to indicate that shift-points are being placed at the vertices v_i. Placing a $\{\mathfrak{C}\}$ on K will preserve all decorations except for each v_i's flower edge assignments which will all be set to 1 (external tangencies).

To avoid some hairy special cases it will be assumed that $F_i \cap F_j = \emptyset$ and $v_i \in \mathrm{int}K$ for all $\mathfrak{C}_i, \mathfrak{C}_j \in \{\mathfrak{C}\}$. Further assume that a complex will be admissible for $A(v_i) = 4\pi$ if $\mathfrak{C}_i \in \{\mathfrak{C}\}$. This is so that admissible complexes will be "admissible for shift-points" by Lemma 7.7 after placing $\{\mathfrak{C}\}$.

Theorem 7.9. *Let $K(I, A)$ be an admissible decorated complex that has been adjusted with a $\{\mathfrak{C}\}$. Then there exists a unique generalized branched motif $K(R, I, A)$ with shift-points at $\{\mathfrak{C}\}$.*

Proof. Theorem 2.13 and 2.14 prove the statement above for complexes without Shift-points. By assumption $K(I, A)$ is admissible for $A(v_i) = 4\pi$ for each $\mathfrak{C}_i \in \{\mathfrak{C}\}$, and so Lemma 7.7 guarantees that the relaxation operator (definition 2.10) can be applied to shift-points.

Surveying the proofs of Theorems 2.13 and 2.14 one finds that the monotone behavior of the traditional flowers and their petal angles is the key behavior (Lemma 2.4). The fact that the center of the flowers are circles plays no other role. The same can be said of Theorem 2.13's other supporting lemmas. Theorem 7.4 provides monotonicity at the shift-points, and Corollary 7.5 provides monotonicity on its petal angles. So the result then follows similarly to Theorem 2.13. □

To the global structure, shift-points provide the same branching qualities of a traditional branch point. Additionally the shift-ratio is a continuous parameter with which the motif can be adjusted (Section 7.3 will introduce another parameter). Just like the fractional branching of Chapter 6, puncturing the sister circles creates a border element with a total turning angle. If the resulting motif is coherent it will necessarily have a total sum that is an integral multiple of 2π. This punctured motif is in every way a traditional circle packing. Yet the local differences at the shift-points express themselves globally creating distinct motifs.

Theorem 7.10. *Let $K(R, I, A)$ be a simply connected motif with $\{\mathfrak{C}\}$. If $K(R, I, A)$ is a generalized branched motif then it is a branched circle packing.*

Proof. The motif exists by Theorem 7.9 and then so does the layout. Since every shift-point is coherent, the holonomy of the closed chain around each shift-point is also coherent. Puncture each of the shift-points in $\{\mathfrak{C}\}$ so that these chains are now border chains of K. Now the result follows by Remark 5.2. □

By Theorem 7.9 the radius r_b in a coherent $\mathfrak{C}$ is determined by its label and ratio x. As such it makes sense to exclude r_b in the notation except when referring to it as a variable, e.g., as in Lemma 2.4. This cleans up the notation nicely for a shift-point; we now just write $\mathfrak{C}(x)$.

7.3 Modified Shift-Points

Definition 7.11. A *modified shift-circle* is a shift-circle defined by the closed path in the normalized position as follows:

$$\gamma(\vartheta) = \begin{cases} r_b e^{i\vartheta} & \text{for } \vartheta \bmod 4\pi \in [0, 2\pi) \\ r_\ell e^{i\vartheta} + (r_b - r_\ell) & \text{for } \vartheta \bmod 4\pi \in [2\pi, 4\pi). \end{cases}$$

The *modified shift-point* at an interior vertex v will be the shift-point $\mathfrak{C}(r_b, x, \varphi)$ where the lead-petal C_0 is placed at $\gamma(\varphi) > 0$ in the layout of the shift-flower. φ is called the *phase angle*.

For the remaining of the thesis all shift-points will be modified; the notation will not change except for the additional decoration, φ.

This type of generalized branching creates two degrees of freedom both of which can be adjusted continuously. These are the sister circle's radii ratio, x, and the lead-petal placement, φ. The former is easier to visualize. Change the ratio and the curve is made longer or shorter. One would expect this to decrease or increase the petal wrapping, respectively. How the latter parameter effects the branching is a little more subtle and less predictable.

Unlike circles, shift-circles do not have constant curvature (as planar curves). Thus a shift-point's angle sum will not only be dependent upon the label but the phase angle. Theorem 7.4 still applies. So monotonicity at the shift-point is unaffected by this additional parameter. However it is not so for the petal angles.

That is, while decreasing r_b will increase $\theta(\mathfrak{C})$, the angle sums of neighboring flowers may decrease (as normal) or increase. This occurs because changing r_b can change the positions of neighboring flowers in relation to the jump-point. To summarize, this structure behaves very much like a traditional branch point from its perspective, but not so for its neighbors. This effect can be seen at C_{j-1} in the right side of Figure 7.4. In the previous sections this issue was avoided by fixing the lead-petal at p.

Refer to the example shown in Figure 7.8. The labels are identical; only the layout method was changed. The petals were laid out counter-clockwise both beginning with the same petal, but differing in the starting location of the the lead-petal (as indicated in the figure). Even though the same label is used, one layout is coherent and the other is not.

The difference in the two layouts was caused by the placement at the jump-point, where the curve transitions from the big to the little sister circle. So unlike a traditional flower where a flower's angle sum is invariant to the petal layout, it matters very much here. This lack of continuity in the curvature opens the possibility for somewhat unpredictable angle changes.

It is the transition between sister circles that creates this issue. Specifically, a decrease of the center circle (r_ℓ and r_b together with x fixed) tends to increase angle, however it may also move a petal onto the larger circle. The petal thus has one of its neighbors increase; a change which can possibly increase its angle sum. For this reason, the phase angle variable was waived so that Theorem 7.9 could be obtained.

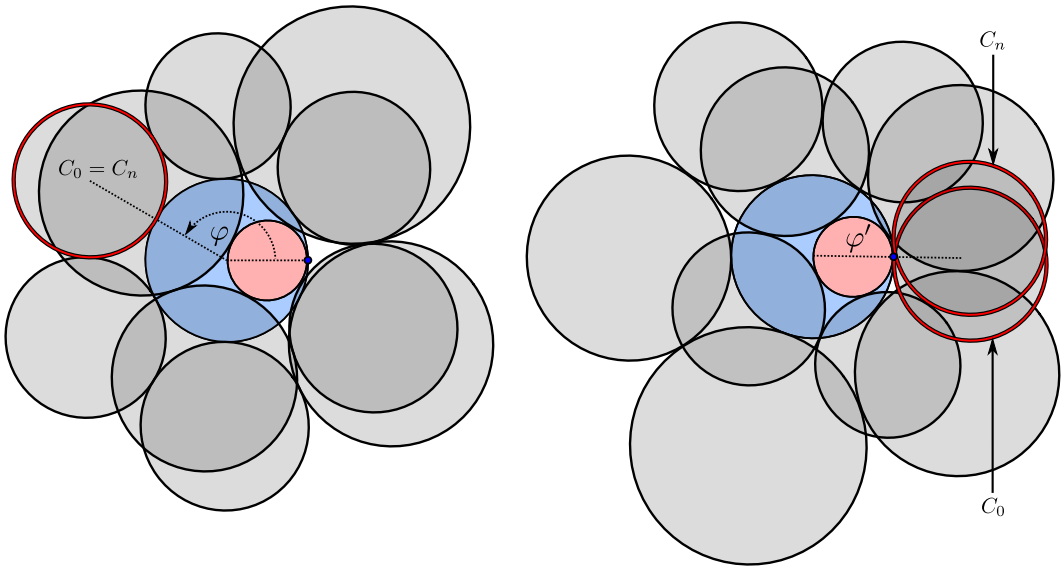


Figure 7.8: How the phase angle changes the layout of a shift-point. On the left is $\mathfrak{C}(1, \frac{1}{2}, \frac{4}{5}\pi)$, and on the right is $\mathfrak{C}(1, \frac{1}{2}, 0)$. C_0 and C_n, outlined in red, are both associated with the same vertex.

The labeling of the petals is arbitrary, and selection of the lead-petal will discretely effect a non-modified shift-point in a manner similar to changing the phase angle. The lead-petal is suppressed as a decoration because it is not a continuous parameter, however it does have the advantage of preserving petal monotonicity.

Remark 7.12. Let $\mathfrak{C}$ be $\mathfrak{C}'$ be two shift-points with petals $\{C_0, C_1, \ldots, C_n\}$ where $\mathfrak{C}$ has lead-petal C_0 and $\mathfrak{C}'$ has lead-petal C_k for $0 < k \leq n$. That is, $\mathfrak{C}$ and $\mathfrak{C}'$ are identical except that their petals are laid in different orders. If $\mathfrak{C}(r_b, x, \varphi)$ is coherent then

$$\mathfrak{C}'(r_b, x, \varphi + \varphi') = \mathfrak{C}(r_b, x, \varphi),$$

for $\varphi' = \theta(\mathfrak{C}; C_0, C_n)$; see Figure 7.9.

Existence and uniqueness came rather easily once monotonicity was established. However it is not unfathomable that Theorems 7.9 and thus 7.10 might be extended to include modified shift-points. Oded Schramm was able to generalize the KAT Theorem for a much broader class of shapes [38, 39]. The convex disks Schramm used should suffer from some of the same monotonicity problems. Although Schramm's results have yet to be generalized to any type of branched packings, methods similar to his might succeed where we have decided to bow out.

For illustration, inspiration, and just plain fun the chapter ends with some pictures. The first set of pictures, Figure 7.10, is an example of a single shift-point with fixed petal radii. The ratio x has been incrementally decreased from $x = 1$ (when the shift-point is a traditional branch circle) to $x \approx 0.0001$. Figures 7.11 and 7.12 are a menagerie of various examples. Included are motifs in $\mathbb{C}$ and $\mathbb{D}$ with multiple shift-points.

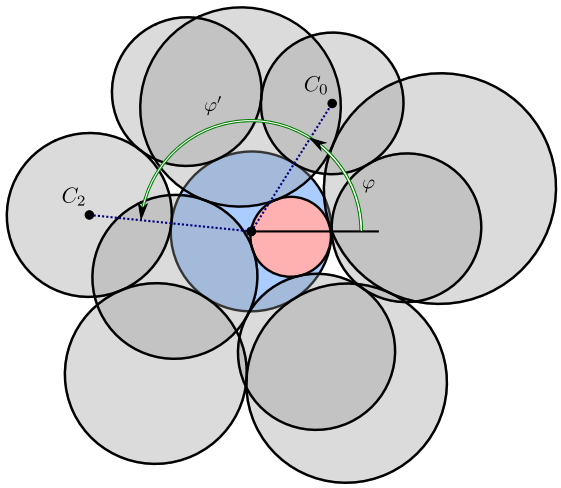


Figure 7.9: The choice of the lead-petal is arbitrary in a modified shift-point. The layout in the picture is of both $\mathfrak{C}(r_b, x, \varphi)$ using lead-petal C_0 and $\mathfrak{C}(r_b, x, \varphi + \varphi')$ using lead-petal C_2.

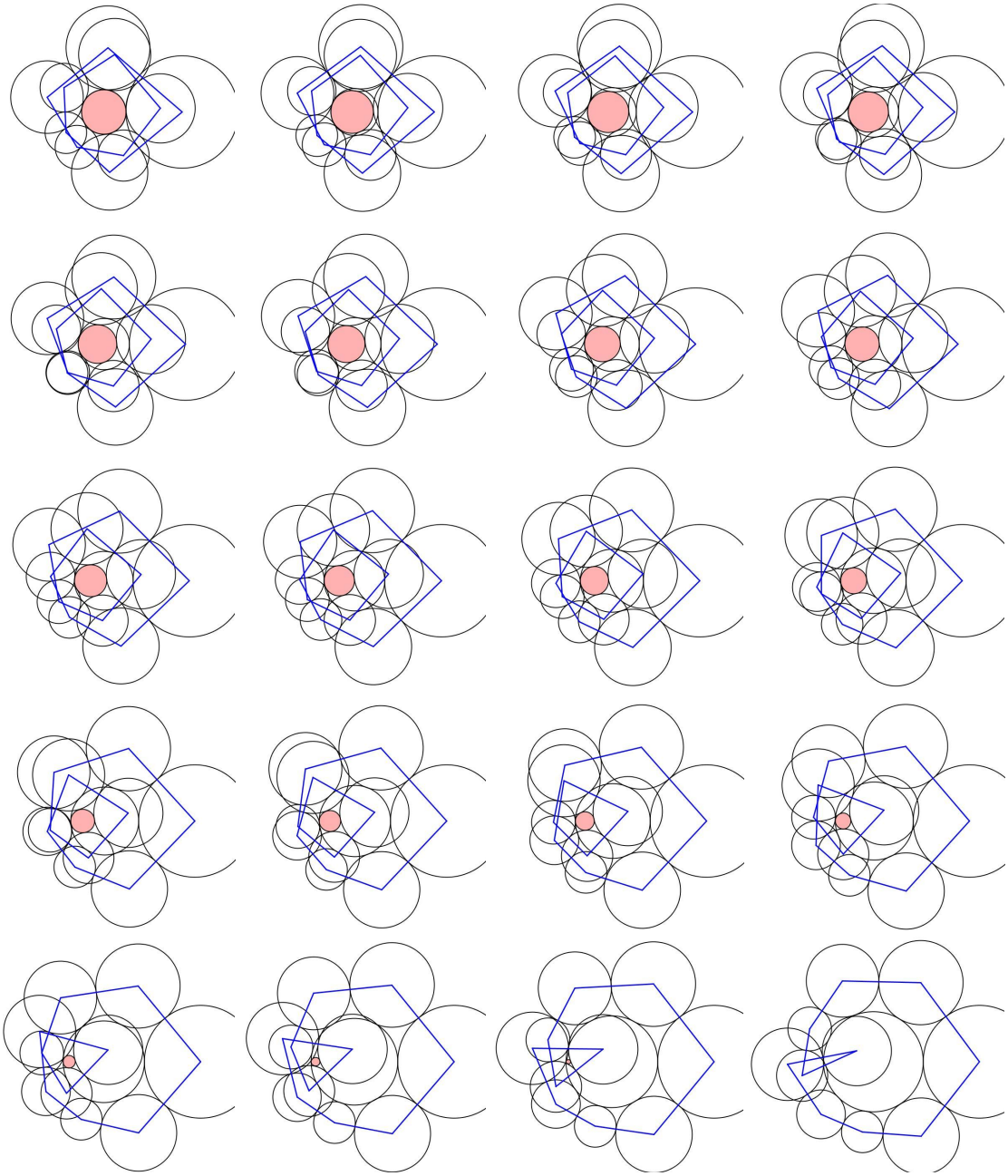


Figure 7.10: Incremental changes of the shift-ratio on a shift-point. The little circle is pink and the border edges are blue.

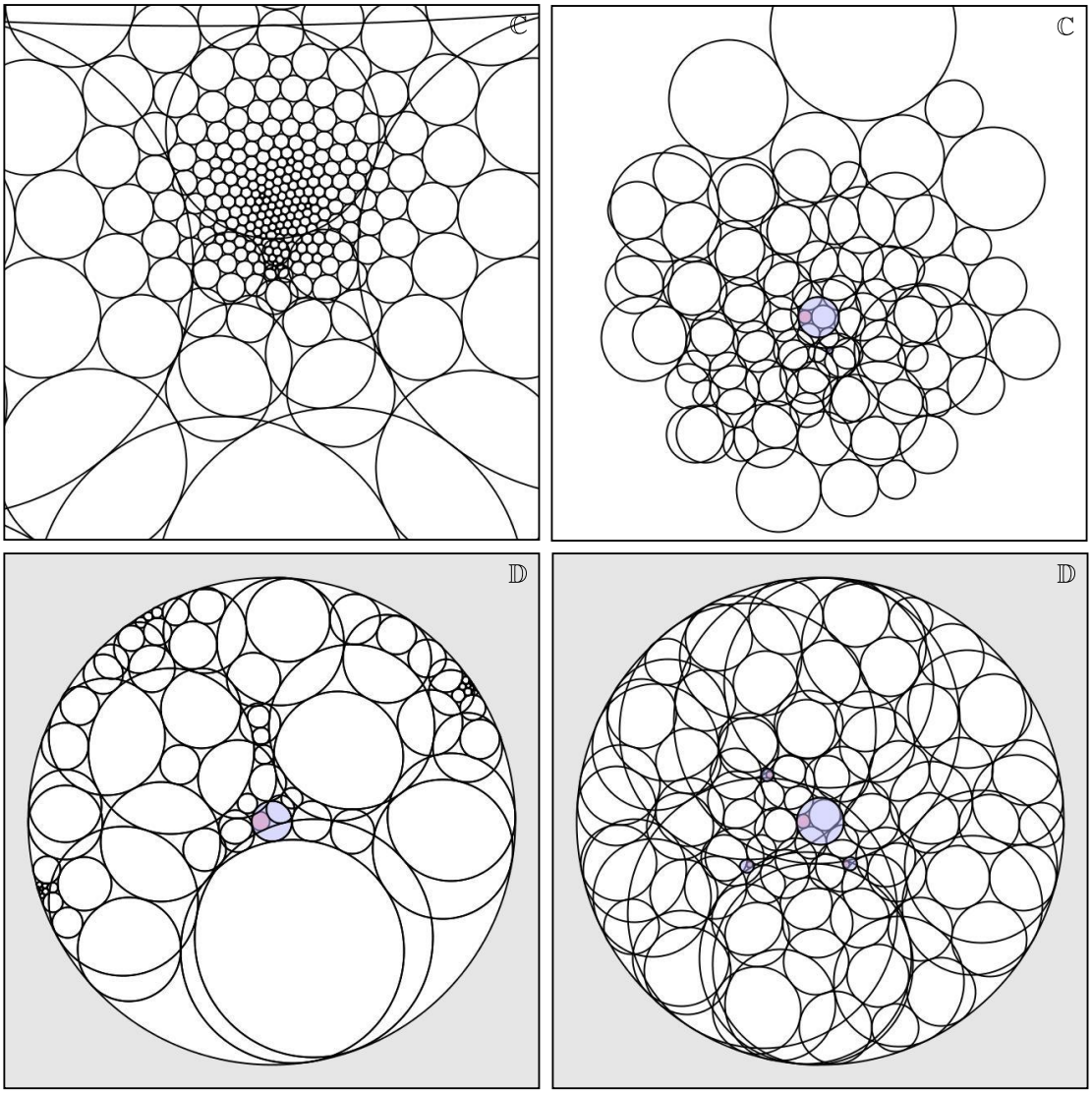


Figure 7.11: Various branched circle packings with shift-points.

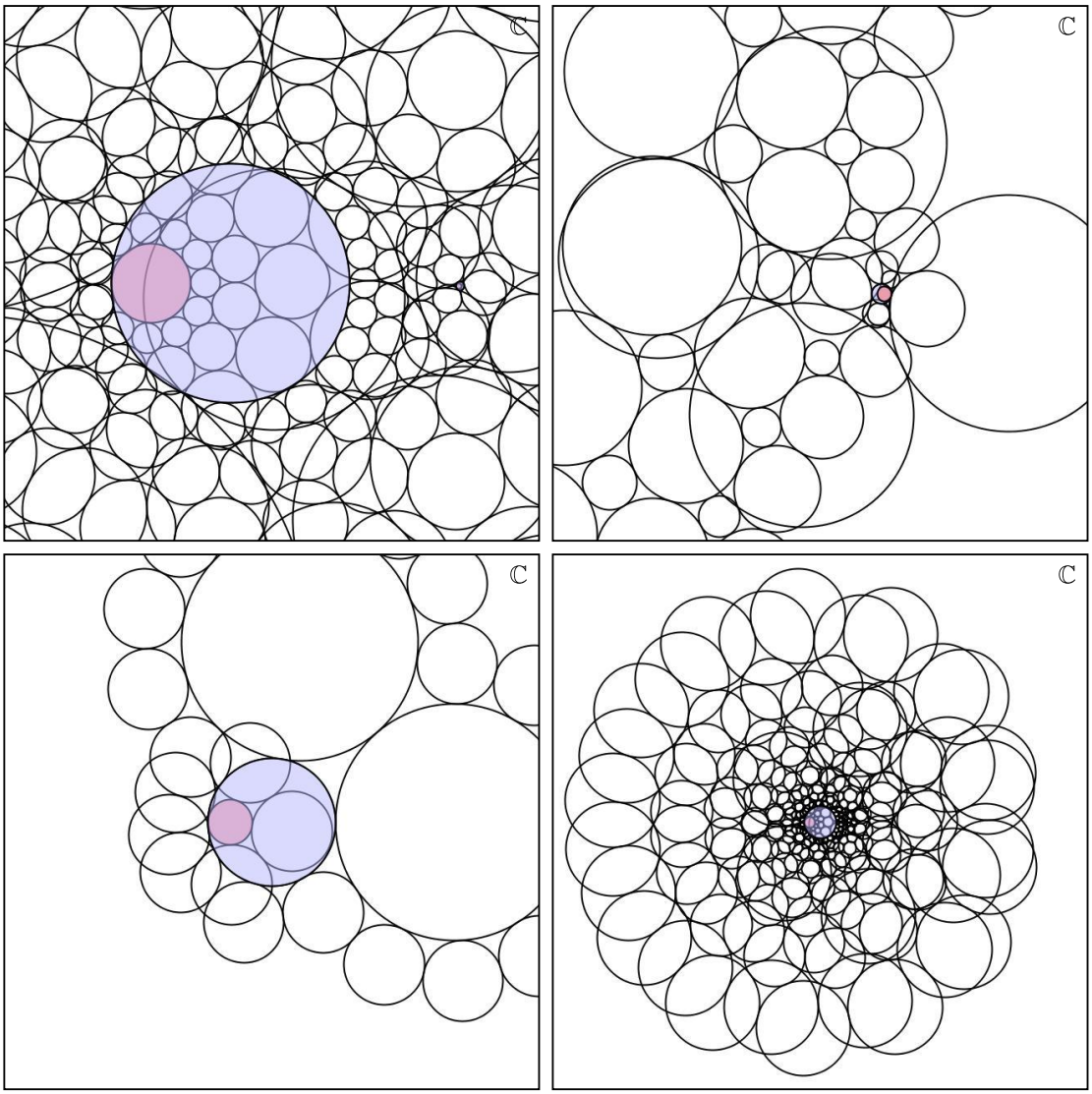


Figure 7.12: More branched circle packings with shift-points.

Chapter 8

Experiments

The geometric behavior of maps between simply connected circle packings parallels that of classical analytic functions quite well, even in the most coarse complexes. Discrete analogies such as the Schwarz lemma, Blaschke products, polynomials, rational functions and others are pleasingly similar to their classical cousins in most aspects (save the methods of their proofs). It has been demonstrated how this parallel deteriorates when multi-connected complexes are considered. The purpose of this chapter is to explore, through illustrative examples, techniques which might reestablish these links.

We have seen that obtaining analogies of the same quality with traditional circle packings is unfortunately not possible. The dance between a motif's combinatorics and its radii creates a geometry which in turn determines the location of vertices. Having a finite number of vertices limits where branching can be induced, the selection of which will be too small in all but the most fortunate of cases. This is the key problem with which we are confronted, and which we saw illustrated in Chapter 4.

Inserting some sort of flexibility will be necessary, and we will do this in a number of ways, all of which will involve a relaxation of the circle packing structure according to some continuous parameter(s). These continuous modifications will be restricted to small localized areas such as a single flower or chain of edges; they will be realizable as the generalized branch points described in Chapter 5. In this way our motifs will be circle packings except in isolated sub-complexes. The goal is to find such parameters with sufficient flexibility to achieve coherence without trading too much global rigidity.

Consider the flower with fixed petal radii. If we treat the radius of the center circle as a continuous parameter it has the qualities we desire. The flower can always achieve coherence, an angle sum of 2π, i.e., its range of effect is sufficient; monotonicity makes it predictable, and the result is unique. Furthermore it does not introduce any unnecessary degrees of freedom. An angle sum of 2π guarantees coherence, a target which is dependent on this single parameter, the central radius. Of course it is also much too restrictive for our purposes as local coherence is necessary but not sufficient for global coherence. However, in toto its behavior is an archetype of what we seek: sufficient scope, predictable behavior, and rigidity.

The nature of circle packings is that the effects seen globally do not exceed the local effects where a change occurred. So the range of an adjustment's effect is inherently somewhat limited. Additionally, independence of parameters is an issue. The endless variety of complexes means that the minimum number of parameters needed may not necessarily be constant. On the positive side, circle packing is ideally suited for computer experimentation and we have the powerful software package `CirclePack` with which to conduct experiments.

There is no ceiling on the number of experiments to try. The variety of different complexes, branch points, and boundary conditions is endless. For the purpose of illustrating key advantages and limitations of different parameters, each section will use a single complex appropriate to its setting. The three examples from Chapter 4 will be examined in turn. Generalized branch points are inserted in an attempt to resolve the issues illustrated in Chapter 4 with varying degrees of success. The different continuous parameters will not be mixed, which admittedly excludes some promising approaches.

8.1 Methods

The underlying mechanics of our methods have been developed in Chapters 2, 5, 6, and 7. Any modification that falls outside the traditional definition of circle packing (Definition 1.2) will be generally referred to as an *adjustment*. Additionally, selective changes of edge assignments will also be called an adjustment. An *adjusted motif* is a motif to which an adjustment has been applied.

Overlapping and separated circles are certainly part of the traditional circle packing catalog, however their place has been as a fixed characteristic which determines the label, i.e., as decorations. The role here will be more like the circles. Rather than finding the radii to fit the decorations (inversive distances, angle sums, and complex), inversive distances are used to help the radii fit the decorations.

This is the viewpoint to be taken with all the adjustments in this chapter. Below, three examples are adjusted in a series of experiments using collections of (modified) shift-points and inversive distances. The former two will be applied at or near a desired branch vertex as described in their respective chapters of introduction. The latter will be applied by increasing or decreasing the inversive assignments of edges emanating from a targeted branch vertex. Call this an *edge adjustment*.

The possibilities for how edge adjustments might be applied are quite broad. We will limit its use to a single flower which then can be viewed as a generalized branch point. In comparison to the endless possibilities, our approach may seem constrained. How global behavior is effected by local modifications can be rather unpredictable due to the variety of complexes. So expansive methods dependent on particular motifs should not be expected to have their results translate well to a more general setting.

The additional parameters afforded by using modified shift-points (as opposed to non-modified shift-points) adds a great deal of flexibility. As of now there is no certainty about the existence and uniqueness of motifs with these types of shift-points (work underway by Edward Crane and Ken Stephenson may answer this). The experiments below begin with an already existing motif. The

adjusted motifs were found with the Circle Packing Algorithm using `CirclePack` (see [14]) which in most cases found a label with very good accuracy.

Admissibility is not being considered with these experiments, however is appears that each decoration parameter in these motifs has a reasonably sized neighborhood of values which can be realized as an adjusted motif. The experiments were not plagued by degenerate or unrealizable labels. Though such problems were encountered they appeared in the most extreme situations, e.g., when shift-ratios were very small.

The shift-point will be treated as dependent upon the shift-ratio x and phase angle φ. In accordance with Remark 7.12 and the note following Theorem 7.10, we write just $\mathfrak{C}_i(x, \varphi)$ for a shift-point at an interior vertex v_i. Computationally the labels appeared to exist when shift-points were inserted. Moreover it is expected that the labels were unique. Although Example 6.6 should be taken as caution against believing that this is in fact true.

Once a motif with shift-points is found, the larger sister circle can be removed. By Theorem 7.6 the smaller sister circle can then be made into a generalized branched flower by simply using the shift-point's layout to assign inversive distances to all of the flower's edges (see Figure 8.1). Call this simple step *converting* the shift-point to a separated flower. This creates a bridge between the shift-point and packings with edge adjustments. Packings with separated circles have a developed and developing theory, e.g., [32, 24]; and some of our unaddressed questions about shift-points may be answered in this way.

For Sections 8.3 and 8.4, the goal will be coherence, the desired classical behavior being already inherent in the decorations. For Section 8.2 this is not the case. Instead a coherent motif will be adjusted with the desired classical behavior being the goal. In each section the different adjustment methods manifest advantages and disadvantages. No clear champion emerges. Rather each method comes with a compromise between outcome and flexibility.

Because modified shift-points and non-admissible decorated complexes are used, coherence is numerically obtained, but not proven. Questions involving existence, uniqueness, and coherence of the labels used in this chapter remain open.

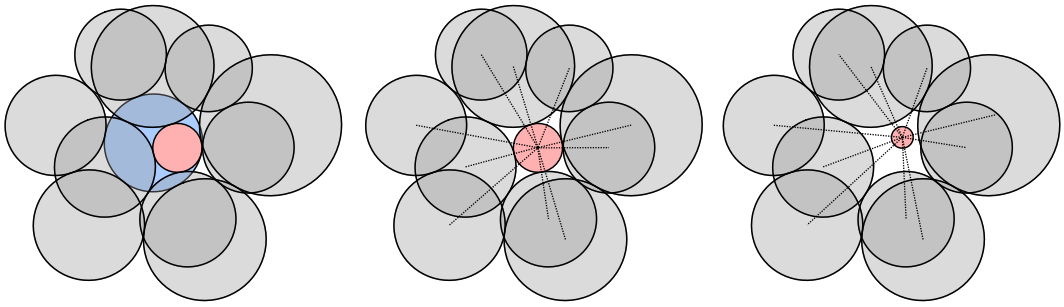


Figure 8.1: A shift-point converted to a generalized branch point. The middle uses the smaller sister circle, and the right uses an arbitrarily small circle.

8.2 Experiments on a Quadratic Polynomial

Let $f^{\#}(v) = |g'|$ where $g(z) = (z - \frac{1}{4})^2$ and $f^{\#}(v)$ is the ratio function. As described in Section 4.3, a discrete function $f : P_{K(R',I,A')} \to P_{K(R,I,A)}$ between Euclidean motifs (R' is the Euclidean label for K_{M}). K is a simply connected disc so coherence is not an issue. As a discrete analogue we would like f to mimic the key behavior of its classical counterpart, that is, to have the layout of the motif place the border circles along the curve $g(z)$ and place the branch point at $g(\frac{1}{4}) = 0$.

The border radii of finite motifs in $\mathbb{C}$ provide a natural and effective means to manipulate the image, however these radii are determined by the function. Neither can the branching be changed, since the location of the branch vertex is one of the target qualities. So traditional means of inserting flexibility are unavailable, and we turn to our toolbox of adjustments.

Shift-points are well suited for this function. Create a branch cut in g's image from the branch point to $(-15/16, 0)$. The two sheets naturally attach themselves to a different sister circle via chains from the border. The consequence of adjusting the shift-ratio x for $\mathfrak{C}(x, \varphi)$ (at the branch point v_1) in our example is that the sister circles pull or push their "closest" border depending on whether they are relatively shrunk or increased, respectively.

It seems to be a general tendency of circle packings that local changes have a greater impact locally, and that this impact lessens moving away (by vertices) from the origin of change. This idea may be somewhat vague, but it is a frequently seen phenomenon when experimenting with circle packings. When applied to how a single radius change affects angle sums, this idea is borne out in the proof of Theorem 2.13. A similar concept was the intuitive inspiration behind Thurston's conjecture that circle packings could approximate classical functions [45]

For reference see Figure 4.2 from Chapter 4. Our goal is to have the discrete version of the function place its border circles in a manner that better imitates its classical version. The result is convincing enough that relying on a formal (and somewhat messy) estimate of error is not necessary.

The image is normalized by placing $f(v_1)$ on the x-axis at $(1/16, 0)$ and v_2 at $(1/16 + r_2, 0)$ (call v_2 the lead-petal; the striped circle in Figure 4.2). We adjust the image of $f(z)$ by inserting a shift-point $\mathfrak{C}(x, \varphi)$ at vertex v_1 with lead-petal v_2. The image motif is then adjusted using the parameters x and φ. When $x = 1$ both sister circles have equal radii, so $\mathfrak{C}(1, \pi)$ is just a traditional branch circle. Figure 8.2 begins with $\varphi = \pi$ and $x = 1$. The ratio x is decreased towards 0. The result shows the shift-point pulling the different segments of f's border; a clear effect, but not in the desired direction.

Next we try $\varphi = 3\pi$. This layout begins by placing the lead-petal on the "little" sister circle. Again, we start with $x = 1$ and then decrease the ratio. (Alternatively the definition for shift-points could be amended to allow $x > 1$; meaning for $x > 1$ the "little" sister would in fact be larger than the "big" sister circle.) The basic shape of the layout's border begins having the sought after shape. Figure 8.3 shows the progression. The two sheets can be seen being pushed and pulled by the sister circles.

There has been unintentional translation due to our choice to identify the shift-point's vertex location with the "big" sister circle. This is easily fixed with one last adjustment. The generalized branched packing pictured on the bottom-left in Figure 8.3 has been adjusted with $\mathfrak{C}(1/30, 3\pi)$. Figure 8.4 shows the same motif after a translation has been applied, fitting its border circles more closely

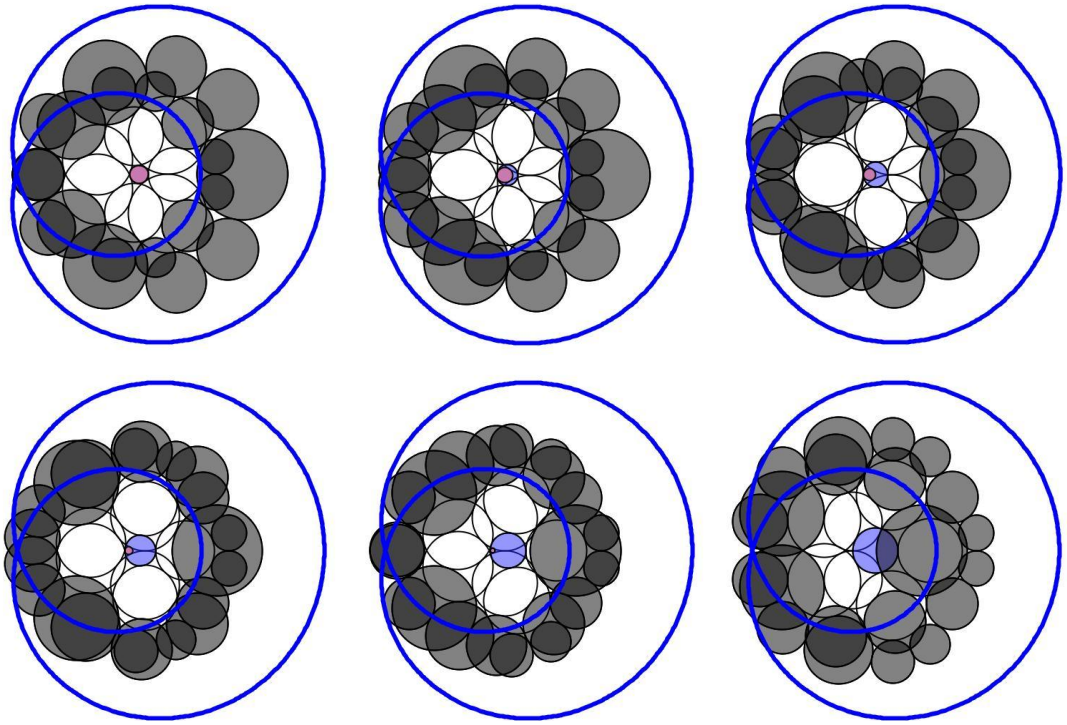


Figure 8.2: Quadratic polynomial adjusted with shift-point $\mathfrak{C}(x, \pi)$ using parameter x. From top-left to bottom-right, the values are $x = 1.0$, 0.75, 0.5, 0.25, 0.125, and 0.0001.

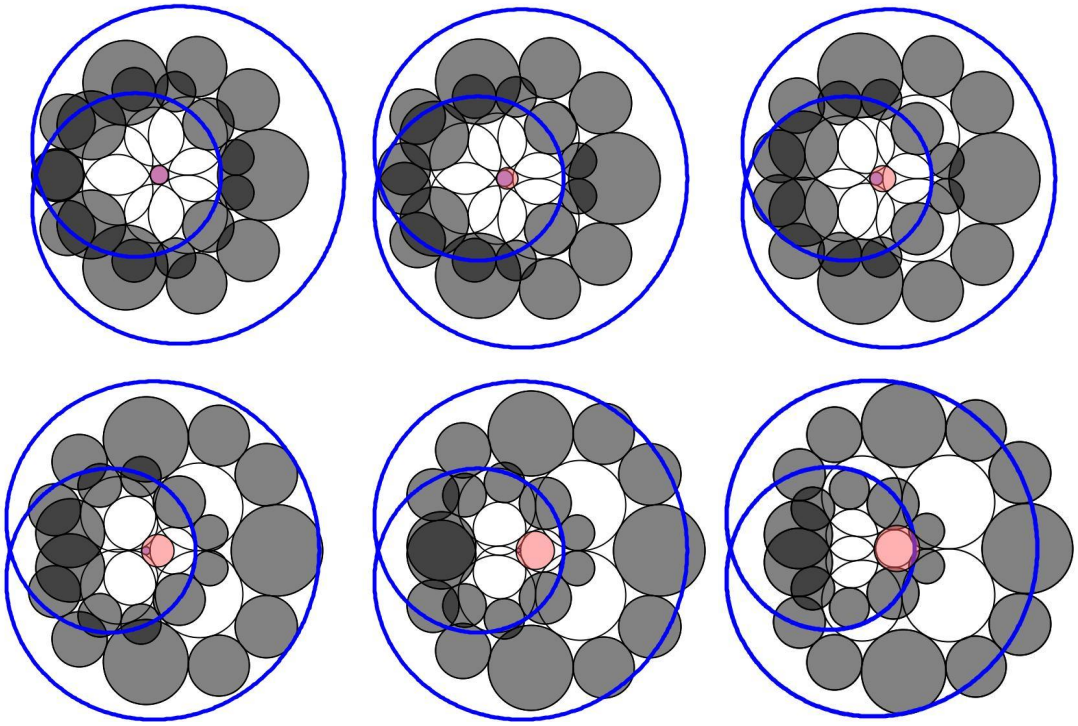


Figure 8.3: Quadratic polynomial adjusted with shift-point $\mathfrak{C}(x, 3\pi)$ using parameter x. From top-left to bottom-right the values are $x = 1.0$, 0.75, 0.5, 0.25, 0.125, and 0.0333.

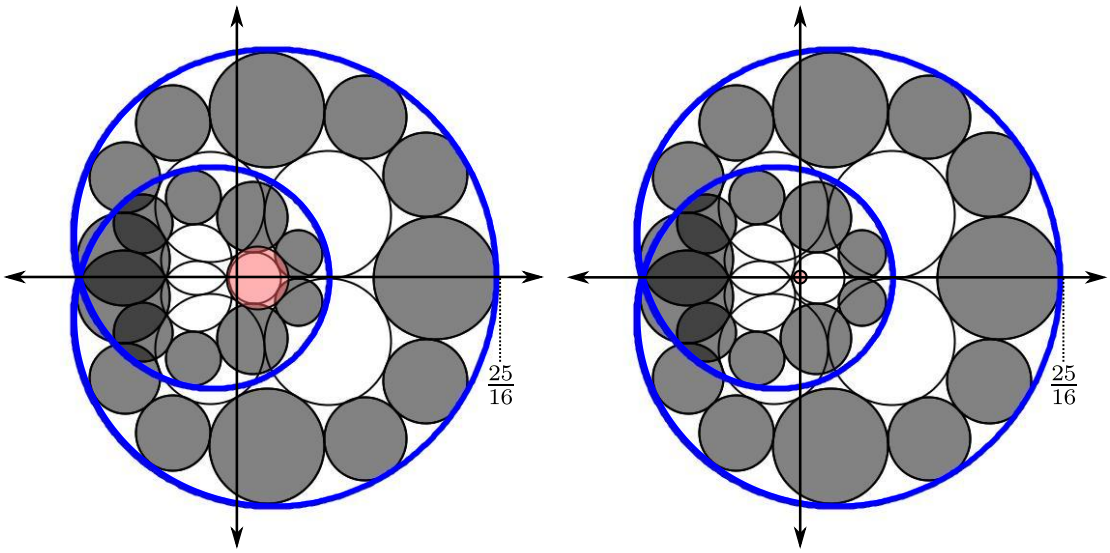


Figure 8.4: The generalized packing from Figure 8.3 adjusted with a separated flower. Using a point inside of $\mathfrak{C}$ and separated edges, the center is fixed at $f(\frac{1}{4}) = 0$.

to the path. The shift-point can be converted to a separated branched flower using a sufficiently small circle centered at $g(\frac{1}{4}) = 0$, and this circle lies inside the generalized branch point $\mathfrak{C}$.

8.3 The Ahlfors Function

In simplest terms we want to find a coherent maximal packing of an annulus in the unit disc. The notation will be the same as used in Section 4.4; R_{A} and $\mathcal{R}$ are labels for a nested annulus and maximal motif, respectively.

In our experiments the domain packing will be the nested annulus $K(R_{\mathrm{A}}, I, A)$, and we seek a discrete map $f\colon K(R_{\mathrm{A}}, I, A) \to K(\mathcal{R}, I, A')$ such that the border circles of the image motif are horocycles and $K(\mathcal{R}, I, A') = K_{\mathrm{M}}$ is a branched circle packing. Furthermore we want to preserve as much of $K(R_{\mathrm{A}}, I, A)$'s characteristics as possible. To this end K_{M}'s angle and edge assignments will be set identical to those in $K(R_{\mathrm{A}}, I, A)$ except where the adjustments are made.

We seek to minimize the holonomy error, E_K (Equation 4.2 as described in Section 4.1), of K's border chains. An annulus is 2-connected so K_{M} is coherent if and only if either of its border holonomies is trivial. However better results, probably due to computational accuracy, were found by using both rather than just one chain.

Our thanks to Edward Crane for providing the annulus in Figure 8.5. It is an annulus with reflexive and translation symmetry. The complex's fundamental domain is on the left; the right has the annulus laid on the sphere. The two selected vertices to be branched (colored gray) are fixed by reflection and swapped by translation. Because of the symmetries, branching at these vertices results in a discrete Ahlfors function motif (a DAF motif; see definition 4.3).

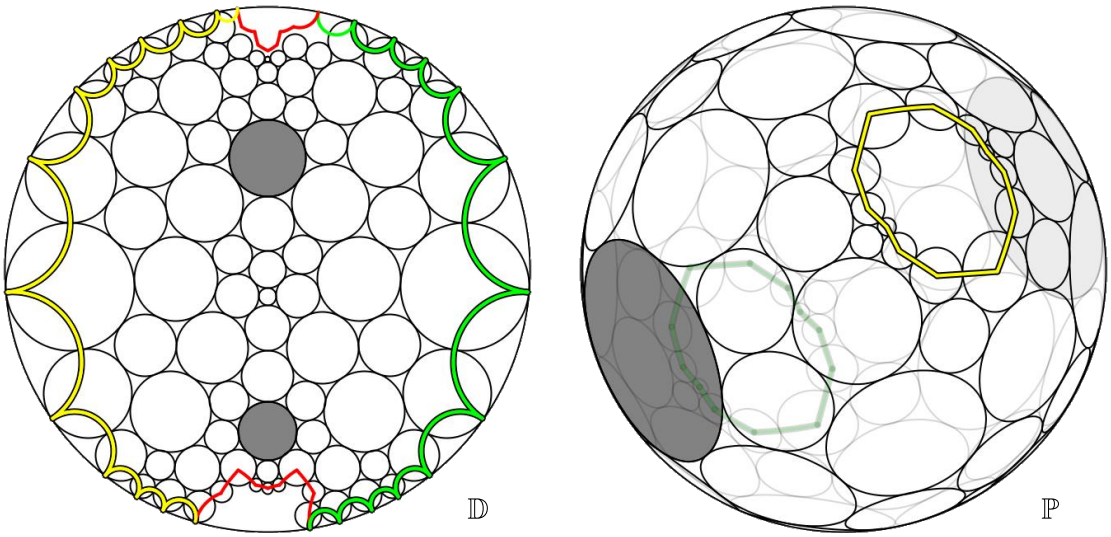


Figure 8.5: An annulus with reflexive and translational symmetry. The two layouts are of the same motif in different geometries. The border edges are colored green and yellow. Circles where branching is to be placed are colored gray. The two red edges on the left identify the same edge.

All the examples in this section are annuli. When branched they will have two branch points and horocycles on the boundaries. All motifs will be branched or generalized branched motifs. For the most part the methods seen here will be applicable to all admissible edge assignments. However for simplicity and clarity (especially concerning pictures) we work with tangency packings, restricting the use of non-tangent edge assignments to generalized branch points.

8.3.1 Example 1: Annulus with Reflexive Symmetry

We break the translational symmetry of Figure 8.5 (but preserve the reflexive symmetry) by conducting a Whitehead move at two symmetric edges as shown in Figure 8.6; call this *Example 1*. The computed branched motif for this decorated complex is not coherent. To better visualize how this flip effects the motif a discrete polynomial construction (see [12]) is used. Briefly we describe how this is done.

Definition 8.1. Given a boundary element, a new vertex called the *ideal vertex* can be added which neighbors all vertices of the boundary element. All the vertices in the boundary element and the ideal vertex become interior vertices.

Let M be the layout of a maximal motif with $n > 0$ border elements. M can be projected to the $\mathbb{P}$ where ideal circles can be added to each boundary element; call the image of this projection $\mathbb{P}(M)$. Identify one of the branch vertices in $\mathbb{P}(M)$, as v_∞, and apply a Möbius transformation mapping it to the outside of $\mathbb{D}$. Then $\mathbb{P}(M)$ can be projected back onto $\mathbb{D}$ with v_∞ as the boundary and its petals as horocycles. Call this last image $\mathbb{D}_v(M)$.

In order for this map to be proper it is necessary that the interior of v_∞'s circle does not intersect any other circle. For externally tangent packings this condition is guaranteed by the fact that half

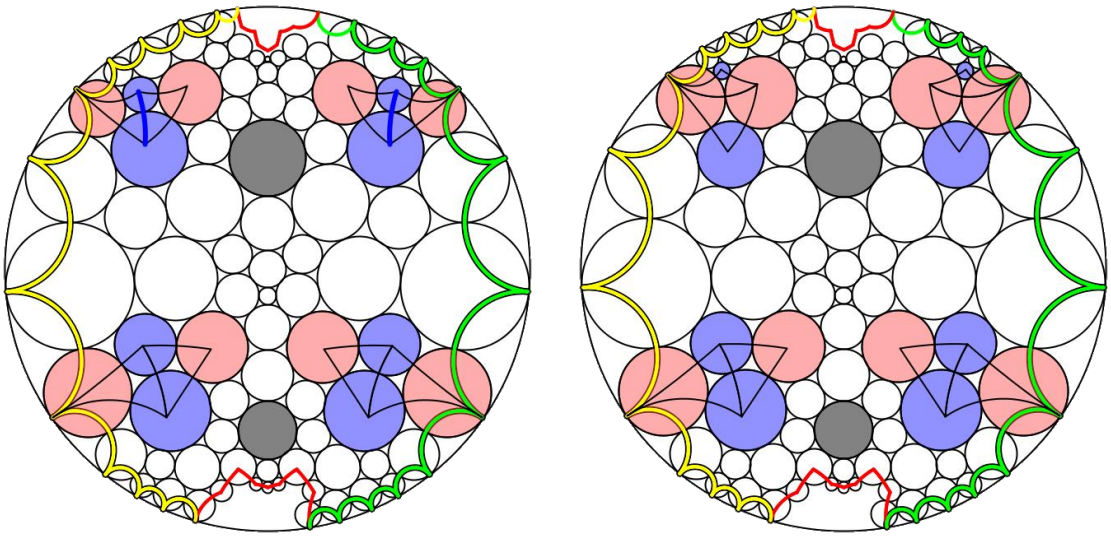


Figure 8.6: Example 1: an annulus with reflexive symmetry. Example 1 (on the right) is derived from the annulus in Figure 8.5 by applying Whitehead moves to the blue edges (on the left), breaking the translational symmetry but retaining the reflexive symmetry.

the branching is at a single branch point. This method allows interior circles to be swapped with the boundary. Call this construction *converting* v (into a boundary), and call the resulting image a *conversion*.

The value of this construction is that $\mathbb{D}_v(M)$ is a simply connected disc with the decorations carried over from M. So the unique label which exists for $\mathbb{D}_v(M)$ creates a coherent motif. Furthermore this motif can be projected back onto $\mathbb{P}$ providing a coherent spherical motif. From here forward it will be assumed that $\mathbb{D}_v(M)$ has this hyperbolic label attached (as opposed to the radii from the image). The ideal circles in $\mathbb{D}_v(M)$ will be mapped such that they coincide if and only if M is coherent. For our example below this will not be the case. Instead we attempt to identically place the ideal circles by adjusting $\mathbb{D}_v(M)$. If this is done then the above steps can be reversed to realize an adjusted Discrete Ahlfors function (DAF) for $K(I, A)$.

Returning to Example 1, swap one of the branch points with the boundary. The two ideal circles are interior circles, but will no longer be identically mapped since the original branched motif was incoherent (see Figure 8.7). Incoherence has been exchanged for an inconsistent border. The two border edges are colored green and yellow, and their associated ideal circles are colored to match.

The two ideal circles represent a single boundary; call one of these circles t. To eliminate the holonomy induced by a DAF map, these two circles must be identically placed in $\mathbb{D}_v(M)$. Any adjustment that reduces the differences of these circles will bring the motif closer to coherence. The shift-point's effect on the boundary in Section 8.2 indicates that it would be a good adjustment candidate, and this is how we shall proceed.

Treating one branch circle as v_∞ leaves the other branch location where an adjustment can be applied, call it v. This vertex was made a shift-point, $\mathfrak{C}(x, \varphi)$. A computational solution was found using `CirclePack` to conduct an exhaustive search over this 2-dimensional parameter space. By a

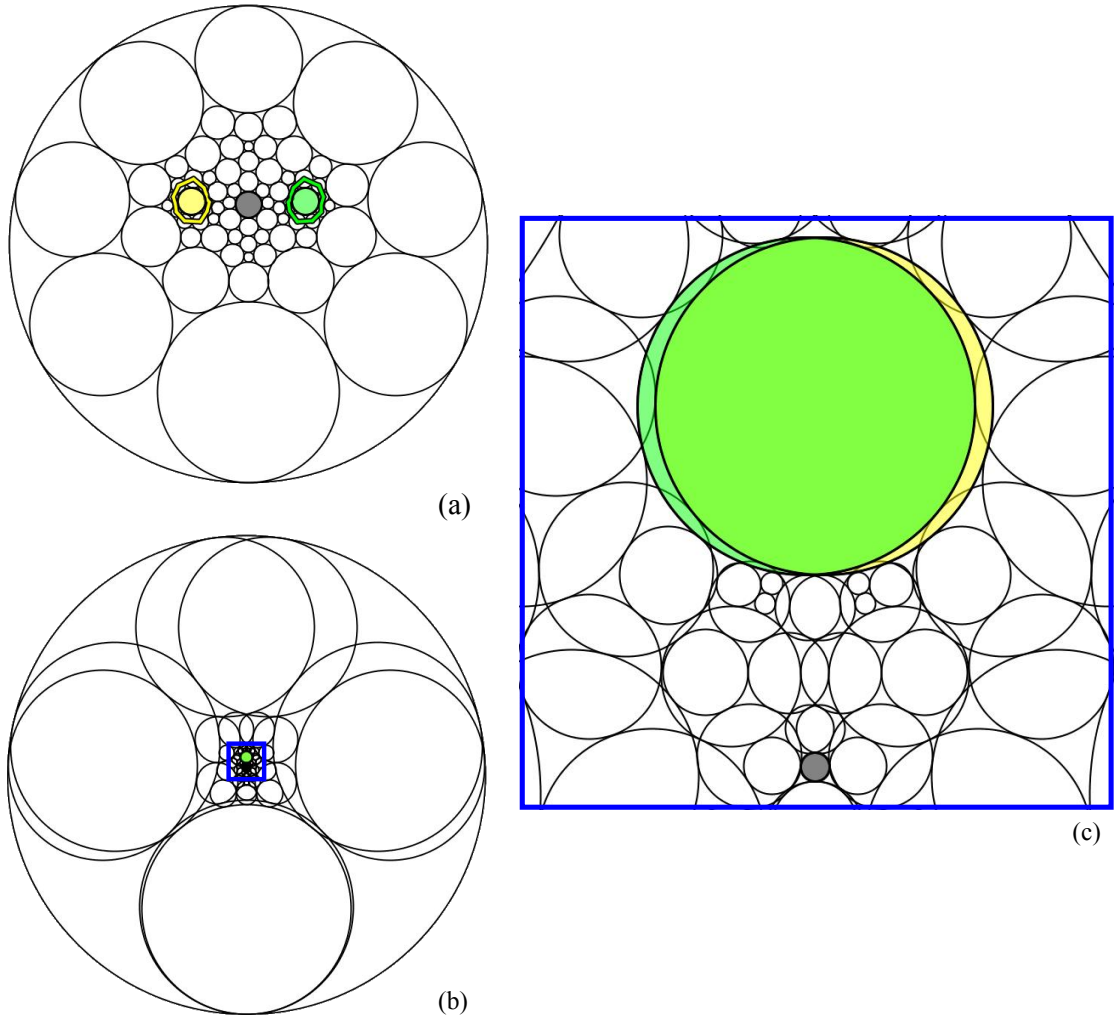


Figure 8.7: A conversion applied to Example 1. (a) is an unbranched $\mathbb{D}_v(M)$, (b) is $\mathbb{D}_v(M)$, and (c) is a detail of the blue box in (b). The ideal circles are colored yellow and green. If the ideal circles were identically mapped then $\mathbb{D}_t(\mathbb{D}_v(M)) = \mathbb{D}_t(\mathbb{D}_v(M))$ would be a coherent DAF (t and u are the vertices of the ideal circles).

solution, we mean values for x and φ such that the holonomy error in $\mathbb{D}_t(\mathbb{D}_v(M))$ is approximately 0. Recall from Remark 7.12 that the selection of the lead-petal is arbitrary, however for simplicity it makes sense to select the lead-petal along the translational axis of symmetry in the image motif.

The motif still has translational symmetry; so it should be expected that the error might be eliminated by adjusting a single parameter. With $\varphi = \pi$, the decreasing x had the general effect of transferring the translation error from the ideal circles to the sister circles of $\mathfrak{C}(x, \varphi)$. A selection of pictures demonstrating this transition (on the conversion $\mathbb{D}_t(\mathbb{D}_v(M))$ is shown in Figure 8.8. A computational solution was found for $x \approx 0.854$; meaning that this motif is a generalized branched packing, and it is the image of a DAF. Lesser ratio values increased the error. So it appears this shift-point's scope of effect easily encompasses the solution.

8.3.2 Example 2: A Non-Symmetric Annulus

By conducting another Whitehead move, the reflexive symmetry of Example 1 can be broken, albeit slightly. The result of such an edge flip is shown in Figure 8.9; call this complex *Example 2*.

As in Example 1, shift-points are used to correct the holonomy (under a DAF map). Unlike Example 1 it was necessary to replace both branch points with shift-points. In the image of the conversion, the ideal circles' center and radii had to match. So in general it would be expected that at least three parameters are required. We needed four to eliminate the holonomy of Example 2; a shift-ratio and phase angle on each shift-point. Improvements were seen when using three, two, and just one of these; but their scope appeared too limited.

Example 2 was modified by replacing the branch points (labeled v_1 and v_2 in Figure 8.9) with $\mathfrak{C}_1(x_1, \varphi_1)$ and $\mathfrak{C}_2(x_2, \varphi_2)$. The extra shift-point prevents us from using a conversion. As in Figure 4.6, two chains serving as function elements layout the motif. The edges of identified circles from each element are colored red.

A single computational solution was found with values $x_1 \approx 1.736$ $\varphi_1 \approx 0.713$ and $x_2 \approx 1.38$ $\varphi_2 \approx 0.858$. The coherent motif and adjustments leading up to it are shown in Figure 8.10. Red edges from the function elements clearly indicate the transformation of the map from a multi-valued function to a DAF. Figure 8.11 shows the image, a generalized branched packing, projected to the sphere.

Figure 8.12 graphs Example 2 with a single shift-point. The graph suggests that the error space is not convex, and makes it seem possible that this solution is not unique. However if another solution does exist it was not to be found after thousands of experiments. It can also be seen how small changes in the parameters can have drastic effects on the holonomy error. It is expected that the apparent discontinuity is actually rapid change, and the jaggedness is likely due to roundoff and computational error.

8.3.3 Example 3: A Coarse Non-symmetric Annulus

Now we return to the annulus from Figure 4.3 in Chapter 4. Call this annulus *Example 3*. Attempting to proceed as in Example 2 only succeeds in illustrating the scope limitations of shift-points. Regardless of where they were placed, we were unable to find a shift-point solution.

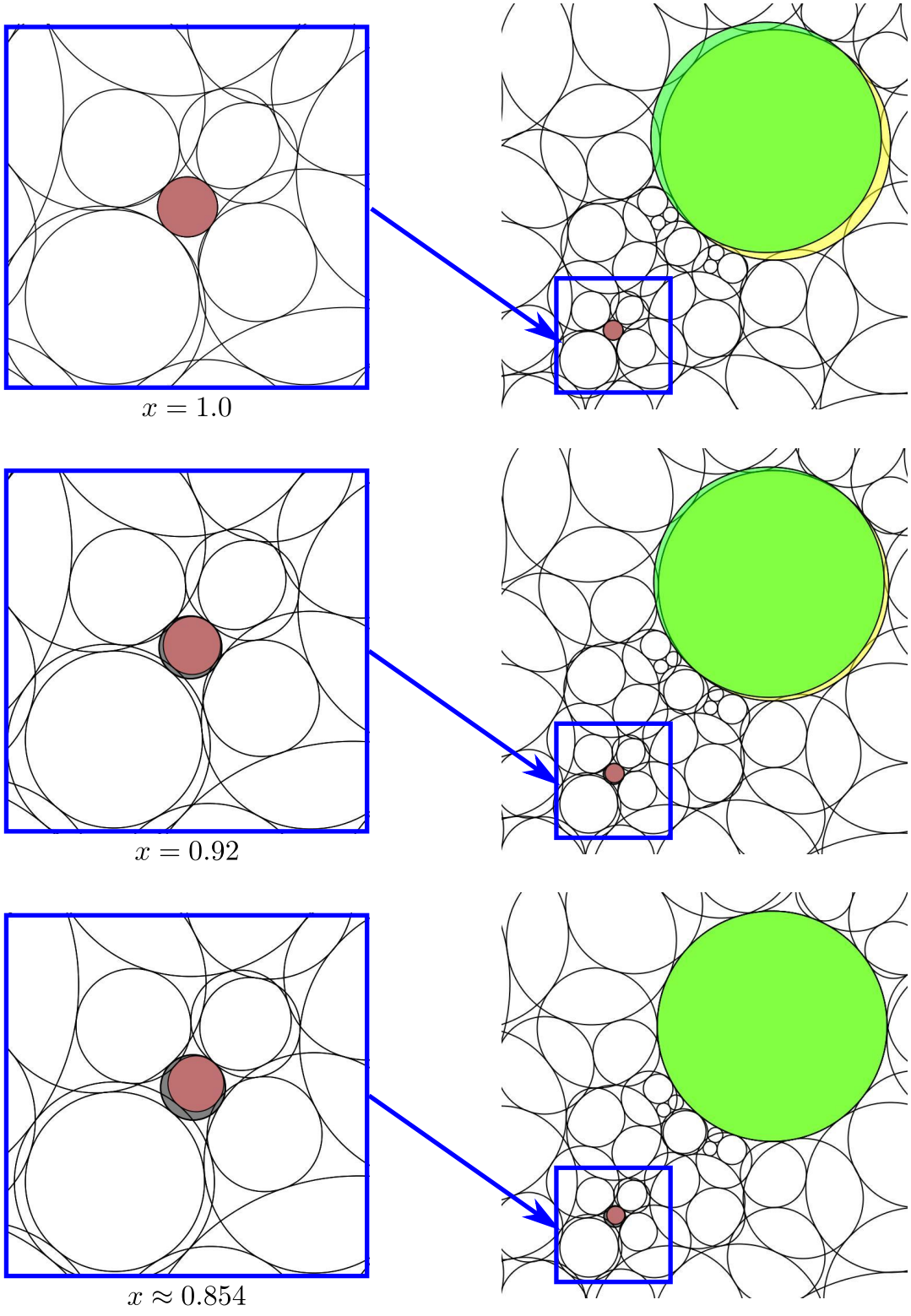


Figure 8.8: Details of the conversion of Example 1. $\mathfrak{C}(x, \varphi)$ on $\mathbb{D}_v(M)$ is shown for varying values of the shift-ratio x.

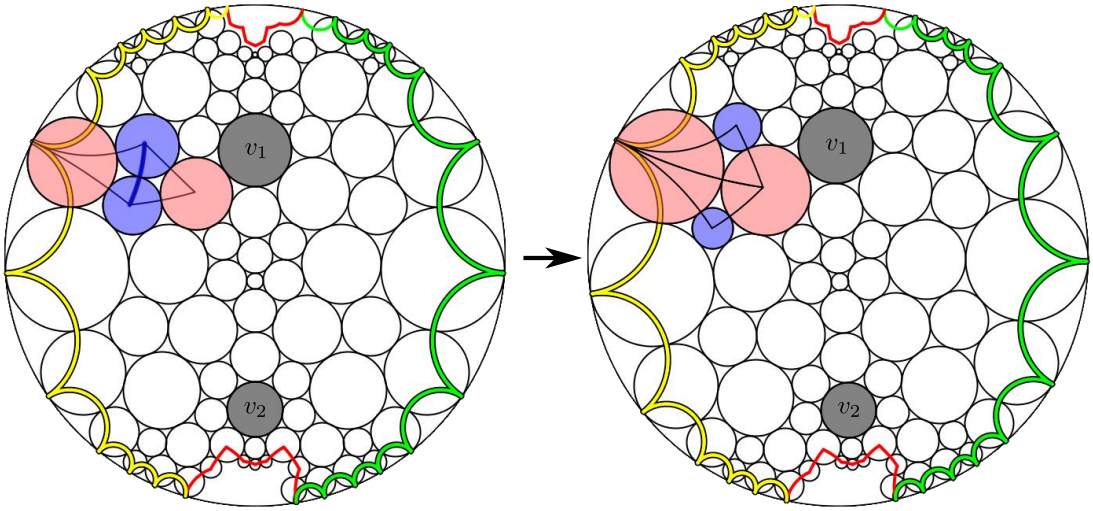


Figure 8.9: Example 2: an annulus with no combinatorial symmetry is created from Example 1. The reflexive symmetry is broken by flipping an edge (blue) in the complex from Figure 8.6 (on the left) creating a non-symmetric annulus, Example 2 (on the right).

We were able to reduce the holonomy error, sometimes substantially. With such coarse combinatorics small adjustments can have an unpredictably disproportionate global effect on the motif, e.g., Figure 8.12. So perhaps a computational solution could be found with greater persistence or improved computational methods. However considering the classical case, it should be expected to have complexes which call for singularities placed between vertices, perhaps on an edge or face, just out of reach of any shift-point's scope.

So we present another adjustment method. Using the same branch points as those highlighted in Figure 4.3, say v_1 and v_2, we adjust the edge assignments of the edges emanating from the branch vertex. Equivalently, we puncture the branch vertices and adjust the border radii along the newly created border edge. This allows a great deal of flexibility at the cost of introducing too many parameters.

We will refer to this adjustment as an *edge assignment adjustment*. There are advantages as viewing the approach both as adjustments on edge assignments and border radii. Both views were used to conduct experiments and construct a computational solution for Example 3. The steps to how this was done are described below.

We converted v_1 to the boundary as in Example 2 with a small alteration. After finding the coherent label for the conversion it was placed in $\mathbb{C}$. This is done by letting all the circles take their Euclidean values and removing the unit circle; call this *puncturing the boundary*. Denote converting and puncturing an interior vertex v in a motif M as $\mathbb{C}_v(M)$. The petals of $v \in M$ are the boundary radii of $\mathbb{C}_v(M)$, and $\mathbb{C}_v(M)$ will be a disc so these boundary radii determine this motif's coherent label.

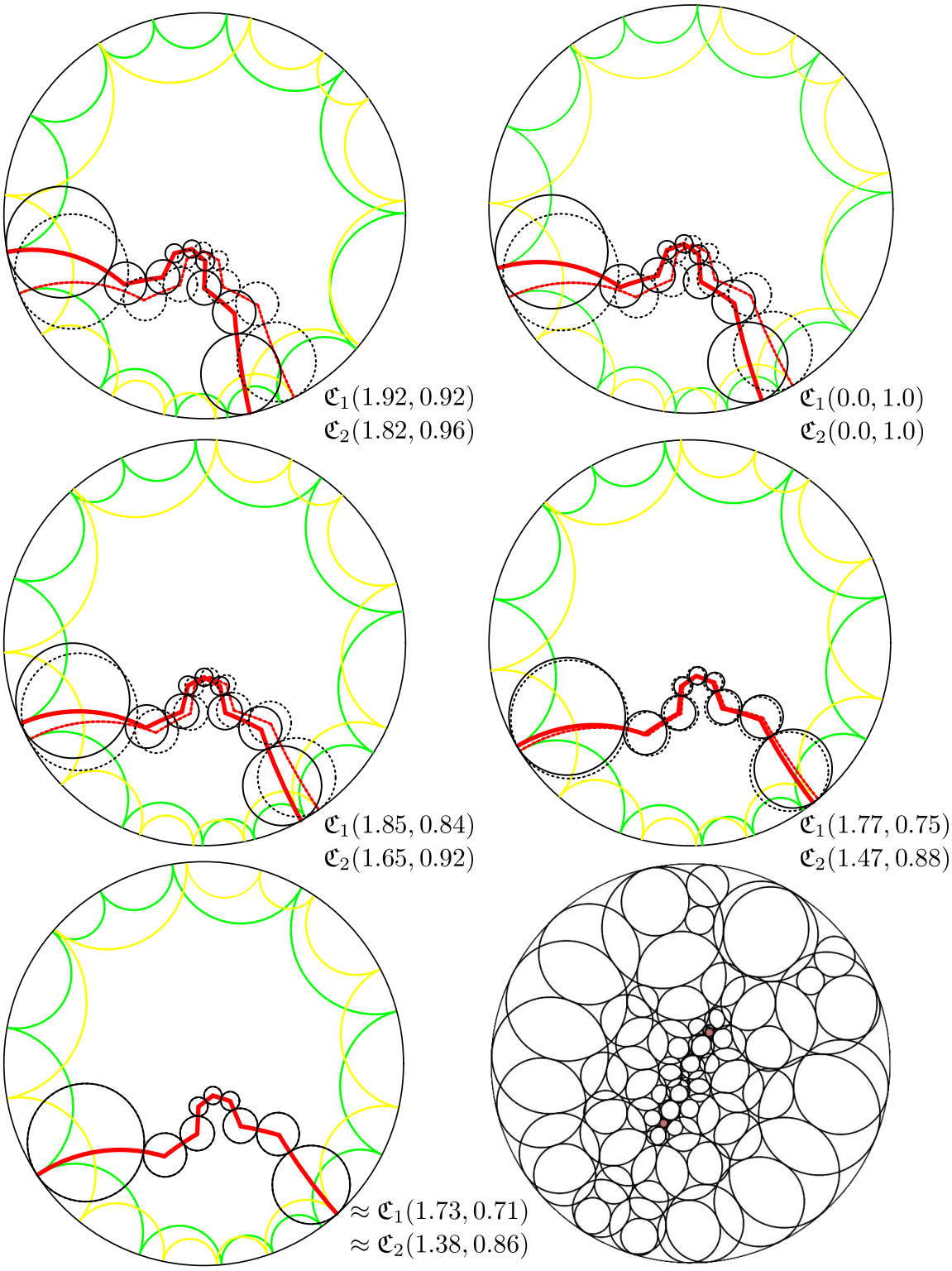


Figure 8.10: Progressive adjustments of Example 2 using shift-points.

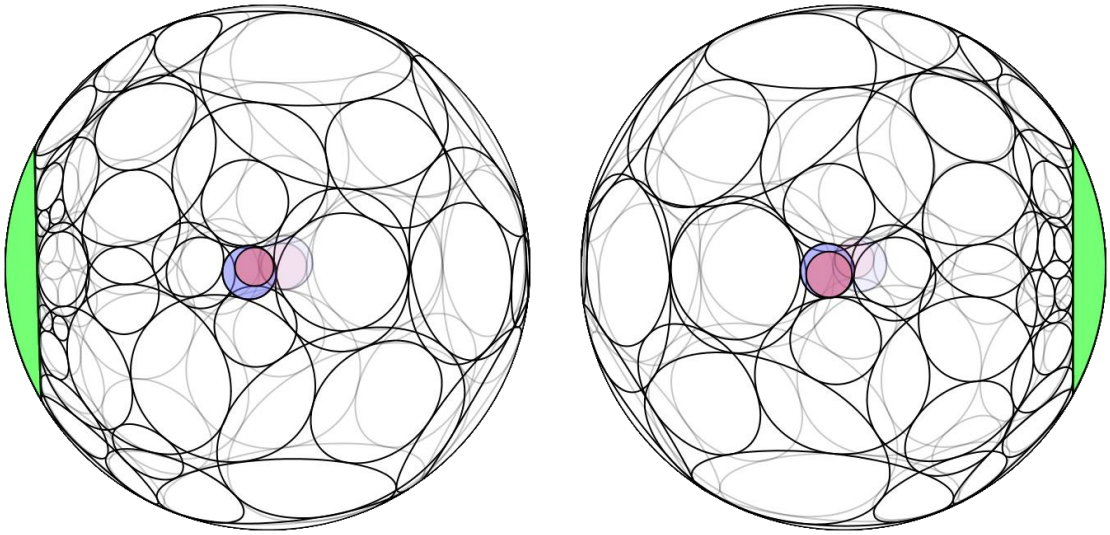


Figure 8.11: Two views of the adjusted solution for Example 2 on $\mathbb{P}$. The views present $\mathfrak{C}_1$ and $\mathfrak{C}_2$ on the left and right, respectively. v_1 was the branch point nearest to the flip in Figure 8.9.

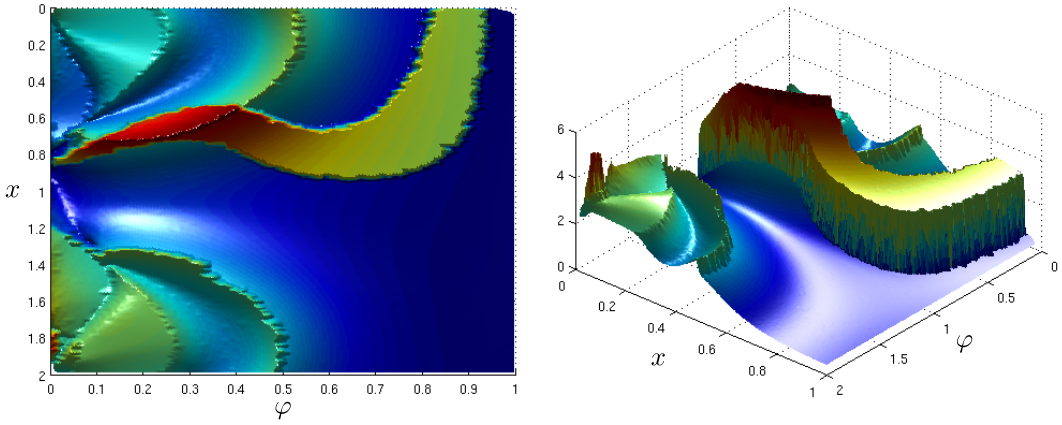


Figure 8.12: The error for Example 2 with a single shift-point. For $\mathfrak{E}(x, \varphi)$: x, φ, E_K are the x, y, and z-axis, respectively.

Let M be the motif for Example 3. We found $\mathbb{C}_{v_1}(M)$, and via a random search sought to minimalism the differences between the ideal circles in $\mathbb{C}_{v_1}(M)$ (the same goal of adjustments in Example 2). A computational solution was not found, but the situation had improved. Then an arbitrary circle was placed in $\mathbb{C}$ such that it encloses $\mathbb{C}_{v_1}(M)$. Projecting to $\mathbb{P}$, this circle is made the circle $C(v_1)$. The edge assignments of M (all greater than or equal to 1) were then adjusted so they matched this image (see Figure 8.13).

Next this process was repeated for v_2. Continuing like this, making adjustments by "ping-ponging" back and forth between v_1 and v_2, refined the motif until a computational solution was found (Figure 8.14). This method has two notable advantages. First, is the greater amount of flexibility over shift-points evidenced by this solution. Second, the computations are much faster. Adjusting border radii allows us to use a packing algorithm which has benefited from years of development. Relatively, our algorithm for finding shift-point labels is rather primitive and slow.

However there is one considerable disadvantage. Using flowers with separated petals, means that the decorated complex is inadmissible, i.e., a label may not exits for the prescribed assignments. Experimentally, this was not a problem, and it is conceivable that existence issues might be avoided by placing reasonable restrictions on the adjustments. The experiment is included in this thesis to highlight the versatility of edge assignments and illustrate the limitations of shift-points.

8.4 The Weierstrass Function

Next we present experiments on the 12-vertex hex torus shown below in Figure 8.15 (also Figure 4.13); call this *Example 4*. This complex was created by conducting flips on the symmetric 12-vertex hex torus from Figure 4.11. Recall from Section 4.5 that a Weierstrass function for Example 4 will require four branch points.

There exists no method for directly computing the labels for a spherical motif. A flower nexus of the spherical complex must be converted to the border (as described in the above section) so that the motif can be computed and laid out in $\mathbb{D}$. Then it can be projected to $\mathbb{P}$ where it will be coherent if and only if it was coherent in $\mathbb{D}$.

If a flower nexus is to be converted to the border it must be a nexus circle whose interior is disjoint from all the other circles in the layout. This means it must be on of the branch circles, adjusting with shift-points is then limited to the three remaining branch circles. Example 4 was rendered from a complex with two translational symmetries by breaking one of them with flips. In light of Examples 1 and 2, one might reasonably assume that three shift-points with a total of six parameters would provide sufficient flexibility.

However the experiments had mixed results. As in the above section, we sought to minimize the holonomy error, E_K. Two non-homotopic generating chains on the torus will be needed, plus the border chain we introduced. The latter chain essentially checks the "local coherence" of the converted vertex's flower the conversion put in $\mathbb{D}$, and `CirclePack` computes the radii for the remaining circles according to their assignments. However, the resulting motif will not in general have a consistent layout.

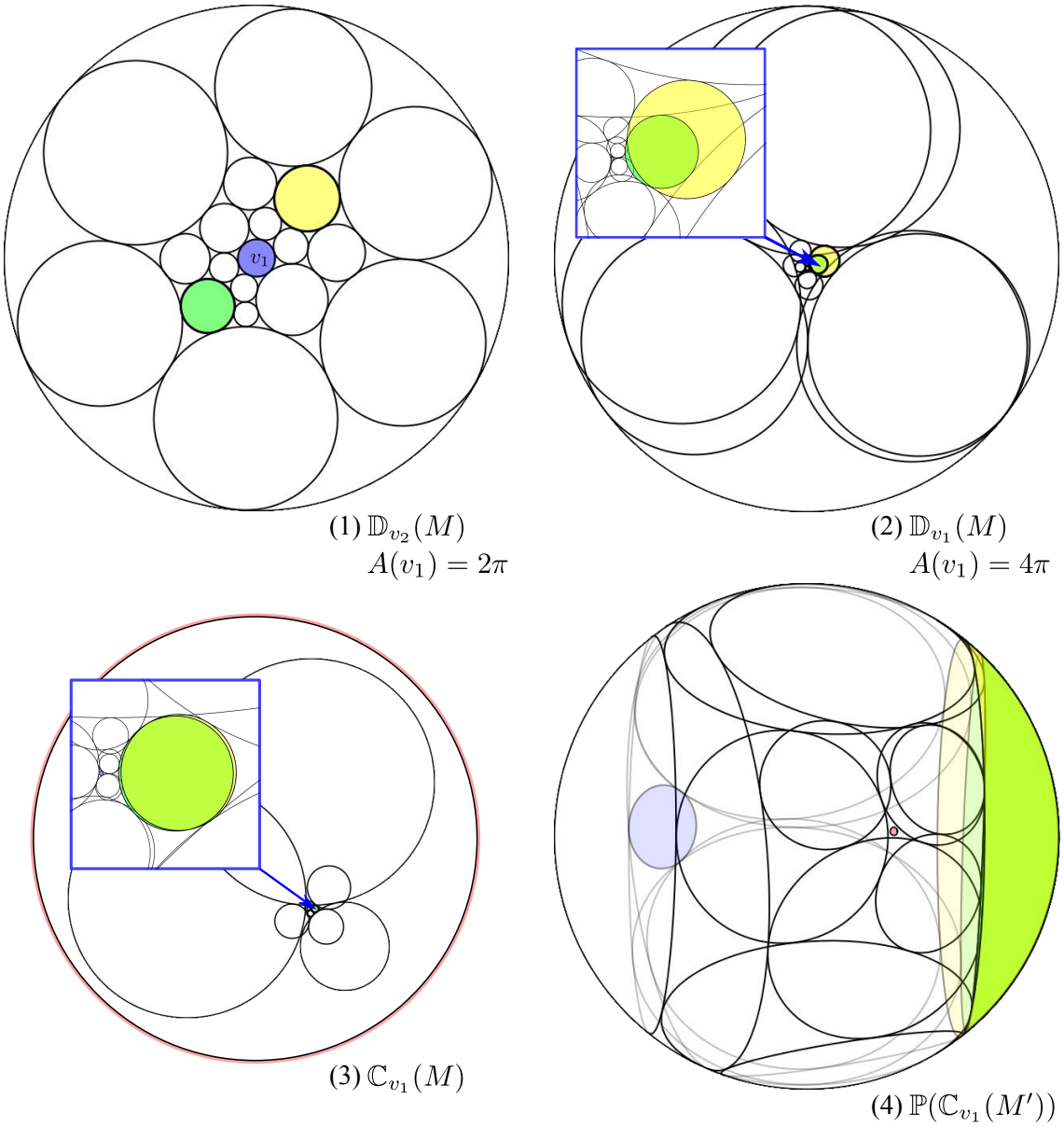


Figure 8.13: The conversion used to adjust the edge assignments for Example 3. (1) The unbranched and (2) branched conversions of v_2. The ideal circles shown in the details are colored green and yellow. (3) The Euclidean border radii have been changed, and $C(v_2)$ has been added as an outer circle. (4) Projection to the sphere, M' is M with v_2's edge assignments (pink circle) set according to their placement on the sphere.

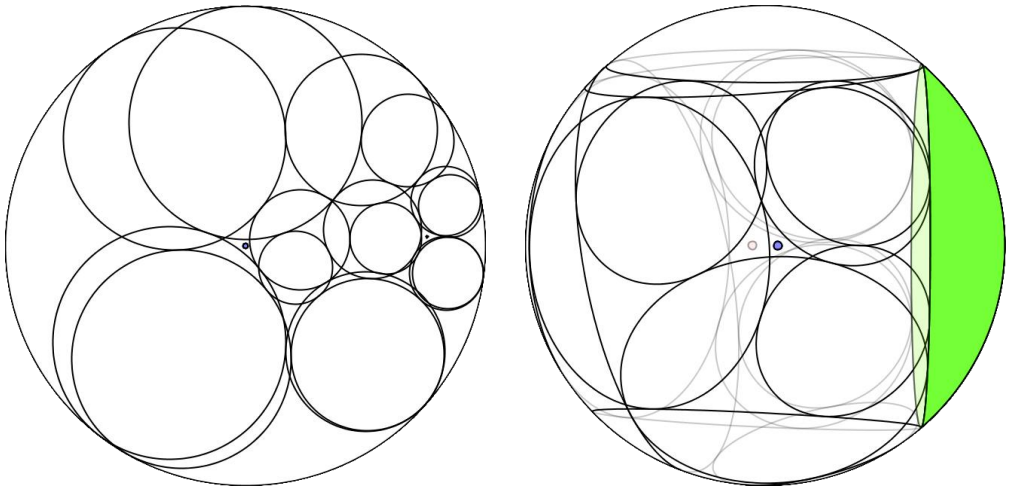


Figure 8.14: Example 3 made coherent via adjusted edge assignments. The generalized branch points are separated branch flowers with center circles colored blue and pink.

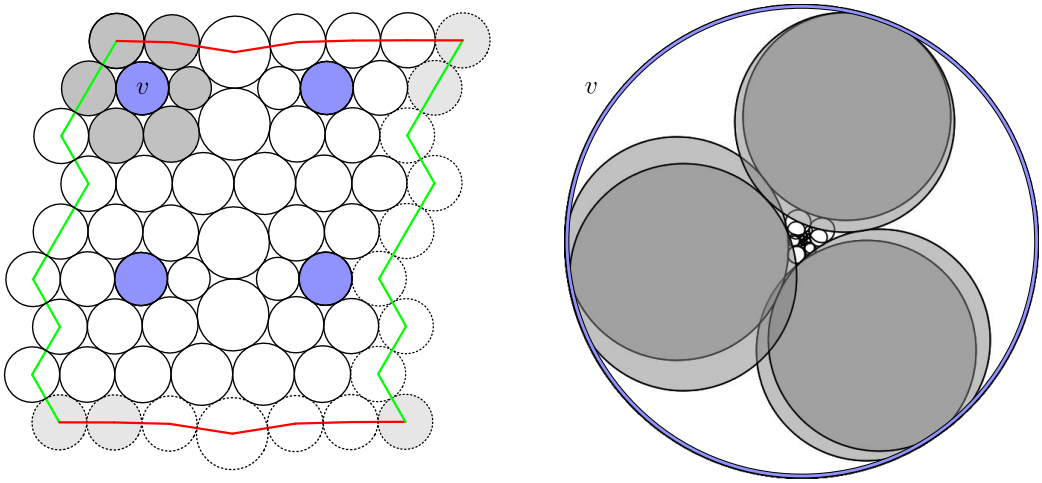


Figure 8.15: The torus used in Example 4. The branch points are colored in blue. On the right is a conversion of v; its petals are colored gray (they are horocycles in the conversion).

By following the steps above, a motif using every possible selection of four traditional branch circles was computed and had its E_K measured. The highlighted circles in Figure 8.15 were the four with the lowest E_K of any set. Next, the conversion of Example 4 was adjusted with (modified) shift-points at the remaining three branch points. Using varying methods to optimize E_K with the six parameters, we were able to significantly reduce the holonomy error (from approximately 3.089 to approximately 0.027).

However we were unable to further improve on this error, and we were unable to achieve the computational or visual success of the previous examples. Progress seems to be impeded by the confluence of several factors. Using more chains and shift-points has a two fold cost in time and accumulative computational error. Small local errors snowball into noticeable amounts; these naturally get expressed in our method of measuring holonomy. Additionally E_K can be very sensitive to relatively small changes in the parameter, and its surface appears to be discontinuous. Figure 8.16 illustrates this behavior when a single shift-point has been inserted.

That a solution exists seems quite possible, but our current methods have met a limiting threshold. An advancement in computational methods or even hardware might yield better results. In regards to the former, applying techniques recently developed by Gerald Orick might resolve the above mentioned cumulative error [35]. However while it is believed that six parameters should suffice, it is unclear exactly why the symmetry of the torus in Section 4.5 actually works.

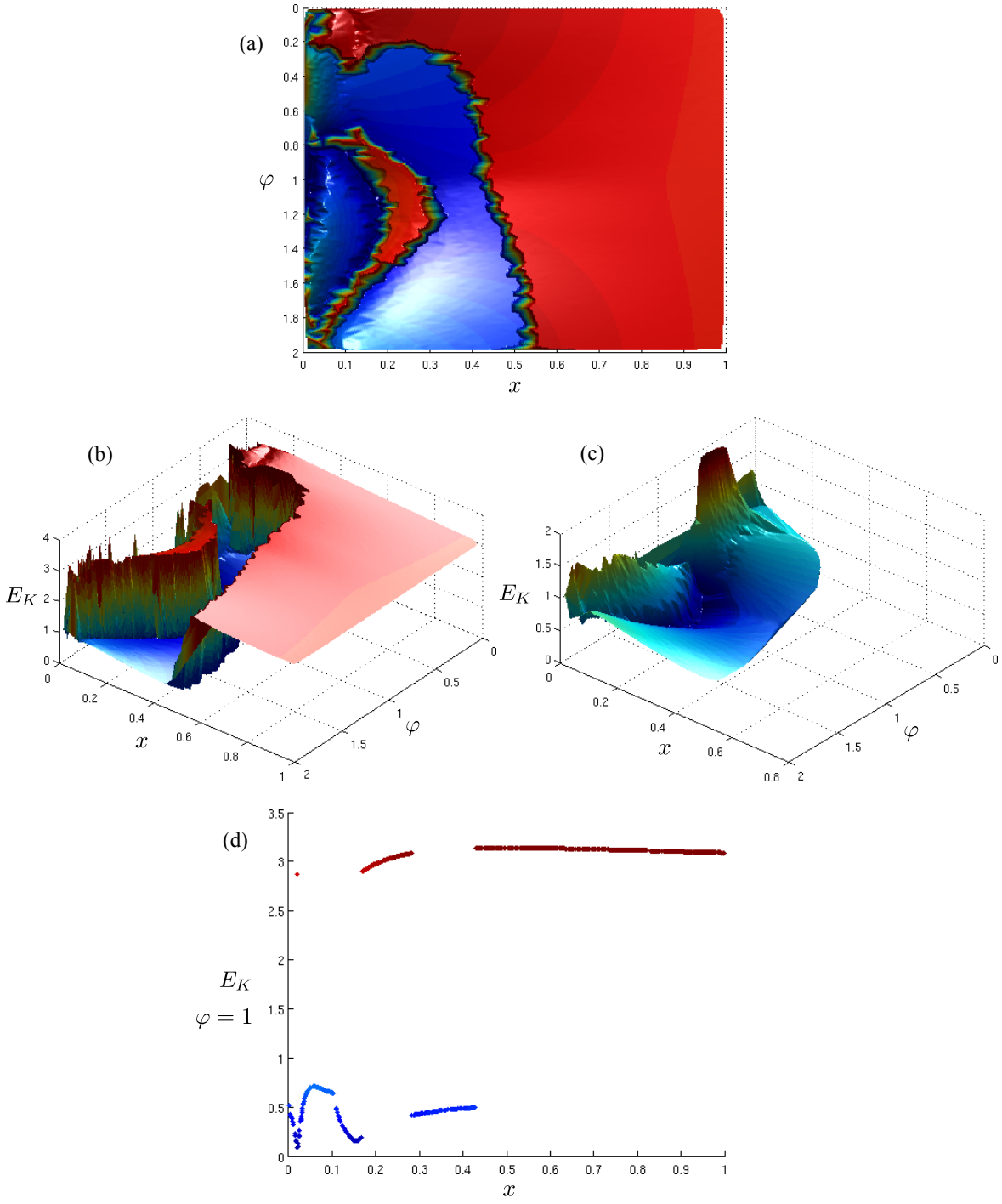


Figure 8.16: Different views of E_K for Example 4 adjusted at a single shift-point. Traditional branching has been placed at the other two branch points. (a) and (b) are a top and isometric view, respectively, (c) is a detail of (b), and (d) is a two-dimensional slice from (b) at $\varphi = 1$.

Bibliography

[1] Lars V. Ahlfors, *Bounded analytic functions*, Duke Math. J. **14** (1947), 1–11. MR 0021108 (9,24a) 43

[2] E. M. Andreev, *Convex polyhedra in Lobačevskiĭ spaces*, Mat. Sb. (N.S.) **81 (123)** (1970), 445–478. MR 0259734 (41 #4367) 9

[3] ———, *Convex polyhedra of finite volume in Lobačevskiĭ space*, Mat. Sb. (N.S.) **83 (125)** (1970), 256–260. MR 0273510 (42 #8388) 9

[4] James Ashe, *Fractured branched circle packings on the plane*, Master thesis, The University of Tennessee, Knoxville, 2004. 59, 68, 71

[5] Alan F. Beardon and David Minda, *The hyperbolic metric and geometric function theory*, Proceedings of the International Workshop on Quasiconformal Mappings and their Applications, Narosa Publishing House, India, 2006, pp. 159–206. 26

[6] Alan F. Beardon and Kenneth Stephenson, *The uniformization theorem for circle packings*, Indiana Univ. Math. J. **39** (1990), no. 4, 1383–1425. MR 1087197 (92b:52038) 39, 43

[7] ———, *The schwarz-pick lemma for circle packings*, Illinois Journal of Mathematics **35** (1991), no. 4, 577–606. 31

[8] Alexander I. Bobenko and Boris A. Springborn, *Variational principles for circle patterns and Koebe's theorem*, Trans. Amer. Math. Soc. **356** (2004), no. 2, 659–689. MR 2022715 (2005b:52054) 70

[9] Philip L. Bowers, *The upper Perron method for labelled complexes with applications to circle packings*, Math. Proc. Cambridge Philos. Soc. **114** (1993), no. 2, 321–345. MR 1230135 (94h:52036) 20

[10] ———, *Introduction to circle packing: the theory of discrete analytic functions [book review of mr2131318]*, Bull. Amer. Math. Soc. (N.S.) **46** (2009), no. 3, 511–525. MR 2507284 2

[11] Philip L. Bowers and Monica K. Hurdal, *Planar conformal mappings of piecewise flat surfaces*, Visualization and mathematics III, Math. Vis., Springer, Berlin, 2003, pp. 3–34. MR 2046999 11

[12] Philip L. Bowers and Kenneth Stephenson, *A branched Andreev-Thurston theorem for circle packings of the sphere*, Proc. London Math. Soc. (3) **73** (1996), no. 1, 185–215. MR 1387087 (97d:52027) 6, 52, 63, 96

[13] ———, *Uniformizing dessins and Belyĭ maps via circle packing*, Mem. Amer. Math. Soc. **170** (2004), no. 805, xii+97. MR 2053391 (2005a:30068) 2

[14] Charles R. Collins and Kenneth Stephenson, *A circle packing algorithm*, Comput. Geom. **25** (2003), no. 3, 233–256. MR 1975216 (2004c:52035) 12, 23, 68, 92

[15] John B. Conway, *Functions of one complex variable*, second ed., Graduate Texts in Mathematics, vol. 11, Springer-Verlag, New York, 1978. MR 503901 (80c:30003) 43

[16] H. S. M. Coxeter, *Inversive distance*, Ann. Mat. Pura Appl. (4) **71** (1966), 73–83. MR 0203568 (34 #3418) 9

[17] Edward Crane, *Branched circle packings and the weierstrass function*, The Barrett Lectures at the University of Tennessee, 2010. 52, 58

[18] Tomasz Dubejko, *Branched circle packings and discrete Blaschke products*, Trans. Amer. Math. Soc. **347** (1995), no. 10, 4073–4103. MR 1308008 (95m:30045) 6, 13, 20

[19] ———, *Infinite branched circle packings and discrete complex polynomials*, J. London Math. Soc. (2) **56** (1997), no. 2, 347–368. MR 1489142 (99h:05025) 6

[20] Tomasz Dubejko and Kenneth Stephenson, *The branched Schwarz lemma: a classical result via circle packing*, Michigan Math. J. **42** (1995), no. 2, 211–234. MR 1342487 (96j:30039) 6

[21] ———, *Circle packing: experiments in discrete analytic function theory*, Experiment. Math. **4** (1995), no. 4, 307–348. MR 1387696 (97f:52027) 6

[22] Clifford J. Earle, *Reviews: Lars Valerian Ahlfors: Collected Papers, Volume I, 1929-1955, Volume II, 1954-1979*, Amer. Math. Monthly **92** (1985), no. 5, 366–368. MR 1540654 43

[23] Brett T. Garrett, *Circle packings and polyhedral surfaces*, Discrete Comput. Geom. **8** (1992), no. 4, 429–440. MR 1176380 (93g:52014) 8, 23, 70

[24] Ren Guo, *Local rigidity of inversive distance circle packing*, to appear in Trans. Amer. Math. Soc. 363 (2011), 4757-4776. 2, 10, 92

[25] Zheng-Xu He, *An estimate for hexagonal circle packings*, J. Differential Geom. **33** (1991), no. 2, 395–412. MR 1094463 (92b:52039) 39

[26] Zheng-Xu He and Oded Schramm, *The inverse riemann mapping theorem for relative circle domains.*, Pacific Journal of Mathematics **171** (1995), no. 1, 157–165. 6

[27] ———, *On the convergence of circle packings to the Riemann map*, Invent. Math. **125** (1996), no. 2, 285–305. MR 1395721 (97i:30009) 39

[28] ———, *The C^∞-convergence of hexagonal disk packings to the Riemann map*, Acta Math. **180** (1998), no. 2, 219–245. MR 1638772 (99j:52021) 39

[29] Gareth A. Jones and David Singerman, *Complex functions*, Cambridge University Press, Cambridge, 1987, An algebraic and geometric viewpoint. MR 890746 (89b:30001) 50

[30] Liliya Kharevych, Boris Springborn, and Peter Schröder, *Discrete conformal mappings via circle patterns*, ACM SIGGRAPH 2005 Courses (New York, NY, USA), SIGGRAPH '05, ACM, 2005. 8

[31] Paul Koebe, *Kontaktprobleme der konformen abbildung. ber. s achs. akad. wiss. leipzig, math*, Phys. Kl **88** (1936), 141–164. 9

[32] Feng Luo, *Rigidity of polyhedral surfaces, iii*, Submitted on 15 Oct 2010. 2, 92

[33] Jiming Ma and Jean-Marc Schlenker, *Non-rigidity of spherical inversive distance circle packings*, Preprint, arXiv:1105.146, 2011. 2

[34] Al Marden and Burt Rodin, *On Thurston's formulation and proof of Andreev's theorem*, Computational methods and function theory (Valparaíso, 1989), Lecture Notes in Math., vol. 1435, Springer, Berlin, 1990, pp. 103–115. MR 1071766 (92b:52040) 24

[35] Gerald L. Orick, *Computational circle packing: Geometry and discrete analytic function theory*, (2010). 107

[36] Igor Rivin, *Euclidean structures on simplicial surfaces and hyperbolic volume*, Ann. of Math. (2) **139** (1994), no. 3, 553–580. MR 1283870 (96h:57010) 10

[37] Burt Rodin and Dennis Sullivan, *The convergence of circle packings to the Riemann mapping*, J. Differential Geom. **26** (1987), no. 2, 349–360. MR 906396 (90c:30007) 1, 39, 71

[38] Oded Schramm, *Packing two-dimensional bodies with prescribed combinatorics and applications to the construction of conformal and quasiconformal mappings*, ProQuest LLC, Ann Arbor, MI, 1990, Thesis (Ph.D.)–Princeton University. MR 2638585 86

[39] ———, *Existence and uniqueness of packings with specified combinatorics*, Israel J. Math. **73** (1991), no. 3, 321–341. MR 1135221 (92k:52039) 86

[40] ———, *Circle patterns with the combinatorics of the square grid*, Duke Math. J. **86** (1997), no. 2, 347–389. MR 1430437 (98a:30061) 9

[41] Hans Schwerdtfeger, *Geometry of complex numbers*, Dover Publications Inc., New York, 1979, Circle geometry, Moebius transformation, non-Euclidean geometry, A corrected reprinting of the 1962 edition, Dover Books on Advanced Mathematics. MR 620163 (82g:51032) 40

[42] Kenneth Stephenson, *A probabilistic proof of Thurston's conjecture on circle packings*, Rend. Sem. Mat. Fis. Milano **66** (1996), 201–291 (1998). MR 1639851 (99m:52024) 39, 71

[43] ———, *Circle packing: a mathematical tale*, Notices Amer. Math. Soc. **50** (2003), no. 11, 1376–1388. MR 2011604 (2004h:52030) 6

[44] ———, *Introduction to circle packing*, Cambridge University Press, Cambridge, 2005, The theory of discrete analytic functions. MR 2131318 (2006a:52022) 2, 4, 6, 10, 20, 31, 32, 43, 58, 70

[45] William P. Thurston, *Geometry and topology of 3-manifolds*, Math. Dept. of Princeton University, Princeton, 1979. 17, 93

[46] ———, *The finite riemann mapping theorem*, Invited talk at the International Symposium at Purdue University on the occasion of the proof of the Bieberbach conjecture, 1985. 1, 9, 39

[47] Jonatan Vasilis, *The ring lemma in three dimensions*, Geom. Dedicata **152** (2011), 51–62. MR 2795235 71

[48] Elias Wegert and David Bauer, *On Riemann-Hilbert problems in circle packing*, Comput. Methods Funct. Theory **9** (2009), no. 2, 609–632. MR 2572659 (2011f:52035) 58

Vita

James Russell Ashe was born in 1975 in Portsmouth, Virginia. In 1994 he graduated from Greeneville High School in Greeneville, Tennessee. James matriculated at East Tennessee State University, TN, where in 1999 he received a B.S. in History with a minor in art. He then graduated with a M.S. in Mathematics at the University of Tennessee in 2004. In 2012 James completed the requirements for a Ph.D. in Mathematics at the University of Tennessee.